

<https://helda.helsinki.fi>

---

## Geochemistry and petrology of the ferropicrite dikes and associated rocks of Vestfjella, western Dronning Maud Land, Antarctica

Heinonen, Jussi S.

Unigrafia

2011-05-27

---

Heinonen , J S 2011 , ' Geochemistry and petrology of the ferropicrite dikes and associated rocks of Vestfjella, western Dronning Maud Land, Antarctica ' , Helsinki . <  
<http://urn.fi/URN:ISBN:978-952-10-6310-7> >

---

<http://hdl.handle.net/10138/229472>

---

acceptedVersion

---

*Downloaded from Helda, University of Helsinki institutional repository.*

*This is an electronic reprint of the original article.*

*This reprint may differ from the original in pagination and typographic detail.*

*Please cite the original version.*

# Geochemistry and petrology of the ferropicrite dikes and associated rocks of Vestfjella, western Dronning Maud Land, Antarctica

Jussi S. Heinonen

Academic dissertation

Department of Geosciences and Geography, Faculty of Science, University of Helsinki, Finland

Department of Geosciences and Geography A7 / Helsinki 201X

49 © Jussi Heinonen (synopsis)  
50 © Reprinted with kind permission of Elsevier (Paper I, III)  
51 © Reprinted with kind permission of Springer-Verlag (Paper II)  
52  
53 This thesis is a contribution to the International Polar Year 2007/2008 and to the project “Anorogenic  
54 magmatism in Dronning Maud Land, Antarctica – AMANDA” that was funded by the Academy of Finland  
55 (Grant no. 210640).  
56  
57 **Author’s address:**  
58 Jussi Heinonen (jussi.s.heinonen@helsinki.fi)  
59 Department of Geosciences and Geography, P.O. Box 64  
60 University of Helsinki (FI-00014), Finland  
61  
62 **Supervised by:**  
63 Arto Luttinen  
64 Curator  
65 Finnish Museum of Natural History  
66 University of Helsinki, Finland  
67  
68 Tapani Rämö  
69 Professor  
70 Department of Geosciences and Geography  
71 University of Helsinki, Finland  
72  
73 **Reviewed by:**  
74 Eero Hanski  
75 Professor  
76 Department of Geology  
77 University of Oulu, Finland  
78  
79 Teal Riley  
80 Head of Survey Mapping  
81 British Antarctic Survey  
82 Cambridge, Great Britain  
83  
84 **Discussed with:**  
85  
86  
87  
88  
89  
90  
91  
92  
93  
94  
95  
96 ISSN-L 1798-7911  
97 ISSN 1798-7911 (print)  
98 ISBN 978-952-10-6309-1 (paperback)  
99 ISBN 978-952-10-6310-7 (pdf)  
100 <http://ethesis.helsinki.fi/>  
101 Helsinki University Print, Helsinki 2010

**Heinonen J.S.**, 2010. *Geochemistry and petrology of the ferropicrite dikes and associated rocks of Vestfjella, western Dronning Maud Land, Antarctica*. Academic dissertation, University of Helsinki, 2010, XX pp., Publications of the Department of Geosciences and Geography A7.

## Abstract

This study provides insights into the composition and origin of ferropicrite dikes ( $\text{FeO}_{\text{tot}} = 13\text{--}17$  wt. %;  $\text{MgO} = 13\text{--}19$  wt. %) and associated meimechite, picrite, picrobasalt, and basalt dikes found at Vestfjella, western Dronning Maud Land, Antarctica. The dikes crosscut Jurassic Karoo continental flood basalts (CFB) that were emplaced during the early stages of the breakup of the Gondwana supercontinent ~180 Ma ago. Selected samples (31 overall from at least 11 dikes) were analyzed for their mineral chemical, major element, trace element, and Sr, Nd, Pb, and Os isotopic compositions.

The studied samples can be divided into two geochemically distinct types: (1) The depleted type (24 samples from at least 9 dikes) is relatively depleted in the most incompatible elements and exhibits initial  $\epsilon_{\text{Nd}}$  of +4.8 to +8.3 and initial  $^{187}\text{Os}/^{188}\text{Os}$  of 0.1256–0.1277 at 180 Ma. (2) The enriched type (7 samples from at least 2 dikes) exhibits trace element characteristics similar to those of oceanic island basalts, initial  $\epsilon_{\text{Nd}}$  of +1.8 to +3.6 and initial  $^{187}\text{Os}/^{188}\text{Os}$  of 0.1401–0.1425 at 180 Ma. Both magma types have escaped significant contamination with the continental crust.

The depleted type is related to the main phase of Karoo magmatism and originated as highly magnesian ( $\text{MgO}$  up to 25 wt. %) partial melts at high temperature (mantle potential temperature > 1600 °C) and pressure (~5–6 GPa) from a sublithospheric, water-bearing, depleted peridotite mantle source. The enriched type sampled pyroxene-bearing heterogeneities that can be traced down to either recycled oceanic crust or melt-metasomatized portions of the sublithospheric or lithospheric mantle.

The source of the depleted type represents a sublithospheric end-member source for many Karoo lavas and has subsequently been sampled by mid-ocean ridge basalts (MORBs) of the Indian Ocean. These observations, together with the purported high temperatures, indicate that the Karoo CFBs were formed in an extensive melting episode caused mainly by internal heating of the upper mantle beneath the Gondwana supercontinent.

My research supports the view that ferropicritic melts can be generated in several ways: the relative Fe-enrichment of mantle partial melts is most readily achieved by (1) relatively low degree of partial melting, (2) high pressure of partial melting, and (3) melting of enriched source components (e.g., pyroxenite and metasomatized peridotite). Ferropicritic whole-rock compositions could also result from accumulation, secondary alteration, and fractional crystallization, however, and caution is required when addressing the parental magma composition.

**Key words:** *ferropicrite, continental flood basalt, Karoo, Gondwana, geochemistry, petrology, Vestfjella, Dronning Maud Land, Antarctica*

## Tiivistelmä (in Finnish)

Mantereiset laakiobasalttiprovinssit ovat suurimpia tunnettuja ilmanalaisia vulkaanisia muodostumia (alkuperäinen tilavuus jopa 2 000 000 km<sup>3</sup>).

152 Laakiobasaltteja esiintyy kaikilla mantereilla ja niitä tiedetään muodostuneen  
153 miltei läpi maapallon historian. Laakiobasalttien purkautumisella on varmasti  
154 ollut huomattava vaikutus maapallon ilmastoon ja elämän kehitykseen, mutta  
155 niiden synnystä tiedetään edelleen varsin vähän. Tämä johtuu osaltaan siitä, että  
156 suurin osa laakiobasalttien kantasulista on reagoinut voimakkaasti mantereisen  
157 litosfäärin kanssa ja niiden alkuperäinen, mahdollisesti litosfäärin alaisesta  
158 vaipasta peritty geokemiallinen sormenjälki on siksi usein vaikeasti  
159 tunnistettavissa ja tulkittavissa.

160 Ferropikriitit ovat poikkeuksellisen rautarikkaita ( $\text{FeO}_{\text{tot}} > 13\text{--}14$  p. %) ja  
161 primitiivisiä ( $\text{MgO} \approx 12\text{--}18$  p. %) laavakiviä, joita on kuvattu joistakin  
162 laakiobasalttiprovinseista. Toisin kuin tavalliset laakiobasaltit, ferropikriitit eivät  
163 yleensä ole merkittävästi reagoineet litosfäärin kanssa ja siksi ne tarjoavat  
164 arvokasta tietoa suoraan laakiobasalttimuodostumien alkulähteiltä – mantereisen  
165 litosfäärin alaisesta vaipasta. Ferropikriitit ovat usein yhdistetty anomaalisen  
166 korkeisiin vaipan lämpötiloihin ja vaippapluumeihin, mutta näiden erikoisten  
167 kivien syntyyn liittyy useita kysymyksiä: Mistä niiden korkea rautapitoisuus on  
168 peräisin? Miten ne kytkeytyvät laakiobasalttien syntyyn?

169 Tässä väitöskirjatyössä käsitellään Vestfjellan (Kuningatar Maudin maa,  
170 Etelämannar) ferropikriittien ( $\text{FeO}_{\text{tot}} = 13\text{--}17$  p. %;  $\text{MgO} = 13\text{--}19$  p. %) sekä  
171 niihin liittyvien muiden primitiivisten magmakivien – pikriittien, meimechiittien,  
172 pikrobasalttien ja basalttien – geokemiaa ja petrologiaa. Nämä suureksi osaksi  
173 aikaisemmin tuntemattomat kivet leikkaavat juonina Karoon suuren  
174 magmaprovinssin laakiobasaltteja, jotka purkautuivat jurakaudella noin 180  
175 miljoonaa vuotta sitten Gondwana-supermantereen repeämisprosessin  
176 alkuvaiheiden aikana. Valikoiduista näytteistä (yhteensä 31 vähintään 11 juonesta)  
177 analysoitiin mineraalien koostumuksia sekä pääalkuaine-, hivenalkuaine-, ja Sr,  
178 Nd, Pb ja Os isotooppikoostumuksia.

179 Analysoidut näytteet voidaan jakaa hivenalkuaine- ja  
180 isotooppikoostumuksensa perusteella kahteen magmatyyppiin: (1) Köyhtynyt  
181 magmatyyppi (24 näytettä vähintään 9 juonesta) on köyhtynyt kaikkein  
182 sopeutumattomimmista alkuaineista ja sen initiaali  $\epsilon_{\text{Nd}}$  vaihtelee välillä +4.8 ja  
183 +8.3 ja initiaali  $^{187}\text{Os}/^{188}\text{Os}$  välillä 0.1256–0.1277 (laskettuna 180 Ma ikäisenä).  
184 (2) Rikastunut magmatyyppi (7 näytettä vähintään 2 juonesta) muistuttaa  
185 geokemiallisesti merellisten saarten basaltteja ja sen initiaali  $\epsilon_{\text{Nd}}$  vaihtelee välillä  
186 +1.8 ja +3.6, ja initiaali  $^{187}\text{Os}/^{188}\text{Os}$  välillä 0.1401–0.1425 (laskettuna 180 Ma  
187 ikäisenä). Kumpikaan magmatyyppi ei ole merkittävästi saastunut kuorellisella  
188 aineksella.

189 Köyhtynyt magmatyyppi on peräisin Karoon päävaiheen aikana hyvin MgO-  
190 rikkaista (jopa 25 p. %) kantasulista, jotka muodostuivat korkeissa lämpötiloissa  
191 (vaipan potentiaalilämpötila  $> 1600$  °C) ja paineissa (n. 5–6 GPa) pääosin  
192 vesipitoisesta, köyhtyneestä ylävaipan peridotiitista. Rikastuneen magmatyyppin  
193 lähteenä ovat vaipan heterogeeniset pyrokseenipitoiset komponentit, jotka  
194 muodostuivat joko subduktoituneen merellisen kuoren reagoidessa vaipan  
195 peridotiitin kanssa tai sulametasomatoosin seurauksena.

196 Geokemiallisen mallinnuksen perusteella monet Karoon laakiobasalteista  
197 ovat alun perin (eli ennen saastumistaan litosfäärin aineksilla) peräisin samasta  
198 vaippalähteestä kuin köyhtynyt magmatyyppi. Tästä lähteestä ovat  
199 todennäköisesti peräisin myös Intian Valtameren keskiselänteen basaltit. Nämä  
200 havainnot ja köyhtyneelle magmatyypille arvioitua korkeat lähdelämpötilat  
201 tukevat käsitystä siitä, että Karoon laakiobasaltit saivat suurimmaksi osaksi

202 alkunsa Gondwana-supermantereen alaisen vaipan sisäisen lämpenemisen, ei  
 203 niinkään ylävaippaan tunkeutuneen syvän vaippapluumin, seurauksena.

204 Tutkimukseni tukee näkemystä siitä, että ferropikriittiset sulat voivat syntyä  
 205 monin eri tavoin: poikkeuksellisen korkea rautapitoisuus saavutetaan helpoimmin,  
 206 jos lähdemateriaali vaipassa sulaa (1) alhaisella asteella (2) ja/tai korkeassa  
 207 paineessa, ja/tai (3) lähdemateriaali sisältää rikastuneita komponentteja (esim.  
 208 pyrokseeniittia tai metasomatoitunutta peridotiittia). On kuitenkin  
 209 huomionarvoista, että ferropikriittinen kokokivikoostumus voi olla myös  
 210 seurausta akkumulaatiosta, sekundaarisesta muuttumisesta tai fraktioivasta  
 211 kiteytymisestä, ja erityistä huomiota on siksi kiinnitettävä kantamagman  
 212 koostumuksen määrittämiseen.

213

## 214 Contents

215

216	Abstract	3
217	Tiivistelmä (In Finnish)	3
218	Acknowledgements	-
219	List of original publications	6
220	Abbreviations	7
221	List of figures	7
222	1. Introduction	8
223	1.1. Continental flood basalts – an unsolved mystery	8
224	1.1.1. The Karoo large igneous province	10
225	1.2. Ferropicrites – continental messengers from the sublithospheric mantle	12
226	1.3. Objectives of this study	14
227	1.4. Analytical methods	18
228	2. Review of the original publications	19
229	2.1. Paper I	19
230	2.2. Paper II	19
231	2.3. Paper III	20
232	3. Discussion	20
233	3.1. Petrogenesis of the Vestfjella ferropicrites	20
234	3.1.1. Depleted type	20
235	3.1.2. Enriched type	24
236	3.2. Implications on the origin of the Karoo continental flood basalt province	25
237	3.2.1. Geochemical comparisons and petrogenetic relationships	25
238	3.2.2. The origin of the Karoo flood basalts	28
239	3.3. Implications on the origin of ferropicrites	29
240	3.3.1. Ferropicrite whole-rocks vs. ferropicrite melts	29
241	3.3.2. Pyroxenite vs. peridotite source	30
242	3.3.3. Hydrous or anhydrous magmas?	35
243	3.3.4. Mantle thermometry and relation to mantle plumes	36
244	3.3.5. The origin of the relative Fe enrichment	38
245	4. In conclusion	39
246	5. References	40
247	Appendix I	
248	Papers I–III	

## List of Original Publications

This thesis is based on the following three publications. References to these publications in the text are made with respect to Roman numerals, as designated below:

- I **Heinonen, J.S.** & Luttinen, A.V. (2008) Jurassic dikes of Vestfjella, western Dronning Maud Land, Antarctica: geochemical tracing of ferropicrite sources. *Lithos*, **105**, 347–364.
- II **Heinonen, J.S.** & Luttinen, A.V. (2010) Mineral chemical evidence for extremely magnesian subalkaline melts from the Antarctic extension of the Karoo large igneous province. *Mineralogy and Petrology*, **99**, 201–217.
- III **Heinonen, J.S.**, Carlson, R.W., & Luttinen, A.V. (2010) Isotopic (Sr, Nd, Pb, and Os) composition of highly magnesian dikes of Vestfjella, western Dronning Maud Land, Antarctica: a key to the origins of the Jurassic Karoo large igneous province? *Chemical Geology*, **277**, 227–244.

### Author's contributions

Paper I: Fully responsible for sample selection, petrographical observations, and geochemical modeling. Mostly responsible for writing, illustrations, and data interpretation.

Paper II: Fully responsible for sample selection, petrographical observations, geochemical modeling, and controlling the mineral chemical analyses. Mostly responsible for writing, illustrations, and data interpretation.

Paper III: Fully responsible for sample preparation and geochemical modeling. Mostly responsible for sample selection, writing, illustrations, isotopic analyses, and data interpretation. Minor contribution to field observations and sampling.

## 297 Abbreviations

298		
299	AFC	= assimilation-fractional crystallization
300	CFB	= continental flood basalt
301	CT1, CT2, CT3, CT4	= continental tholeiite magma types of Vestfjella
302	EC-AFC	= energy-constrained assimilation-fractional crystallization
303	EM	= enriched mantle
304	F	= degree of melting
305	HFSE	= high field strength element
306	ICP-MS	= inductively coupled plasma mass spectrometry/spectrometer
307	$K_d$	= mineral/melt partition coefficient
308	$K_D$	= mineral/melt bulk partition coefficient
309	LILE	= large-ion lithophile element
310	LIP	= large igneous province
311	LOI	= loss on ignition (~volatile content)
312	Ma	= million years / million years ago
313	MORB	= mid-ocean ridge basalt
314	N-MORB	= normal mid-ocean ridge basalt
315	OIB	= oceanic island basalt
316	P	= pressure
317	SCLM	= subcontinental lithospheric mantle
318	T	= temperature
319	$T_{ex}$	= excess potential temperature relative to ambient upper mantle
320	$T_p$	= mantle potential temperature
321	TIMS	= thermal ionization mass spectrometry
322	TTG	= tonalite-trondjemite-granodiorite
323	XRF	= X-ray fluorescence
324		

## 325 List of figures

326	
327	Fig. 1. <i>Locations of Phanerozoic ferropicrites and LIPs with CFB affinities, page XX</i>
328	Fig. 2. <i>Schematic model of flood basalt generation, page XX</i>
329	Fig. 3. <i>Distribution of Mesozoic CFBs in reconstructed Gondwana supercontinent, page XX</i>
330	Fig. 4. <i>Classification and nomenclature for the highly magnesian volcanic rocks, page XX</i>
331	Fig. 5. <i>Variations of <math>FeO_{tot}</math>, <math>Al_2O_3</math>, <math>TiO_2</math>, and <math>(Sm/Yb)_N</math> vs. <math>MgO</math> for ferropicrites, page XX</i>
332	Fig. 6. <i>Ferropicrites shown in <math>\epsilon_{Nd(t)}</math> vs. <math>t</math> diagram, page XX</i>
333	Fig. 7. <i>Distribution of Jurassic CFBs in western Dronning Maud Land and ferropicrites and associated rocks in Vestfjella, page XX</i>
334	
335	Fig. 8. <i>Geochemical characteristics of Vestfjella ferropicrites and associated rocks shown in <math>FeO_{tot}</math> vs. <math>MgO</math> diagram and <math>La/Sm</math> vs. <math>Sm/Yb</math> diagram, page XX</i>
336	
337	Fig. 9. <i>Clinopyroxene phenocryst chemistry of a Vestfjella depleted ferropicrite, enriched ferropicrite, and meimechite shown in <math>TiO_2</math> vs. <math>MgO</math> diagram, page XX</i>
338	
339	Fig. 10. <i>Results of lithospheric contamination modeling illustrated in primitive mantle –normalized incompatible element patterns along with representative CT lava compositions, page XX</i>
340	
341	Fig. 11. <i>Geochemical characteristics of ferropicrites compared with peridotite and pyroxenite experimental partial melts and continental picrites and komatiites in <math>FeO_{tot}</math> vs. <math>MgO</math>, <math>CaO</math> vs. <math>Al_2O_3</math>, and <math>TiO_2</math> vs. <math>Na_2O</math> diagrams, page XX</i>
342	
343	
344	Fig. 12. <i>Ferropicrites shown in <math>Zn/Fe</math> (<math>\times 10^4</math>) diagram, page XX</i>
345	Fig. 13. <i>Phanerozoic ferropicrites shown in initial <math>\epsilon_{Nd}</math> vs. <math>^{87}Sr/^{86}Sr</math>, <math>^{87}Sr/^{86}Sr</math> vs. <math>^{206}Pb/^{204}Pb</math>, <math>^{207}Pb/^{204}Pb</math> vs. <math>^{206}Pb/^{204}Pb</math>, and <math>^{208}Pb/^{204}Pb</math> vs. <math>^{206}Pb/^{204}Pb</math> diagrams, page XX</i>
346	
347	Fig. 14. <i>Ferropicrites shown in logarithmic <math>Nb/Y</math> vs. <math>Zr/Y</math> diagram, page XX</i>
348	
349	
350	



# 1. Introduction

## 1.1. Continental flood basalts – an unsolved mystery

Several times in the history of planet Earth, enormous volumes ( $>0.1 \text{ Mkm}^3$ ) of magma have emplaced into the crust and on the surface of the Earth far away from major plate boundaries in relatively short periods of time ( $\leq 50 \text{ Ma}$ ;  $>75\%$  of total volume within  $\sim 5 \text{ Ma}$ ; Bryan & Ernst 2008). The remains of these catastrophic events have been termed Large Igneous Provinces (LIP) and they include oceanic plateaus, ocean basin flood basalts, giant continental dike swarms, silicic LIPs, Archean tholeiite-komatiite associations, volcanic rifted margins, and continental flood basalt (CFB) provinces (Bryan & Ernst 2008). CFB provinces (Fig. 1) are of particular importance as their formation commonly preceded or was coeval with continental break-up and their emplacement likely had a significant effect on the contemporary climate and biosphere.

CFBs have been extensively studied, but their origin is still a matter of considerable debate: a great variety of models have been proposed in order to explain their petrogenesis and geological characteristics (see, e.g., Macdougall 1988; Saunders 2005; Bryan & Ernst 2008). The formation of CFBs was traditionally considered to be controlled by crustal tectonics and/or ambient mantle convection (e.g., Gibson 1966; Clifford 1968; Cox 1978) until Richards *et al.* (1989) suggested that the arrival of the “head” of a lower-mantle-sourced thermal upwelling, i.e., mantle plume (Morgan 1971) onto the base of the continental lithosphere could be held responsible for the extensive magma production. The plume hypothesis (to explain CFB origins) was further developed during the 1990’s (e.g., Campbell & Griffiths 1990; Kent *et al.* 1992; Farnetani & Richards 1994; Bercovici & Mahoney 1994), but has been increasingly challenged by recently developed lithosphere-focused models that include decompression melting triggered by delamination (Elkins-Tanton & Hager 2000; Elkins-Tanton 2005), melting of fertile mantle components (Anderson 1994, 2005, 2007) associated with extension (Foulger 2007), and edge-driven convection (King & Anderson 1995, 1998). Furthermore, the Siberian Traps CFB province has been considered by Jones *et al.* (2002) as the result of melting related to an impact of an extraterrestrial projectile. In some models plate tectonic processes are accompanied by mantle plumes (White & McKenzie 1989) and temperature increases in the subcontinental mantle explained by “passive” processes, such as internal heating of supercontinent-insulated mantle (e.g., Gurnis 1988; Coltice *et al.* 2007). Nevertheless, a central question in the discussion on the CFB origins is whether these huge manifestations of basic magmatism were associated with notable positive thermal anomalies in the subcontinental upper mantle ( $T_{\text{ex}} \geq 100 \text{ }^\circ\text{C}$ ; e.g., Richards *et al.* 1989; White & McKenzie 1989; Johnston & Thorkelson 2000; Thompson & Gibson 2000; Coltice *et al.* 2007) or not ( $T_{\text{ex}} \approx 0 \text{ }^\circ\text{C}$ ; e.g., King & Anderson 1995; Anderson 2000, 2005; Elkins-Tanton 2005; Foulger 2007).

The debate on the origin of CFBs is largely fueled by the lack of knowledge on the parental magmas and mantle sources involved. This stems from the fact that CFBs usually are fairly evolved ( $\text{MgO} < 10 \text{ wt. } \%$ ) and generally show strong lithospheric geochemical signatures, which hinder the identification of their parental melt compositions and ultimate mantle sources (Fig. 2; e.g., Hawkesworth *et al.* 1992; Hooper & Hawkesworth 1993; Lightfoot *et al.* 1990, 1993; Wooden *et al.* 1993; Pik *et al.* 1999; Luttinen & Furnes 2000; Sano *et al.*

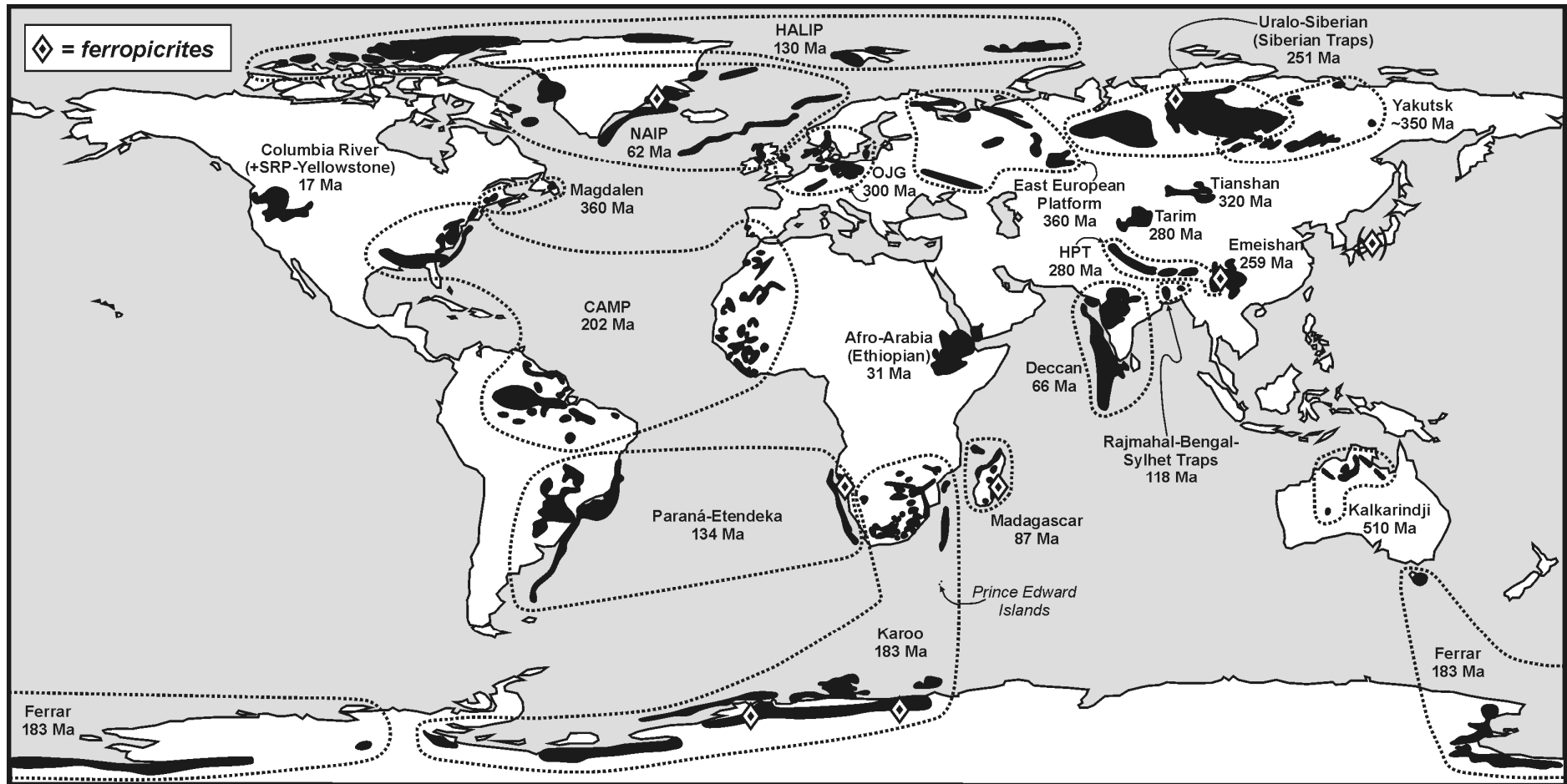


**Figure 1.** Locations of Phanerozoic ferropicrites and LIPs with CFB affinities (after Bryan & Ernst 2008). Prince Edward oceanic island group also shown. Ages denote the onset of the first major magmatic pulse (cf. Bryan & Ernst 2008). HALIP = High Arctic Large Igneous Province; NAIP = North Atlantic Igneous Province; CAMP = Central Atlantic Magmatic Province; OJG = Oslo-Jutland-NE Germany; HPT = Himalaya-Panjal Traps; SRP = Snake River Plain.

2001; Tommasini *et al.* 2005; Jourdan *et al.* 2007a). Some have even questioned whether sublithospheric sources are needed at all and have suggested that some CFBs may have formed by wholesale melting of mantle lithosphere (e.g., Turner *et al.* 1996). There is also a considerable debate on whether the possible sublithospheric end-member components represent mantle sources similar to those of mid-ocean ridge basalts (MORBs; derived from ambient depleted upper mantle) and/or ocean island basalts (OIB; derived from anomalous upper mantle or mantle plume) (e.g., Macdougall 1988; Ellam & Cox 1989, 1991; Ellam *et al.* 1992; Menzies 1992; Horan *et al.* 1995; Ellam & Stuart 2000; Peate *et al.* 2003; Carlson *et al.* 2006; Ellam 2006).

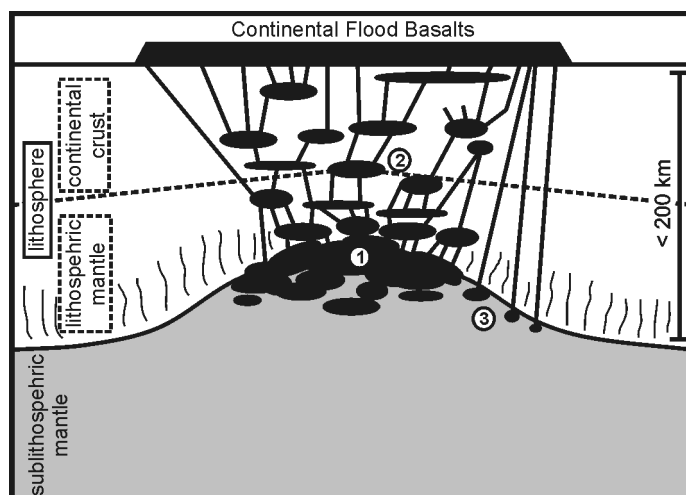


**Figure 2.** Schematic model of flood basalt generation. The parental melts originate in the subcontinental mantle (1) and subsequently evolve, assimilate, and mix in magma chambers within the lithosphere (2). In rare occasions (such as in the case of many ferropicrites), sublithospheric mantle-derived melts avoid lithospheric contamination (3).

### 1.1.1. The Karoo large igneous province

The Karoo LIP is a Jurassic CFB province that manifests huge outpourings of basaltic magma (up to  $2 \times 10^6$  km<sup>3</sup>; Richards *et al.* 1989) in a developing rift between Africa and Antarctica during the early stages of the breakup of the Gondwana supercontinent (Fig. 1, 3). Other CFB provinces related to the early stages of Gondwana dispersal are the coeval Ferrar CFB province and the Cretaceous Paraná-Etendeka CFB province (Fig. 3). The bulk of the exposed Karoo CFBs are located in southern Africa, but their remnants can also be found in several nunataks of western Dronning Maud Land, Antarctica (Fig. 1, 3). Karoo-related dike swarms and sills are more widespread than the lavas (Fig. 3) and, in places, also overlap with contemporaneous Ferrar-type intrusive rocks (Leat *et al.* 2006; Riley *et al.* 2006). The <sup>40</sup>Ar/<sup>39</sup>Ar datings of Karoo-related rocks indicate that magmatism was active over ~16 Ma (190–174 Ma) with the main volume of mafic magmas being emplaced within ~184–178 Ma (Duncan *et al.* 1997; Zhang *et al.* 2003; Jourdan *et al.* 2005, 2007b; Riley *et al.* 2005).

Most of the Karoo CFBs and related rocks show geochemical evidence of strong lithospheric influence (e.g., Hawkesworth *et al.* 1984; Sweeney *et al.* 1994; Luttinen *et al.* 1998; Luttinen & Furnes 2000; Riley *et al.* 2005; Ellam 2006; Jourdan *et al.* 2007a) and, presumably, undisturbed sublithospheric compositions are rare. Even the most primitive Karoo volcanic rocks found in southern Africa, the Mwenezi picrites (Fig. 3), are characterized by enriched lithospheric

geochemical signatures (Ellam & Cox 1989, 1991; Sweeney *et al.* 1991; Ellam *et al.* 1992; Ellam 2006). In southern Africa, some of the MORB-like basaltic dikes of Rooi Rand (Fig. 3) are the only known examples of Karoo rocks that have been thought to preserve sublithospheric mantle-derived compositions (Duncan *et al.* 1990). They have been ascribed to the final stages of Karoo magmatism at ~174 Ma and mark the initiation of ocean floor spreading between Africa and Antarctica (Duncan *et al.* 1990; Watkeys 2002; Jourdan *et al.* 2007b).

Most of the Karoo-related rocks with sublithospheric geochemical affinities have been found within the Antarctic extension of the Karoo LIP. They include MORB-like dikes (CT2 subtype) at Vestfjella (Luttinen & Furnes 2000) and ferropicrite dikes and related rocks at Ahlmannryggen (Group 3; Riley *et al.* 2005) and Vestfjella (OIB-like CT4 magma type; Luttinen *et al.* 1998) (Fig. 3). The ferropicrites of Ahlmannryggen have been dated at ~190 Ma, although with considerable uncertainty, and could thus be related to the initial stages of the Karoo magmatism (Riley *et al.*, 2005). The absolute ages of the uncontaminated mantle-derived magma types of Vestfjella have not been reliably constrained (cf. Zhang *et al.* 2003).

The Karoo province has been at the focus of CFB research throughout the history of modern petrology. Notable studies of, e.g., Cox *et al.* (1965, 1967) and Cox (1970, 1972) and the South African National Geodynamics Programme “Petrogenesis of the Volcanic Rocks of the Karoo Province” (Erlank 1984) laid down the guidelines and resulted in significant amounts of geochemical data on Karoo volcanic rocks. The plume model for Karoo volcanism was first invoked by Burke & Dewey (1972). Richards *et al.* (1989) further considered Karoo CFBs to represent magmas produced by the plume “head” and the Prince Edward islands in the Indian Ocean (Fig. 1) to manifest the current location of the hotspot and volcanism caused by the subsequent thermal upwelling related to the plume “tail”. The plume model has recently been supported by paleostress and liquidus temperature estimates for some Karoo dikes in Antarctica (Riley *et al.* 2005; Curtis *et al.* 2008). Structural analyses, geochemical affinities, and temporal relationships of the great majority of Karoo-related rocks, however, point to a strong control of lithosphere on the magmatism (Cox *et al.* 1967; Cox 1988; Duncan *et al.* 1984; Ellam & Cox 1989; Sweeney *et al.* 1991, 1994; Luttinen *et al.* 1998; Luttinen & Furnes 2000; Jourdan *et al.* 2005, 2006, 2007a, 2007b), and in many cases, question a plume origin. Recently, rifting associated with prolonged period of internal mantle heating beneath an insulating supercontinent has been also suggested as the dominant cause for the Karoo magmatism (Coltice *et al.* 2009; cf. Silver *et al.* 2006).

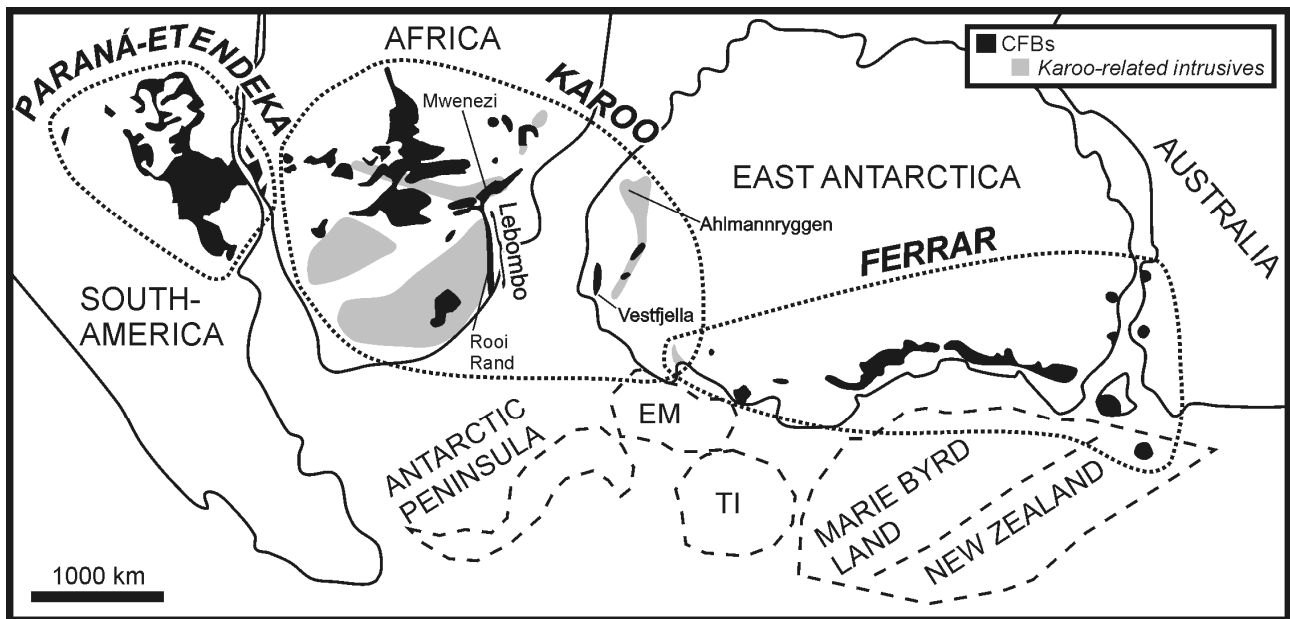


**Figure 3.** Distribution of Mesozoic CFBs in reconstructed Gondwana supercontinent. In the case of the Karoo province, the known extent of intrusive equivalents (found outside CFBs) is also shown. Reconstruction modified after Hergt *et al.* (1991), Storey *et al.* (1992), Segev (2002), Leat *et al.* (2006), and Jourdan *et al.* (2004). EM = Ellsworth-Whitmore Mountains, TI = Thurston Island.

## 1.2 Ferropicrites – continental messengers from the sublithospheric mantle

Ferropicrites (Fig. 4) are subalkaline or mildly alkaline primitive rocks that were first described from the Paleoproterozoic Pechenga volcanic belt in Fennoscandia (Hanski & Smolkin 1989, 1995; Hanski 1992). Since then, they have been found to represent a volumetrically minor, yet petrologically fundamental magma type in several Precambrian volcanic belts with LIP-affinities (e.g., within Dharwar Craton in India, Onverwacht Group volcanic succession in South Africa, and Slave and Superior Provinces in North America; Table 1; Stone *et al.* 1995; Francis *et al.* 1999; Gibson 2002; Goldstein & Francis 2008) and in Phanerozoic CFB provinces (Karoo, Paraná-Etendeka, North Atlantic Volcanic Province, Siberian Traps, and Madagascar; Table 1; Fig. 1; Gibson *et al.* 2000; Gibson 2002; Riley *et al.* 2005). Ferropicritic whole-rock compositions have also been published from the Phanerozoic Emeishan CFB province (Zhang *et al.* 2006) and highly magnesian olivine-cumulates from a Permian accreted oceanic plateau in Japan have been considered as “ferropicritic” in character (Ichiyama *et al.* 2006, 2007) (Fig. 1). Phanerozoic ferropicrites are found as lava flows that represent the lowermost stratigraphic portions of CFB provinces and/or as dikes that crosscut the CFBs and/or the surrounding basement rocks (Table 1; Gibson *et al.* 2000; Gibson 2002; Riley *et al.*, 2005). Where stratigraphic correlations are possible, ferropicrites are commonly found as basal lavas also in Precambrian successions (Table 1; e.g., Hanski 1992; Gibson 2002).

The mineral composition of unaltered ferropicrites is dominated by olivine phenocrysts and groundmass consisting of clinopyroxene, plagioclase, and Fe-Ti oxides (e.g., Gibson *et al.* 2000). Igneous amphibole and spinifex textures have also been described from some Precambrian ferropicrites (e.g., Hanski 1992; Hanski & Smolkin 1995; Stone *et al.* 1995, 1997). In addition to high  $\text{FeO}_{\text{tot}}$  contents, the geochemical characteristics of ferropicrites include relatively low

Al<sub>2</sub>O<sub>3</sub>, high TiO<sub>2</sub>, high Sm/Yb, and generally positive (depleted) initial  $\epsilon_{\text{Nd}}$  values (Fig. 5, 6).

Ferropicrites and some picrites, meimechites, and Precambrian komatiites (Fig. 4) are among the few continental intraplate volcanic rock types that have crystallized largely from uncontaminated, sublithospheric mantle-derived near-primary melts (Fig. 2). Ferropicrites are generally void of xenolithic material and, when Phanerozoic, relatively unaltered (as opposed to, e.g., meimechites and continental komatiites). In addition, the geochemical characteristics of ferropicrites indicate derivation by lower degree of mantle melting (and/or from more enriched sources) at higher pressures relative to common CFB picrites/komatiites that originate as more homogenized and voluminous melt patches at lower pressures (Fig. 2; e.g., Gibson 2002). Therefore, ferropicrites are more likely to sample relatively small-scale heterogeneities and are particularly important in constraining the composition of the subcontinental upper mantle and understanding the origin of CFBs

Several workers have discussed the mantle sources of ferropicrites. Hanski (1992) and Hanski & Smolkin (1995) were the first to recognize that ferropicrites, such as those found in the Pechenga complex, cannot represent primary melts derived from ambient mantle peridotite at any reasonable pressure. They suggested that the ferropicrite mantle sources were metasomatized by Fe- and incompatible element-enriched low-degree melts shortly prior to the main melting event. Their conclusions were also supported by subsequent studies on Archean ferropicrites (e.g., Stone *et al.* 1995). The expanding dataset of Archean ferropicrites led Francis *et al.* (1999) to suggest that Archean mantle reservoirs were enriched in iron relative to modern mantle. This suggestion was questioned on the basis of subsequent findings of several Phanerozoic ferropicrites, however (Gibson *et al.* 2000; Gibson 2002). Gibson (2002) provided a general petrogenetic model that emphasizes the significance of recycled oceanic crust as a “re-fertilizer” of peridotite in the starting-heads of mantle plumes since the Archean times. Such re-fertilized peridotites would melt at higher pressures relative to ambient mantle and, at CFB settings, thick continental lithosphere would restrict subsequent mixing with larger-fraction picritic melts at lower pressures (Gibson 2002; Tuff *et al.* 2005). Accordant models, with recycled eclogite-bearing (Ichiyama *et al.* 2006) or pyroxenitic (Tuff *et al.* 2005) mantle source, have been subsequently developed for Phanerozoic Fe-rich suites, whereas peridotitic mantle sources have been favored for Precambrian ferropicrites (Goldstein & Francis 2008). In the recycled source models, the relative Fe-enrichment has been ascribed to partial melting of pyroxenite at high pressures ( $\geq 5$  GPa; Tuff *et al.* 2005) and/or entrainment of relatively Fe-rich subducted oceanic crustal component (Ichiyama *et al.* 2006), whereas in the most recent peridotite source models it has been attributed to melting of primordial, Fe-rich olivine cumulates in the mantle (Goldstein & Francis 2008). Jakobsen *et al.* (2005), in their study concerning silicate liquid immiscibility, suggested that ferropicrites could also form by mixing of evolved, immiscible Fe-rich liquids with picritic mantle melts.

In addition to discussion on the composition and the lithology of the ferropicrite mantle sources, opinions differ whether these sources were water-bearing (Hanski 1992; Stone *et al.* 1997) or anhydrous (Gibson 2002). Nevertheless, although high water contents have profound implications for the estimated liquidus temperatures of ferropicrite melts (by lowering them), ferropicrites have generally been attributed to anomalously hot mantle sources and

mantle plumes (e.g., Hanski & Smolkin 1995; Stone *et al.* 1995; Walker *et al.* 1997; Gibson *et al.* 2000; Gibson 2002; Riley *et al.* 2005; Goldstein & Francis 2008).

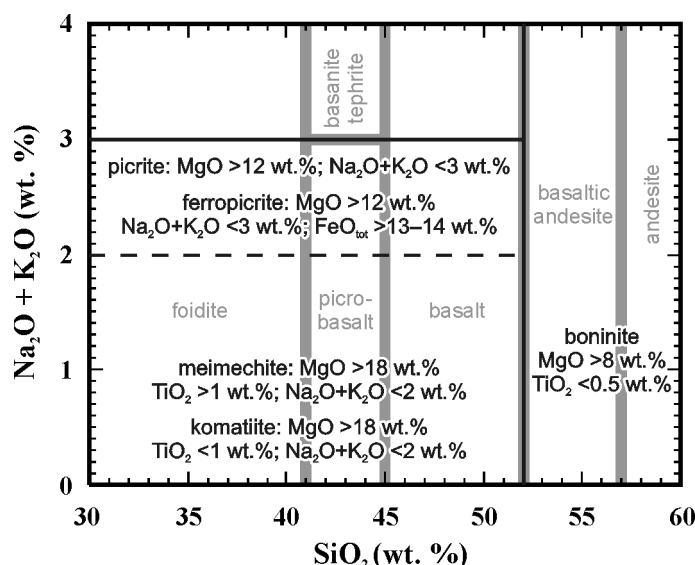


**Figure 4.** Classification and nomenclature for the highly magnesian volcanic rocks (black lines) after Le Bas (2000), except ferropicrite classification after Hanski & Smolkin (1989), Gibson *et al.* (2000), and Paper I. Total alkali-silica classification scheme for common volcanic rocks shown in gray in the background (Le Bas *et al.* 1986).

### 1.3 Objectives of this study

The Karoo-related ferropicrites of Vestfjella were first described in the studies of Luttinen *et al.* (1998) and Luttinen & Furnes (2000) as the CT4 magma type, one of the four Karoo “continental tholeiite” magma types of Vestfjella area. The main emphasis in these studies was on the abundant lithosphere-signatured lava flows (CT1–CT3) and CT4 was only superficially treated as a rare occurrence of OIB-like volcanic rocks, possibly derived from a mantle plume. The subsequent realization of their anomalously high Fe contents and findings of previously unknown ferropicrites with relatively depleted, more MORB-like incompatible trace element composition (Luttinen & Huhma 2005) were the initial sparks for my Ph.D. study, which I started immediately after finishing my M.Sc. studies in March 2006.

Given the overall rarity of primitive, sublithospheric mantle-derived volcanic rocks related to CFB provinces, my main goals were to provide high precision geochemical, mineral chemical, and isotopic data on these extraordinary rocks and their differentiates, define the nature of their mantle sources, and find answers to the greatly discussed origins of Karoo CFBs and ferropicrites in general. Related field studies at Antarctica were performed during December 2007 – January 2008; detailed map of the study area with sampling locations is given in Fig. 7.

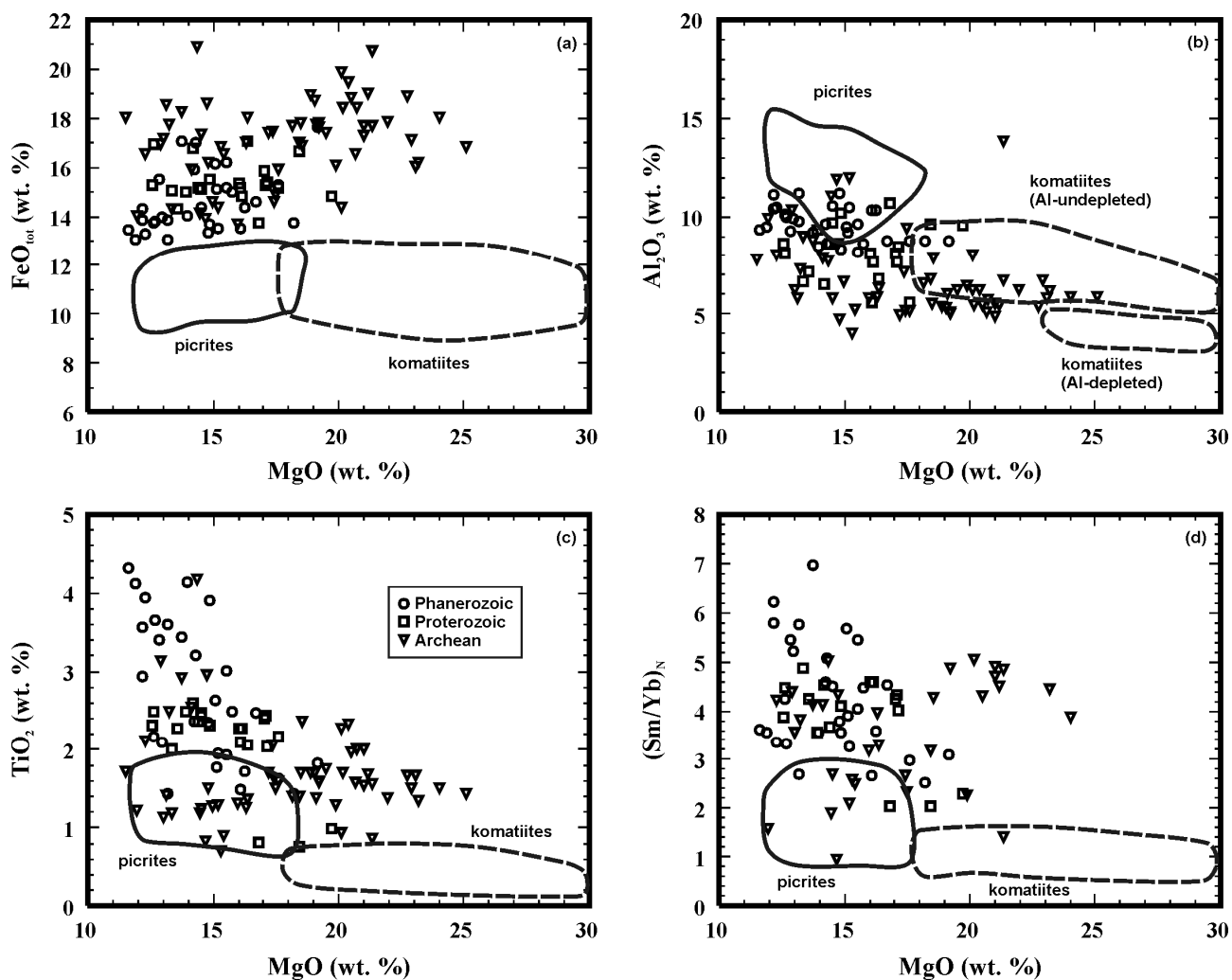


**Figure 5.** Variations of FeO<sub>tot</sub> (a), Al<sub>2</sub>O<sub>3</sub> (b), TiO<sub>2</sub> (c), and (Sm/Yb)<sub>N</sub> (d) vs. MgO for ferropicrites. Fields for continental picrites and komatiites are shown for comparison (compiled from GEOROC: <http://georoc.mpchmainz.gwdg.de/georoc/>). Legend is shown in c.

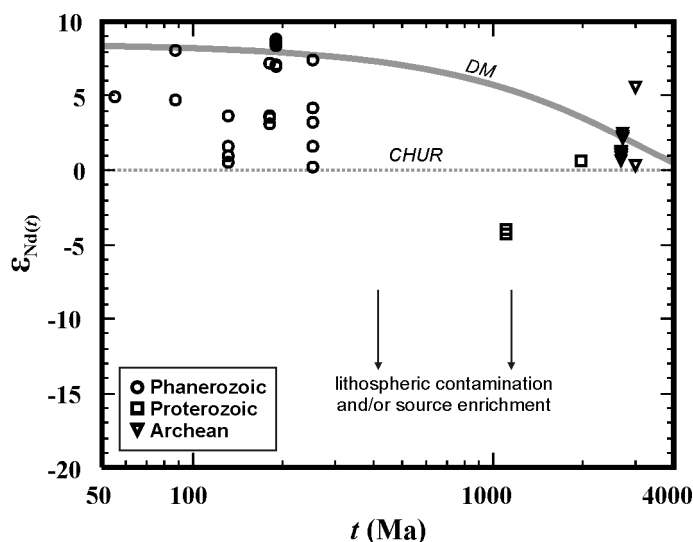


**Figure 6.** Ferropicrites shown in  $\epsilon_{Nd(t)}$  vs.  $t$  diagram. CHUR (the chondritic uniform reservoir) denotes the evolution of undifferentiated Earth (Wasserburg *et al.* 1981). The evolution path of the depleted mantle (DM) is after DePaolo (1981a).  $\epsilon_{Nd(t)}$  calculated using  $^{143}\text{Nd}/^{144}\text{Nd} = 0.512636$  and  $^{147}\text{Sm}/^{144}\text{Nd} = 0.1966$ . Data sources are given in Table 1.



**Table 1.** Ferropicrites of the world and their characteristics (average CFB picrite and Precambrian komatiite shown for comparison).

Suite and age	Samples	Occurrence	MgO*	FeO <sub>tot</sub> *	LOI*	Nb/Y	(Sm/Yb) <sub>N</sub> <sup>@</sup>	Olivine Fo <sup>\$</sup>	Nature <sup>#</sup>	References
NAVP/East Greenland Phan. (55 Ma)	MF91-57b, MF91-57c	basal lava flows	12.2–13.2	13.9	3.5–3.6	?	5.8	?	uncertain	Fram & Leshner 1997
Madagascar Phan. (88 Ma)	MAN90-45, MAN90-47	basal lava flows	13.7–15.1	16.1–17.1	3.5–3.6	0.9–1.0	5.7–7.0	?	uncertain	Storey <i>et al.</i> 1997
Paraná-Etendeka/ Namibia Phan. (132 Ma)	97SB63, 97SB73	dike & basal lava	12.2-14.3	14.3-15.9	0.9-1.6	0.9-1.1	4.6-6.2	76-85 (82)	primary	Gibson <i>et al.</i> 2000
	96SB48, 97SB67, 97SB68	basal lava flows	12.6-15.5	13.8-15.1	0.2-0.5	0.5-0.7	3.9-4.2	64-81 (67)	cumulate	Gibson <i>et al.</i> 2000
	SMG105, SMG016	basal lava flows	15.2-16.2	13.5-14.4	?	0.6-0.9	3.3-3.6	?	uncertain	Ewart <i>et al.</i> 1998
Karoo/Vestfjella depleted type Phan. (180 Ma)	AL/B14e-98, AL/B16-98, AL/WM1b-98	two dikes	14.5-16.7	14.4-15.0	1.1-3.8	0.4-0.5	4.5	79-89 (83)	primary (but differentiated)	Paper I, II
Karoo/Vestfjella enriched type Phan. (180 Ma?)	AL/B20a-98, 14-KHG-90, JSH/B006	a dike	12.8-15.5	15.5-17.0	2.4-5.5	0.7-0.8	5.1-5.5	78-83 (81)	primary	Paper I, III
Karoo/ Ahlmannryggen Phan. (190 Ma?)	Z.1812.1, Z.1812.2, Z.1812.3, Z.1813.1, Z.1816.2, Z.1817.2	dikes	11.6-14.8	13.1-14.0	0.9-2.6	0.2-0.3	3.3-3.6	70-86 (?)	uncertain	Riley <i>et al.</i> 2005
Siberian Traps/ Gudchichinsky Phan. (250 Ma)	SG-32 2245.5, SG-32 2301, SG-32 2332.7, 1F(18)	basal lava flows	13.2-18.2	13.1-15.3	7.4-8.4	0.4-1.0	2.7-3.0	72-81? (78?)	cumulate?	Wooden <i>et al.</i> 1993 Lightfoot <i>et al.</i> 1993 Olivine: see Sect. 3.1.1.
Emeishan/Lijiang Phan. (250 Ma)	DJ-2, DJ-35	basal lava flows	13.0-14.8	13.4-14.0	4.1-5.2	1.3-1.4	3.8-5.2	?	uncertain, alkaline?	Zhang <i>et al.</i> 2006
	DJ-26	basal lava flow	19.1	17.7	5.2	1.1	3.1	85-88 (86)	primary	Zhang <i>et al.</i> 2006
Average CFB picrite	compilation (n=375)	lavas and dikes	14.7	11.0	2.9	0.6	2.1	commonly <90	-	GEOROC database <sup>§</sup>
Keweenawan Rift Prot. (1100 Ma)	PC-7, PC-8, TK-13	basal lava flows	16.8-19.7	13.7-16.7	?	0.1-0.2	2.0-2.3	?	uncertain	Shirey <i>et al.</i> 1994
Pechenga complex Prot. (1980 Ma)	1–4, Locations: 1Or, 2Ki–4Ki, 6Sh–13Sh (cf. References)	basal lava flows	12.5-17.6	14.3-17.0	3.8-11.5	0.8-0.9	3.6-4.9	olivine not preserved	likely primary	Hanski 1992 Hanski & Smolkin 1995
Slave Province/ Lake of the Enemy Arch. (2660 Ma)	EN-3, EN-5, EN-9, EN-12, EN-14, EN-16, EN-18, EN-22	amphibolite lenses within metasediments	12.3-17.4	14.6-20.9	0.7-2.0	0.7-1.2	2.7-5.0	olivine not preserved	likely primary	Francis <i>et al.</i> 1999

**Table 1.** Continued...

Suite and age	Samples	Occurrence	MgO*	FeO <sub>tot</sub> *	LOI*	Nb/Y	(Sm/Yb) <sub>N</sub> <sup>@</sup>	Olivine Fo <sup>§</sup>	Nature <sup>#</sup>	References
Western Superior Province/Grassy Portage Bay Arch. (2700 Ma)	GP-1, GP-3, GP-5–GP-9, GP-10–GP-20	amphibolite facies metatuffs within metasediments	14.5–24.0	13.7–19.9	0.8–5.6	0.8–1.1	2.7–4.9	olivine not preserved	likely primary	Goldstein & Francis 2008
Western Superior Province/Lumby Lake Arch. (2700 Ma)	LM-27–LM29, LM-33–LM35, LM-37, LM-42, LM-43	greenschist facies metatuffs relatively high in the stratigraphy	11.5–25.1	16.2–20.8	1.0–14.3	0.4–1.8	1.4–4.8	olivine not preserved	likely primary	Goldstein & Francis 2008
Western Superior Province/Boston Creek Flow Arch. (2720 Ma)	1-J29, 1-36, 1-43	metalavas (basal?)	13.0–15.4	16.6–17.2	3.3–4.8	0.6–0.8	2.5–3.5	olivine not preserved	likely primary	Stone <i>et al.</i> 1995
Kolar Schist Belt (India) Arch. (2900 Ma)	13-4, 17-10, 18-10, 19-7, 23-9	amphibolite facies metalavas	14.5–19.9	13.9–16.1	?	0.2–0.4	1.0–2.3	olivine not preserved	likely primary	Rajamani <i>et al.</i> 1985
Western Superior Province/Steep Rock belt Arch. (3000 Ma)	SR-1, SR-3–SR-7, SR-17, SR-26–SR-28, SR-30, SR-48	greenschist facies basal metatuffs	14.8–22.8	15.9–19.0	5.7–13.5	1.1–1.6	4.5–5.0	olivine not preserved	likely primary	Goldstein & Francis 2008
Onverwacht Group (S Africa) Arch. (3500 Ma)	5048–5050	basal metalavas	12.0–20.1	14.0–14.4	0.5–3.5	0.2–0.3	1.6	olivine not preserved	likely primary	Jahn <i>et al.</i> 1982
Average Prec. komatiite	compilation (n=897)	metavolcanic rocks	24.7	10.9	5.9	0.2	1.2	<95 (rare)	-	GEOROC database <sup>¶</sup>

\* MgO, FeO<sub>tot</sub>, and LOI (loss on ignition) given in wt. %. <sup>@</sup> Normalized to chondrite of McDonough & Sun (1995). <sup>§</sup> Range of core values and average (shown in parentheses) given. <sup>#</sup> Primary nature of the suites assessed (cf. Paper I). <sup>¶</sup> <http://georoc.mpch-mainz.gwdg.de/georoc/>

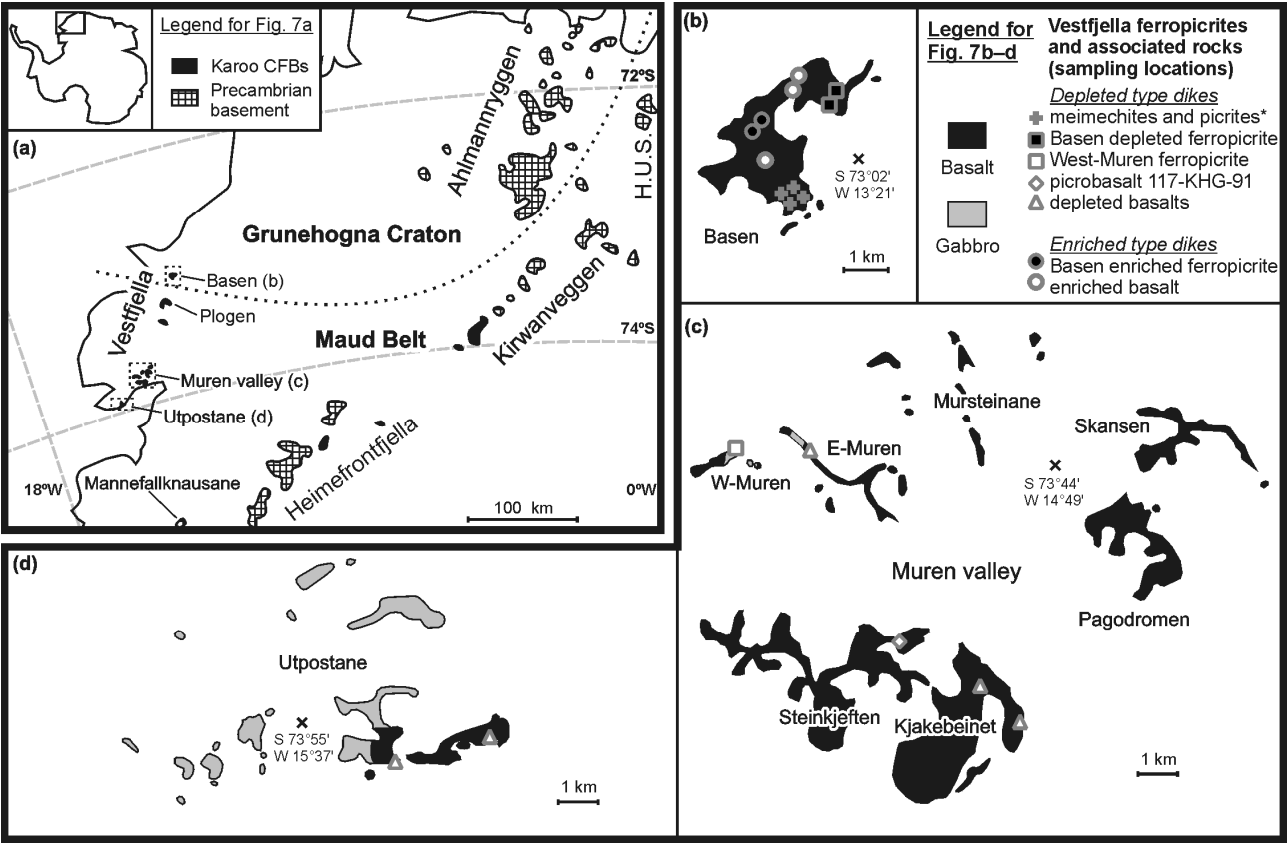


**Figure 7.** Distribution of Jurassic CFBs in western Dronning Maud Land (a) and ferropicrites and associated rocks (sampling locations shown) in Vestfjella (b–d). Lithospheric boundary between Archean Grunehogna craton and Proterozoic Maud Belt in (a) is after Corner (1994). H.U.S. = H. U. Sverdrupfjella. \* Meimechites and picrites are only found as dike-derived boulders.

### 1.4 Analytical methods

Major and trace element data presented in Papers I and III have been obtained with X-ray fluorescence spectrometer (XRF) and inductively coupled plasma mass spectrometer (ICP-MS) at the GeoAnalytical Laboratory of the Washington State University. In addition to Paper I, detailed descriptions of the GeoAnalytical Laboratory procedures are given in Johnson *et al.* (1999) and Knaack *et al.* (1994), respectively. Mineral chemical major element data presented in Papers I–III have been obtained with electron microprobe by using five wavelength-dispersive spectrometers (at the Geological Survey of Finland; Paper II, III) or one energy-dispersive spectrometer (at the Department of Earth Sciences, University of Cambridge; Paper I). Operation conditions and statistical data for the microprobes are given in Papers I and II. Isotopic data have been obtained by using thermal ionization mass spectroscopy (TIMS) at the Unit for Isotope Geology, Geological Survey of Finland (for Sr and Nd; Papers I and III) and by using TIMS and ICP-MS at the Department of Terrestrial Magnetism, Carnegie Institution of Washington (for Sr, Nd, Pb, and Os; Paper III). Detailed descriptions of the analytical methods are given in Papers I and III, respectively.

## 2. Review of the original papers

### 2.1 Paper I

Paper I provides field, petrographic, and whole-rock geochemical descriptions of the ferropicrite dikes and associated rocks of Vestfjella and discusses the nature of their mantle sources. In addition, olivine chemical data are presented for two ferropicrite samples. On the basis of trace element and isotope geochemical characteristics, the ferropicrites are divided into two distinct groups: (1) The relatively depleted type exhibits chondrite-normalized  $(\text{La}/\text{Sm})_{\text{N}}$  of 1.2–1.3 and  $(\text{Sm}/\text{Yb})_{\text{N}}$  of 4.5, and initial  $\epsilon_{\text{Sr}}$  from -18 to -19 and  $\epsilon_{\text{Nd}}$  from +7 to +8 (at 180 Ma). (2) The relatively enriched type (CT4 magma type of Luttinen *et al.* 1998) exhibits chondrite-normalized  $(\text{La}/\text{Sm})_{\text{N}}$  of 1.7 and  $(\text{Sm}/\text{Yb})_{\text{N}}$  of 5.1–5.4, and initial  $\epsilon_{\text{Sr}}$  from 0 to +1 and  $\epsilon_{\text{Nd}}$  from +3 to +4. Geochemical modeling and the presence of relatively Mg-rich olivine phenocrysts ( $\text{Fo}_{79-88}$ ) indicate that at least the depleted ferropicrites are likely to represent near-primary mantle melts that have largely avoided lithospheric contamination and have been derived from anomalous hot mantle sources. The meimechite ( $\text{MgO} > 18$  wt. %) and basalt ( $\text{MgO} \leq 10$  wt. %) samples are considered as cumulates and differentiates from ferropicritic magmas, respectively. The relatively high Fe and Ti contents and oceanic island picrite- and OIB-like trace element signatures of the ferropicrites are considered to indicate derivation from recycled, pyroxenitic mantle sources. On the basis of the unusually high primitive-mantle-normalized  $(\text{V}/\text{Lu})_{\text{N}}$  of the depleted ferropicrites (1.9–2.2), the recycled component in their case is thought to comprise of oceanic Fe-Ti gabbros. Global comparison reveals that many samples described as ferropicrites in the literature may in fact represent olivine cumulates or altered alkaline rocks and not crystallized equivalents of exceptionally Fe-rich subalkaline melts. High  $(\text{V}/\text{Lu})_{\text{N}}$  appears to be a characteristic feature of several ferropicrites and is thought to indicate that Fe-Ti gabbro component was prevalent in the mantle sources of such suites.

### 2.2 Paper II

Paper II concentrates on the mineral chemistry (~400 analyses) of some of the depleted meimechite ( $n = 4$ ) samples of Vestfjella, and their petrological implications. For comparison, mineral chemical data are also provided for two samples from a depleted ferropicrite dike. Two of the meimechites are characterized by “ferropicritic” olivines ( $\text{Fo}_{84-85}$ ) and they obviously represent cumulates from ferropicritic magmas (cf. Paper I). The other two meimechites, however, are characterized by olivines that show extremely high Fo contents ( $\text{Fo}_{90-91}$ ; up to  $\text{Fo}_{92}$ ). These olivines are euhedral to subhedral, exhibit high CaO ( $\geq 0.19$  wt. %), and contain Ti-rich (volcanic) spinel inclusions, and are thus considered likely to represent true phenocrysts and not xenocrysts from mantle peridotite. Moreover, the presence of igneous amphibole as inclusions in these olivines is thought to indicate that the olivines crystallized from magmas that had  $\text{H}_2\text{O}$  contents of ~1–2 wt. %. Calculations based on olivine-liquid equilibria indicate that the meimechite parental magmas were very MgO-rich (up to 25 wt. %) and were derived from extremely hot mantle sources ( $> 1600$  °C) compatible with the plume theory. The highly magnesian nature of the meimechites and their geochemical and mineral chemical similarity to the depleted ferropicrites is thought to cast doubt on the previously purported pyroxenite origins for the

depleted magma type (cf. Paper I) and, instead, suggest dominantly peridotitic sources for them. Major and trace element comparisons with other highly magnesian Phanerozoic magma types reveal similarities between the Vestfjella meimechites, meimechites from the Siberian Traps LIP, and the purported komatiite parental melts associated with the Paraná-Etendeka LIP, and indicate their derivation from broadly similar sources and/or by similar melting processes in anomalously hot sublithospheric mantle.

## 2.3 Paper III

Paper III presents high-precision whole-rock isotope (Sr, Nd, Pb, and Os) geochemical data on the meimechites, ferropicrites, and associated rocks of Vestfjella ( $n = 8$ ), and progresses on to place tighter constraints on their mantle sources and interpret implications on the origins of the Karoo LIP and the breakup of the Gondwana supercontinent. Additional reference datasets are presented for samples of CT1, CT3, and MORB-like Low-Nb magma types of Vestfjella ( $n = 5$ ). Major and trace element whole-rock geochemical data and olivine chemical data are also provided for a relatively fresh sample of the enriched ferropicrite dike. The isotopic data confirm that, unlike most of the Karoo magmas, the depleted ferropicrites and associated rocks have not been significantly contaminated by lithospheric materials. Their isotopic signature is indistinguishable from that of SW Indian Ridge MORB and the MORB-like Low-Nb type dikes of Vestfjella. This is thought to suggest their derivation from long-term depleted upper mantle sources and cast doubt on their previously purported plume origin (cf. Paper I, II). The enriched ferropicrites and associated rocks are likely to sample pyroxenitic heterogeneities (cf. Paper I), but whether this source was present in the lithospheric mantle (e.g., as metasomatic veins) or sublithospheric mantle (e.g., as metasomatic veins or recycled lithospheric materials) remains an open question. The overall isotopic similarity to EM-signatured OIBs could indicate a recycled component with up to ~15 % of sedimentary material. Given the probability that the enriched type and especially the depleted type have been derived from anomalously hot upper mantle sources, the recently introduced internal heating model of the upper mantle beneath a supercontinent (Coltice *et al.* 2007, 2009) is considered to be the most likely cause for the generation of the Karoo LIP.

## 3. Discussion

### 3.1. Petrogenesis of the Vestfjella ferropicrites

In this section, I analyze and summarize the interpretations on the origin of the Vestfjella ferropicrites (Paper I–III) and present some views that were not considered in the original papers. All the available data support the division of the Vestfjella ferropicrites and related rocks to relatively depleted and enriched types that sampled distinct mantle sources (Paper I–III). Accordingly, I treat them separately in two subsections.

#### 3.1.1. Depleted type

One of the most important findings on the depleted type ferropicrites was that they do not represent undifferentiated mantle melts, as ferropicrites often are presumed

731 (cf. Paper I), but were likely derived by olivine fractionation from even more  
732 magnesian meimechitic parental melts (Paper II). The geochemical and isotopic  
733 modeling further indicated that these parental melts were likely derived from  
734 hydrated Indian Ridge MORB-source upper mantle peridotite at high pressures  
735 (~5–6 GPa) and temperatures ( $T_p > 1600$  °C) (Paper II, III). Preliminary  $^{40}\text{Ar}$ - $^{39}\text{Ar}$   
736 age data for three ferropicrite-related basaltic dikes (Kurhila *et al.* 2008; A. V.  
737 Luttinen *et al.* in prep.) are compatible with interpretations that suggest the  
738 crystallization of depleted type magmas during the main phase of Karoo  
739 magmatism at ~180 Ma (cf. Paper III).

740 The depleted type has been treated as a largely coherent magma type (Paper  
741 I–III), but there are indications that some of the dikes may have crystallized from  
742 separately evolved melt batches. For example, the relatively large within-group  
743 variations in  $\text{FeO}_{\text{tot}}$ ,  $\text{La}/\text{Sm}$ , and  $\text{Sm}/\text{Yb}$  ratios are difficult to explain solely by  
744 differentiation (e.g., olivine-fractionation and contamination), but rather require  
745 differences in mantle melting conditions (Fig. 8). At least three subtypes that  
746 likely derive from distinct parental magmas can be distinguished: (1) the  
747 meimechites and picrites (and possibly also depleted basalts), (2) Basen  
748 ferropicrite, and (3) West-Muren ferropicrite (Fig. 8). These observations along  
749 with the overall undifferentiated nature of the rocks imply that the most primitive  
750 magmas did not significantly mix or homogenize in large crustal magma  
751 chambers, but rather intruded as relatively fast-moving separate magma pulses in  
752 a way somewhat similar to kimberlitic magmas (cf. Paper II). On the other hand,  
753 relatively wide within-sample variations in olivine phenocryst compositions  
754 (Paper II), reversely zoned olivines in the West-Muren ferropicrite (Paper I; cf.  
755 Appendix I) and rare, resorbed, and oscillatory zoned clinopyroxenes in  
756 meimechite sample AL/B5-03 (Fig. 9) indicate that minor mixing took place in  
757 some of the individual magma feeding channels. Although magma ascent  
758 velocities likely were high (cf. Section 3.3.3), the nature of the ascent may have  
759 been pulsating, thus allowing some mixing of cogenetic magmas in various stages  
760 of differentiation (cf. Larsen & Pedersen 2000). Importantly, sample AL/B5-03  
761 with evidence of mixing of clinopyroxene-saturated magmas has not been used in  
762 the parental melt calculations (cf. Paper II).

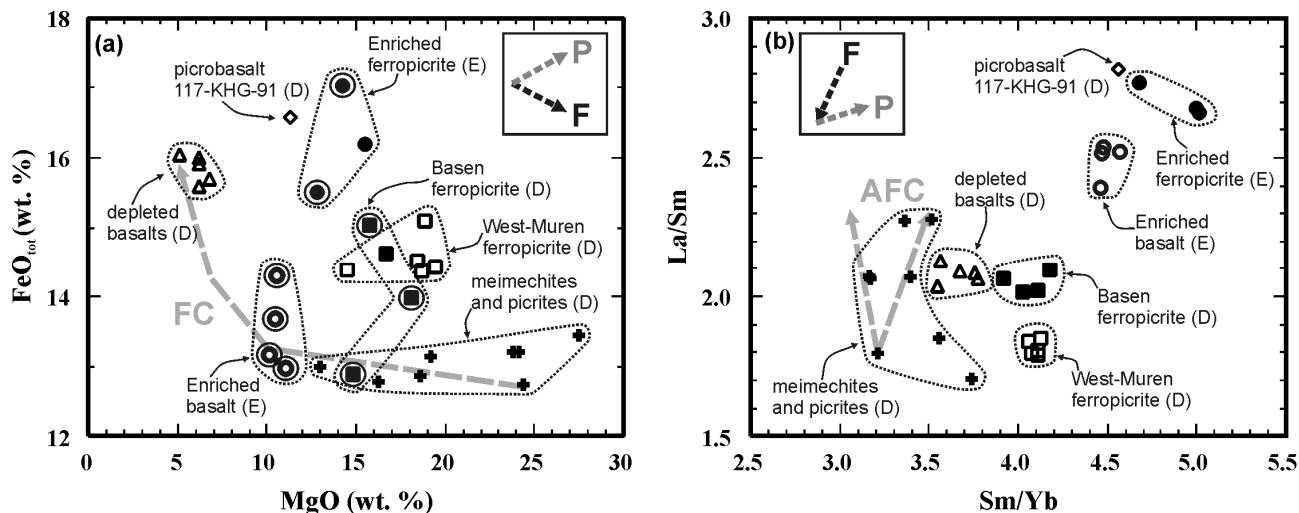
763 Although the major element and isotopic compositions of the depleted type  
764 indicate derivation from depleted upper mantle peridotite, comparison of the  
765 Vestfjella data with experimental results on peridotite partial melting reveal some  
766 minor discrepancies related to minor and trace elements. Firstly, the  $\text{TiO}_2$  contents  
767 of the depleted type ( $> 1$  wt. % in the parental melts; Paper II) are higher than in  
768 partial melts of KLB-1 peridotite (estimated to correspond to depleted MORB-  
769 source) even at very low degrees of melting ( $< 1$  wt. % in general; cf. Herzberg &  
770 Zhang 1996). Ti is not enriched in our samples relative to other similarly  
771 incompatible elements (e.g., Eu and Gd; cf. Paper I), however, indicating a  
772 general enrichment in all incompatible elements relative to KLB-1 partial melts. I  
773 provide five alternative explanations for this discrepancy: (1) The peridotitic  
774 source is not as depleted in incompatible elements as KLB-1; e.g., partial melting  
775 experiments on fertile (“pyrolitic”) garnet peridotite have resulted in partial melt  
776  $\text{TiO}_2$  contents up to 1.7 wt. % at ~10 % of melting (Walter 1998). (2) The  
777 peridotitic source contains subordinate pyroxenite components. (3) The peridotitic  
778 source has been enriched by metasomatic fluids. This had to happen relatively  
779 shortly before melt generation or otherwise it would likely have affected the  
780 isotope systematics. (4) The incompatible trace element characteristics have been

inherited from very low-degree, high-pressure initial peridotite partial melts, whereas the major element compositions reflect subsequent more extensive melting processes at lower pressures (McKenzie 1985; Saunders *et al.* 1988). (5) The presence of water affected the partial melting process by decreasing  $K_D$  values (e.g., Gaetani *et al.* 2003) thus resulting in high incompatible element concentrations in the partial melts. It should be noted that the Indian Ridge MORB do not represent N-MORB, but show relatively enriched compositions indicative of possible subordinate enriched source components in the upper mantle beneath Indian Ocean (e.g., Janney *et al.* 2005; Nishio *et al.* 2007); importantly, Indian Ocean MORB and the Vestfjella depleted type are both characterized by similar mild enrichments in large-ion lithophile elements (LILE) (Paper III). Bearing this in mind, none of the aforementioned alternatives is in discordance with the purported ambient upper mantle source for the depleted type.

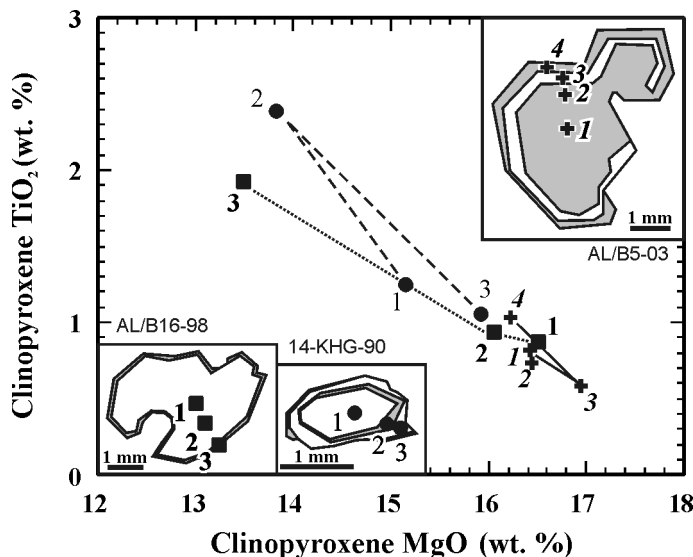
One problem that was highlighted in Paper III is that the mantle potential temperatures calculated for the depleted type parental magmas ( $T_p \approx 1640\text{--}1700$  °C; Paper II) exceed those predicted by the internal mantle heating model ( $\sim 1600$  °C at maximum; Coltice *et al.* 2007). Temperature calculations in Paper II were based on olivine-liquid equilibration following the method of Putirka *et al.* (2007), but here I also performed additional thermobarometric modeling by using the method of Lee *et al.* (2009). The advantage of this method is that it can be utilized on any subalkaline whole-rock that is thought to represent olivine-controlled melt composition derived from a peridotitic mantle source. By using the samples AL/WM1b-98, AL/B16-98, and AL/B9-03 as the melt compositions (cf. Paper I, II), altering the  $H_2O^{liq}$  between 1 and 2 wt. % (cf. Paper II), and assuming depleted (KLB-1; Davis *et al.* 2009) or fertile (KR4003; Xue *et al.* 1990) peridotite as the source material, the method results in  $T_p$  values ranging  $\sim 1630\text{--}1740$  °C and pressures ranging 4–7 GPa. The minimum temperatures are marginally lower compared to those calculated in Paper II and were attained with  $H_2O^{liq} = 2$  wt. % and fertile peridotite source. The fertile peridotite source alternative is particularly important as it may correspond to the possible entrainment of subordinate enrichments (cf. above) that are likely to decrease the solidus temperatures. It should also be noted that the estimated errors of the methods of Lee *et al.* (2009) and Putirka *et al.* (2007) are  $\sim 3$  % and  $\sim 5$  % that correspond to  $T_p$  variations of  $\sim 48$  and  $\sim 80$  °C at 1600 °C, respectively. One additional factor that could lower the calculated temperatures and has not been considered is the  $CO_2$  content of the parental magma. There is growing evidence that carbonated peridotites may comprise a significant source component for the alkaline OIBs (e.g., Dasgupta *et al.* 2006, 2007). In addition,  $CO_2$  has been suggested to be involved in the petrogenesis of the meimechites of the Siberian Traps and lower the melt origination temperatures on the order of 100–150 °C (Elkins-Tanton *et al.* 2007). The overall subalkaline character of the depleted type and the absence of associated carbonatites do not indicate marked mantle  $CO_2$  influence in the case of Vestfjella, however (cf. Gibson *et al.* 2000; Elkins-Tanton *et al.* 2007). In summary, it seems that the Vestfjella depleted type is difficult to explain without an involvement of a significant thermal anomaly ( $T_p > 1600$  °C) in the sub-Gondwanan upper mantle (cf. Paper II).

Overall, the depleted type was a challenging magma type to study. When more and more data came available during the course of this project, some of the original fundamental hypotheses on their origin were subjected to significant revisions. In Paper I, the depleted type was thought to originate by plume-induced

831 partial melting of pyroxenite sources that entrained significant amounts of  
 832 recycled oceanic Fe-Ti gabbros. In Paper II, the mineral chemical data indicated  
 833 that the depleted type actually had fractionated from highly magnesian parental  
 834 magmas that derive from dominantly peridotitic, instead of pyroxenitic, mantle  
 835 sources. Paper III presented isotopic evidence on the upper mantle origin of the  
 836 depleted type and thus questioned its plume origin (cf. Paper I, II). The depleted  
 837 type may be considered a prime example how scientific knowledge is revised and  
 838 refined on the basis of new – and sometimes unexpected – findings.  
 839



840  
 841 **Figure 8.** Geochemical characteristics of Vestfjella ferropicrites and associated rocks shown in (a)  $\text{FeO}_{\text{tot}}$  vs.  $\text{MgO}$   
 842 diagram and (b)  $\text{La/Sm}$  vs.  $\text{Sm/Yb}$  diagram. Highly altered samples ( $\text{LOI} > 3$  wt. %) are encircled in (a); D = depleted  
 843 types; E = enriched types. Fractional crystallization model (FC) as in Paper I, but with sample AL/B9-03 as a starting  
 844 composition. Assimilation-fractional crystallization modeling (AFC;  $r = 0.5$ ) performed by using lamproite (AL/KB8-  
 845 98; Luttinen *et al.* 2002) and average upper continental crust (Rudnick & Gao 2003) as contaminants. Effects of  
 846 pressure (P) and degree of melting (F) estimated on the basis of the experiments of Walter (1998) and Adam & Green  
 847 (2006).



848  
 849 **Figure 9.** Clinopyroxene phenocryst chemistry of a Vestfjella depleted ferropicrite (AL/B16-98),  
 850 enriched ferropicrite (14-KHG-90), and meimechite (AL/B5-03) shown in  $\text{TiO}_2$  vs.  $\text{MgO}$  diagram.  
 851 The phenocryst in 14-KHG-90 represents a part of a glomerocryst ( $\varnothing \approx 6$  mm). Data from Paper II  
 852 and Appendix I.



### 3.1.2. Enriched type

In contrast to the depleted type ferropicrites, there are no indications of highly magnesian parental magmas for the enriched type ferropicrites. Their relatively low MgO contents, high FeO<sub>tot</sub> and TiO<sub>2</sub> contents, and enriched OIB-like trace element and isotopic signatures are all compatible with their derivation from pyroxene-rich (recycled?) mantle source (Paper I, III).

Similar to the depleted type, the enriched type dikes also show relatively large differences in FeO<sub>tot</sub> contents and La/Sm and Sm/Yb ratios suggesting that they evolved as two separate magmatic systems. Generalizing, the higher FeO<sub>tot</sub>, La/Sm, and Sm/Yb of the enriched ferropicrite suggest derivation by lower degree of melting and from more garnet-rich mantle relative to the enriched basalt (Fig. 8). Although one enriched ferropicrite sample contains a glomerocryst of oscillatory zoned clinopyroxene (and minor altered olivine) that could indicate magma mixing (Fig. 9), the absence of such glomerocrysts and other mixing-related textures in all the other samples and the overall compositional homogeneity of the olivine population (Paper III) indicate that the geochemical effect of possible mixing processes has been negligible.

The implication of pyroxene-rich source notably hinders estimating the physical conditions of mantle melting (e.g.,  $P$ ,  $T_p$ ), because the available models are only compatible with peridotite sources (e.g., Putirka *et al.* 2007; Lee *et al.* 2009). Nevertheless, the melting conditions of the enriched type parental magmas can be tentatively estimated on the basis of melting experiments performed by Tuff *et al.* (2005) on geochemically similar Paraná-Etendeka ferropicrites (Gibson *et al.* 2000; cf. Paper III). The experiments indicated that the Paraná-Etendeka parental melts originated at pressures of  $\geq 5$  GPa and  $T_p$  of  $\sim 1550$  °C from a garnet-pyroxenitic source. Although it is tempting to suggest similar conditions also for the enriched type, it should be noted that whereas the Paraná-Etendeka ferropicrites were thought to originate from an anhydrous source (Gibson *et al.* 2000; Gibson 2002), the enriched type shows evidence of hydrous parental melts by containing igneous amphibole in olivine-hosted inclusions and as a groundmass phase (Paper III; Appendix I). Petrography-based correction for 50% crystallization of an anhydrous mineral assemblage (olivine + clinopyroxene) indicates that the enriched type parental magma contained  $\sim 1.5$  wt. % of H<sub>2</sub>O (cf. Paper II). If this difference in primary H<sub>2</sub>O contents between the enriched type and Paraná-Etendeka ferropicrites is real and not a result of false interpretations (cf. Section 3.3.3), it could indicate lower temperatures of initial melting for the former relative to the latter.

Although all the evidence point to a pyroxene-rich source for the enriched type, the nature and origin of this source have not been tightly constrained: recycled ferrobasalts (Paper I), sediment-bearing oceanic crust (Paper III), and metasomatic veins (Paper III) have been suggested, but, e.g., linking specific recycled crustal materials to EM-like mantle reservoir signatures has been proven to be a complicated task at best (Paper III; cf. Stracke *et al.* 2003). Moreover, the whole idea of recycled crust as a major OIB source contributor has recently been questioned on the basis of several basic geochemical and geophysical observations, and more emphasis has been given to the role of recycled lithospheric mantle sections (e.g., Niu & O'Hara 2003; Niu 2009). Bearing this in mind and given the significant pitfalls in modeling the alteration, subduction, dehydration, metamorphism, blending, and recycling of oceanic crust (e.g.,

Stracke *et al.* 2003), the ultimate origin of the enriched type source remains ambiguous until more sophisticated methods for such evaluations are available (cf. Paper III).

The temporal position of the enriched type relative to Karoo magmatism is unclear. The fact that they sample relatively small-scale heterogeneities in the sub-Gondwanan mantle, however, may imply that they originated either shortly before or after the main magmatic phase (~184–178 Ma) that was likely associated with relatively large-scale mantle melting (cf. Paper I; Gibson 2002). The fact that the enriched type is found as dikes that further show reverse paleomagnetic polarity (Peters 1989) – as opposed to the normally polarized CFBs that they crosscut (Hargraves *et al.* 1997) – is more compatible with the latter option.

In summary, there are many open questions in the petrogenesis of the enriched type: the ultimate nature of the source components, the melting conditions in this source, as well as the temporal relationship to the Karoo magmatism remain uncertain. Although their rarity (only two dikes known) indicates that they represent a rather anomalous type of magmatism which probably did not contribute significantly to the Karoo magmatism in general (cf. Paper III, Section 3.2.1), they are important in providing evidence that the sub-Gondwanan upper mantle contained enriched sources similar to those of OIB.

## **3.2. Implications on the origin of the Karoo continental flood basalt province**

### **3.2.1. Geochemical comparisons and petrogenetic relationships**

Geochemical comparisons between Vestfjella ferropicrites and other Karoo magma types have been minutely performed in Papers I and III. In general, the lack of detailed trace element and isotopic (namely Pb and Os) data on the Karoo CFBs restricts comparisons and, in the case of many Karoo lavas and related intrusive rocks, any kind of compositional information has not been published (e.g., parts of Zambia, Zimbabwe, and South Africa; cf. Jourdan *et al.* 2007a). Moreover, the fact that ferropicrites initiate under anomalous melting conditions (e.g., relatively low-degree and high pressure of melting; Section 3.3; Paper I) makes the comparison with common CFBs difficult even in the case of a possible common mantle source. As a starting point, the Vestfjella ferropicrites have potential to sample Karoo source end-members, because they derive directly from the subcontinental mantle (Paper III).

Volcanic rocks that exhibit identical compositional characteristics (e.g., combination of high Fe and Sm/Yb) with the Vestfjella ferropicrites are not known from the Karoo province. Some Fe-rich lavas of Lebombo (Sweeney *et al.* 1994) have been speculated to represent contaminated differentiates of enriched ferropicrite-like parental magmas (Paper I), but further comparison is hampered by inadequate geochemical data also in their case (cf. Paper III). On the other hand, their relatively low Ti contents (cf. Fig. 12 of Paper I) may imply that they sampled a more Ti-poor source relative to the enriched type. The relatively high Nb content of the enriched type is also a very peculiar feature within the Karoo framework (Paper III). Such a characteristic is difficult to explain by lithospheric contamination and indicates derivation from an anomalous source component (Paper III). On the other hand, effective contamination of such Nb-rich magmas

952 with crustal materials may result in Nb-depleted volcanic rocks, possibly  
953 represented by some Karoo CFBs (cf. Fig. 7 in Paper III). Given the peculiar OIB-  
954 like compositional characteristics of the enriched type, and the fact that it is only  
955 known from two dikes on Basen nunatak (Fig. 7b), I suggest that they derive from  
956 some anomalous pyroxene-rich upper mantle source that was not involved in the  
957 generation of the majority of Karoo CFBs (cf. Paper III).

958 The Vestfjella depleted type, on the other hand, originated from the same  
959 ambient upper mantle source that produced the MORB-like low-Nb dikes of  
960 Vestfjella (Paper III). These magma types are isotopically indistinguishable and  
961 the differences in their major and trace element composition can be readily  
962 attributed to differences in initial melting conditions (Paper III). In order to  
963 investigate the importance of this upper mantle source in the petrogenesis of  
964 Antarctic Karoo CFBs in general, I modeled lithospheric contamination of low-  
965 Nb type magmas that, rather than depleted ferropicrites that originated as low-  
966 degree melts at extremely high pressures, are likely to provide more feasible  
967 parental magma compositions for the modeling. Accordingly, I used a  
968 fractionation-corrected (~30 % of olivine) low-Nb sample P27-AVL with the  
969 highest initial  $\epsilon_{Nd}$  (+7.7) and lowest initial  $\epsilon_{Sr}$  (-15.7) as the parental melt  
970 composition (cf. Luttinen & Furnes 2000). I modeled contamination with crustal  
971 and subcontinental lithospheric mantle (SCLM) material separately (cf. Paper III).  
972 Energy-constrained assimilation and fractional crystallization (EC-AFC; Bohrsen  
973 & Spera 2001; Spera & Bohrsen 2001) modeling of crustal contamination takes  
974 into account the latent heat of crystallization and partial melting of wall rock.  
975 Crustal contaminants used in the model are an Archean TTG (representing  
976 Grunehogna craton; Fig. 7) and average upper and lower continental crust  
977 (representing Maud Belt; Fig. 7). Conventional AFC modeling (DePaolo 1981b)  
978 was preferred in the case of SCLM, because of significant uncertainties regarding  
979 its physicochemical nature (cf. Paper III). Lamproitic contaminant is thought to  
980 represent a fair approximation of a SCLM-derived low-degree partial melt  
981 composition (Luttinen *et al.* 2002). The input parameters for the contamination  
982 models are presented in Table 2 and the results that are most reminiscent of the  
983 various CT lava signatures are presented in Fig. 10. Modeling was utilized only  
984 on high field strength elements (HFSE) that, unlike LILE, are not mobile during  
985 secondary alteration.

986 The CT1 lavas exhibit strong indications of lithospheric contamination by  
987 showing, e.g., high Th/Ta, La/Sm, Ce/Nb, and Ce/P and low Ti/Zr ratios and  
988 highly unradiogenic initial  $\epsilon_{Nd}$  (Fig. 10a). The model replicates the CT1 signature  
989 fairly well by 4% contamination of a low-Nb parental melt with Archean crustal  
990 material (Fig. 10a). It is important to note, however, that, e.g., the Ti contents of  
991 the most depleted CT1 samples are lower than in the hypothetical parental melt  
992 (Fig. 10a). This feature, along with the differences in the heavy rare earth element  
993 contents between the model and CT1 lavas (Fig. 10a), can be readily explained by  
994 derivation of CT1 and low-Nb parental melts by distinct melting conditions (e.g.,  
995 higher degree of melting at higher pressure in the case of CT1). The CT2  
996 signature is replicated even more satisfactorily by 2% contamination of average  
997 (Proterozoic) upper crust (Fig. 10b). The CT3 signature, on the other hand, is  
998 possible to explain by negligible (1%) contamination with SCLM and/or lower  
999 crust (Fig. 10c). In fact, the most depleted CT3 samples show incompatible  
1000 element compositions that approach those of the hypothetical low-Nb parental  
1001 magma.

In summary, my contamination modeling indicates that the major geochemical characteristics of the CT lavas could be explained by lithospheric contamination of low-Nb type parental magmas. Importantly, the application of EC-AFC modeling overcomes the previous shortcomings related to AFC modeling of crustal contamination that suggest superfluous (e.g., >20 % in the case of CT1) degrees of contamination to produce CT geochemical signatures (cf. Luttinen & Furnes 2000). Therefore, given that the low-Nb dikes are likely to represent the uncontaminated correlatives of many Vestfjella CFBs and, accordingly, similar CFBs of Sabie River Basalt Formation in the African part of Karoo (Duncan *et al.* 1984; Hawkesworth *et al.* 1984; Sweeney *et al.* 1994; cf. Luttinen & Furnes 2000), depleted ferropicrites seem to have sampled a sublithospheric upper mantle end-member source of Karoo magmatism (cf. Paper III). It is possible that this sublithospheric mantle source was variably LILE-enriched (cf. Luttinen and Furnes, 2000) and had much less important role in the petrogenesis of most of the strongly lithosphere-signatured Karoo lavas of southern Africa (cf. Jourdan *et al.* 2007a). It is important to note that if the low-Nb dikes had not been discovered, finding the apparent petrogenetic relationships between the depleted ferropicrites and CT lavas would have been difficult to impossible (cf. Paper III).

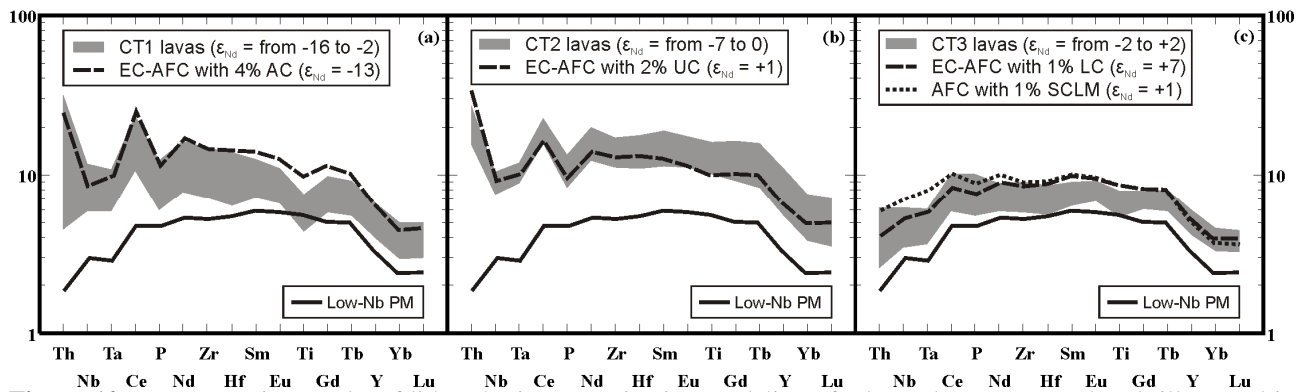


**Figure 10.** Representative results of lithospheric contamination modeling of a low-Nb type parental melt illustrated in primitive mantle (Sun & McDonough 1989)-normalized incompatible element patterns along with representative CT1 (n=29) (a), CT2 (n=14) (b), and CT3 (n=20) (c) lava compositions. See Table 2 for model parameters.

1044

**Table 2.** Input parameters for the EC-AFC and AFC models.

Variable	PM <sup>†</sup>	AC <sup>*</sup>	UC <sup>**</sup>	LC <sup>***</sup>	SCLM <sup>#</sup>
Model	EC-AFC + AFC	EC-AFC	EC-AFC	EC-AFC	AFC (r=0.5)
Magma liquidus T (initial T) [°C]	1600	-	-	-	-
Assimilant liquidus T [°C]	-	1000	1000	1100	-
Assimilant initial T [°C]	-	300	300	600	-
Solidus T [°C]	-	900	900	950	-
Equilibration T [°C]	-	1100	1100	1100	-
Isobaric specific heat [J/kg K]	1668	1370	1370	1388	-
Crystallization enthalpy [J/Kg]	600000	-	-	-	-
Fusion enthalpy [J/Kg]	-	270000	270000	350000	-
	K <sub>D</sub> <sup>@</sup>				
Th [ppm]	0.16 (0.001)	3.6	10.5	1.2	26.1
Nb [ppm]	2.19 (0.02)	5	12	5	170
Ta [ppm]	0.12 (0.01)	0.4	0.9	0.6	14.6
Ce [ppm]	8.55 (0.001)	64	63	20	502
P [ppm]	458 (0.05)	698	655	436	15099
Nd [ppm]	7.37 (0.003)	22	27	11	229
Zr [ppm]	60 (0.05)	132	193	68	1076
Hf [ppm]	1.72 (0.05)	3.4	5.3	1.9	26.6
Sm [ppm]	2.7 (0.003)	3.52	4.7	2.8	36.4
Eu [ppm]	1.00 (0.01)	1.01	1.0	1.1	10
Ti [ppm]	7428 (0.08)	1739	3837	4916	23860
Gd [ppm]	3.04 (0.02)	3.8	4.0	3.1	23
Tb [ppm]	0.55 (0.02)	0.4	0.7	0.48	2.91
Y [ppm]	15.40 (0.06)	10	21	16	37
Yb [ppm]	1.21 (0.06)	0.5	1.96	1.5	1.48
Lu [ppm]	0.18 (0.06)	0.1	0.31	0.25	0.23
<sup>143</sup> Nd/ <sup>144</sup> Nd <sup>§</sup>	0.512829	0.510551	0.511800	0.511806	0.512275
ε <sub>Nd</sub> <sup>§</sup>	+8.3	-36.2	-11.8	-11.7	-2.5

1045

1046

1047

1048

1049

1050

1051

1052

1053

1054

1055

1056

1057

1058

1059

1060

1061

1062

1063

1064

1065

1066

1067

1068

All thermal parameters after Paper III. <sup>†</sup> Parental melt: trace element composition after fractionation-corrected Low-Nb sample P27-AVL (Section 3.2.1; cf. Luttinen & Furnes 2000); Nd isotopic composition after the model in Paper III. <sup>\*</sup> Archean crust: trace element and Nd isotopic composition after TTG sample 96/203 (Kreissig *et al.* 2000; Ta and Hf estimated after Kleinhanns *et al.* 2003). <sup>\*\*</sup> Upper (Proterozoic) crust: trace element composition after the average upper crust of Rudnick & Gao (2003); Nd isotopic composition after the model of Jourdan *et al.* (2007a). <sup>\*\*\*</sup> Lower (Proterozoic) crust: trace element composition after the average lower crust of Rudnick & Gao (2003); Nd isotopic composition after granulite 21BD6 (Talarico *et al.* 1995). <sup>#</sup> Subcontinental lithospheric mantle: trace element and Nd isotopic composition after lamproite AL/KB8-98 (Luttinen *et al.* 2002). AFC process has been modeled to take place after the same level of fractionation of PM than in the case of lower crust. <sup>@</sup> K<sub>D</sub> values for the parental melt estimated from GERM database (<http://earthref.org/>); All K<sub>D</sub> values for the crustal contaminants are 0.1. <sup>§</sup> Calculated at 180 Ma except for SCLM-derived lamproite at 159 Ma.

### 3.2.2. The origin of the Karoo flood basalts

The ferropicrites of Vestfjella, namely the depleted type, provide an important addition into the debate on the origins of the Karoo flood basalts. The association of the depleted type with the main phase of Karoo magmatism at ~180 Ma, and its petrogenetic relationship with Karoo lavas (Paper III; cf. previous Section) indicate that it sampled an important sublithospheric end-member for Karoo magmatism. These findings are in strong discordance with studies that suggest that the parental melts of the Karoo CFBs formed solely in the lithospheric mantle (e.g., Hawkesworth *et al.* 1984; Elburg & Goldberg 2000; Scenario 1 of Jourdan *et al.* 2007a).

The derivation of the depleted type from anomalously hot mantle sources (> 1600 °C; Paper II) indicate that sub-Gondwanan mantle was heated to

temperatures of at least ~200 °C above that of ambient mantle. The fact that the depleted type represents melts largely derived from ambient MORB-source mantle is more compatible with the internal mantle heating model (Coltice *et al.* 2007, 2009) than the plume model (Morgan 1971; Richards *et al.* 1989), however (Paper III). Although there is a possibility that some other processes suggested for CFB generation (cf. Section 1.1; Bryan & Ernst 2008) were also active, I propose that the internal heating effect significantly enhanced the melt production in the sub-Gondwanan mantle and was largely responsible for the generation of vast amounts of basaltic magma represented by Karoo (and Ferrar) CFBs at ~180 Ma (cf. Paper III).

### 3.3. Implications on the origin of ferropicrites

#### 3.3.1. Ferropicrite whole-rocks vs. ferropicrite melts

Paper I highlights some important issues that should be considered when interpreting the petrogenesis of ferropicrites: ferropicritic whole-rock compositions do not necessarily represent crystallized equivalents of ferropicrite melts (i.e. primary ferropicrites), but may also record accumulation of relatively Fe-rich olivine (< Fo<sub>80</sub>) in basaltic melts or by hydrothermal alteration of alkaline volcanic rocks (i.e. secondary ferropicrites). Careful examinations on petrography, geochemistry, and mineral chemistry of ferropicrites are required in order to evaluate whether their compositions are of primary or secondary origin. Obviously, the trace element or isotope compositions of secondary ferropicrites should not be utilized in order to study the petrogenesis of ferropicrite melts.

Normative mineral calculations (CIPW) performed on highly magnesian ferropicrite whole-rock compositions (e.g., FeO<sub>tot</sub> ≈ 14 wt. %; MgO ≈ 18 wt. %) result in normative olivine contents less than 40 vol. %. Broadly, this could mean that if the modal olivine content in a ferropicrite sample is higher, the rock may contain accumulated olivine. More elaborate means to address the cumulate issue is to perform detailed chemical analyses on olivine phenocrysts and evaluate whether they are in or out of equilibrium with the host whole-rock composition (Paper I). Unfortunately, this evaluation is impossible for highly altered or metamorphosed ferropicrites that do not contain primary igneous olivine: in the case of Precambrian ferropicrites, the samples that have been collected close to presumed chilled margins of the lava flows or from pyroclastic successions have been thought to be void of accumulation effects and closely represent primitive Fe-rich liquid compositions (e.g., Hanski & Smolkin 1995; Stone *et al.* 1995; Goldstein & Francis 2008; cf. Table 1). Surprisingly limited olivine chemical data exist for ferropicrites that contain fresh olivine (Table 1; cf. Paper I): specific analyses have only been provided for the ferropicrites of Vestfjella (Paper I–III; Appendix I), Paraná-Etendeka (Gibson *et al.* 2000), and Emeishan (Zhang *et al.* 2006). The Vestfjella ferropicrites, the most Fe-rich Emeishan ferropicrite, and two Paraná-Etendeka samples have likely crystallized from primitive Fe-rich melts as they are characterized by relatively Mg-rich olivines (≥ Fo<sub>81</sub>; Table 1; Paper I–III). Three of the Paraná-Etendeka samples, however, show evidence of olivine accumulation (Table 1; Paper I) and likely do not derive from ferropicritic melts. Importantly, these samples can also be distinguished from the primary Paraná-Etendeka ferropicrites on the basis of trace element characteristics (Table 1) and thus they possibly represent separately evolved magma type (or types). Accordingly, these cumulate Paraná-Etendeka samples have been excluded from

the following discussion on ferropicrite petrogenesis. Less detailed olivine data (e.g., not sample-specific) have been provided for Ahlmannryggen (Riley *et al.* 2005) and Siberia (Ryabov *et al.* 1977; Zolotukhin & Al'mukhamedov, 1991; Zolotukhin *et al.* 1991). Without further olivine analyses, the primitive nature of these and all the other ferropicrite suites that lack olivine chemical data and do not sample chilled margins remains uncertain (Table 1; cf. Paper I).

Many ferropicrites show petrographical and geochemical (e.g., LOI > 3 wt. %; Table 1) evidence of post-crystallization hydrothermal alteration. In addition, Archean ferropicrites have unanimously been subjected to greenschist-to-amphibolite facies metamorphism (Table 1). During alteration or metamorphism, volcanic rocks are prone to gain or lose fluid mobile elements (such as Si, Na, and K) which may complicate the identification of primary subalkaline and alkaline magma types (cf. Paper I). Pearce (1996) tried to tangle this problem by introducing a trace element classification diagram that utilizes immobile trace element ratios Zr/Ti and Nb/Y, where Nb/Y is considered to be an indicator of alkalinity (cf. Fig. 10 in Paper I). Volcanic rocks that show Nb/Y ratios of higher than about 1 are likely to be of alkaline origin. For example, some of the lavas from Prinsen af Wales Bjerre formation, East Greenland (Peate *et al.* 2003) exhibit ferropicritic whole rock compositions (e.g., MgO = 13.2–19.9 wt. %; FeO<sub>tot</sub> = 13.5–16.1 wt. %; Na<sub>2</sub>O + K<sub>2</sub>O = 2.5–3.1), but are slightly altered (e.g., LOI = 1–3 wt. %) and show high Nb/Y ratios (1.7–3.1) and thus likely derive from alkaline parental magmas (Peate *et al.* 2003). Ferropicritic whole-rock compositions have also been described from oceanic settings (e.g., Hawaii; Reiners & Nelson 1998) where they are also characterized by high degrees of hydrothermal alteration and are thus unlikely related to ferropicrite parental melts (cf. Paper I). I emphasize, however, that rock classification schemes are designed by people and commonly not followed by nature: for example, the distinction between ferropicrites and highly alkaline Mg-rich volcanic rocks may simply relate to differences in mantle melting conditions (e.g., degree of melting; cf. Section 3.3.2) and, theoretically, a whole spectrum of subalkaline to alkaline Fe- and Mg-rich melt compositions may be generated from the same mantle source under favorable conditions (cf. Gudfinnsson & Presnall 2005). Although most of the CFB-related alkaline volcanic rocks have been thought to derive from the lithospheric mantle (e.g., Harmer *et al.* 1998; Gibson *et al.* 2006; Song *et al.* 2008; Srivastava *et al.* 2009), the Prinsen af Wales Bjerre lavas have been interpreted to sample sublithospheric mantle heterogeneities (Peate *et al.* 2003) and should thus be considered as important in studying deep origins of CFBs as ferropicrites.

### 3.3.2. Pyroxenite vs. peridotite source

It is evident that ferropicrite liquids cannot originate by direct partial melting of ambient, depleted mantle peridotite (Hanski 1992; Stone *et al.* 1995; Gibson *et al.* 2000; Gibson 2002; Goldstein & Francis 2008; Paper I). In Vestfjella, however, the depleted ferropicrites are likely to represent differentiates from even more primitive (meimechitic) parental magmas that derive by relatively low-degree, high-pressure melting of a mantle source dominated by depleted upper mantle peridotite (Paper II, III). The question of whether ferropicrites represent near-primary or already significantly differentiated melts should thus be carefully addressed in every case (cf. Fig. 11). It should also be noted that mixing of peridotite-derived picritic melts with evolved Fe-rich basalts or immiscible liquids could theoretically result in ferropicritic whole-rock compositions (Jakobsen *et al.*

2005). Such mixing processes would be expected to result in significant igneous disequilibrium textures and textural and geochemical heterogeneities within individual magma bodies, however, and these are not characteristic of ferropicrites. In addition, this model provides no explanation for the fact that ferropicrites are only found in CFB provinces and not, for example, in mid-ocean ridges. These observations strongly suggest that liquid immiscibility (and subsequent mixing) is very unlikely cause for the generation of most ferropicrite melts (cf. Goldstein & Francis, 2008). The most likely mantle sources for unfractionated ferropicrite melts are enriched peridotite and pyroxenite – the only mantle lithologies that exhibit Mg and Fe contents high enough to produce these exceptional liquid compositions (cf. Paper I).

Whether pyroxenite represents a major melt-producing lithology in the sources of several oceanic islands and CFB provinces has been debated (e.g., Putirka 1999; Stolper *et al.* 2004; Sobolev *et al.* 2005, 2007; Herzberg 2006; Elkins *et al.* 2008). The situation is similar in the field of ferropicrite research: Tuff *et al.* (2005) concluded on the basis of melting experiments that Paraná-Etendeka ferropicrites are most likely to represent partial melts of garnet pyroxenite at high pressures ( $\geq 5$  GPa), whereas Goldstein & Francis (2008) maintained that peridotite-basalt mixtures and most garnet pyroxenite xenoliths have insufficient Fe, Mg, or both to produce melts that correspond to the exceptionally Fe-rich Archean ferropicrites (cf. Fig. 5; Table 1). The geochemical similarities of the Vestfjella ferropicrites with pyroxenite partial melts and purported pyroxenite-sourced Hawaiian picrites initially led to the suggestion that the former also represent partial melts of recycled pyroxenites (Paper I). Nevertheless, the question arises if there are any means to distinguish between Fe-enriched peridotite and pyroxenite as ultimate sources for ferropicrite melts.

Melting experiments on pyroxenites are relatively few. Moreover, experiments on enriched peridotites are lacking, the closest correlatives being experiments performed on fertile (pyrolitic) peridotite starting material (e.g., Walter 1998). The published major element data on pyroxenite and fertile peridotite partial melts at pressure range of 2.5–6 GPa are compared with the Phanerozoic, Proterozoic, and Archean ferropicrites in Fig. 11. Firstly, it is important to note that only one of the experimental partial melts exceed 14 wt. % of  $\text{FeO}_{\text{tot}}$  (14.03 wt. %; pyroxenite partial melt at 2.5 GPa,  $F = 18$  %; Fig. 11a) which may reflect the absence of both anomalous (e.g., Fe-rich) starting materials and data on low-degree melt compositions ( $F < 0.1$ ) in the melting experiments, or that the experimental melts represent isobaric batch melts and not polybaric aggregate melts that are likely to have higher Fe content (cf. Gibson 2002). Although relatively high  $\text{FeO}_{\text{tot}}$  and  $\text{TiO}_2$  of ferropicrites are more compatible with pyroxenitic rather than peridotitic sources on the basis of available experimental data (cf. Paper I), the high MgO of some Archean ferropicrites have not been attained in pyroxenite melting experiments (Fig. 11a and c; Goldstein & Francis 2008). It is also evident from Fig. 11 that the effects of pressure, degree of melting, and source compositions on the partial melt compositions are difficult to distinguish from each other (cf. Hirschmann *et al.* 1999). For example, the relatively higher  $\text{Al}_2\text{O}_3$  of the Phanerozoic ferropicrites relative to the Archean ferropicrites may indicate that the Phanerozoic samples derive by (1) higher degree of pyroxenite melting, (2) lower pressure of pyroxenite melting, (3) lower degree of peridotite melting, (4) lower pressure of peridotite melting, or (5) from more pyroxene-rich sources relative to the Archean samples (Fig. 11b). Although



1219 the first alternative is not very likely on the basis that mantle melting was more  
1220 extensive in the early Earth in general, the rest of the alternatives seem equally  
1221 viable. The considerably higher Na<sub>2</sub>O of the Phanerozoic ferropicrites at a given  
1222 TiO<sub>2</sub>, however, is difficult to explain solely by melting conditions and may  
1223 suggest that Phanerozoic ferropicrites contained more pyroxene-rich mantle  
1224 sources in general (Fig. 11c). Nevertheless, it should also be kept in mind that  
1225 Na<sub>2</sub>O contents of some Precambrian ferropicrites have likely been modified  
1226 during metamorphism (cf. Section 3.3.1).

1227 In Paper I, the high V/Lu ratio of many ferropicrites was thought to indicate  
1228 a major role for recycled Fe-Ti gabbro component in their mantle sources. Many  
1229 incompatible trace element ratios, including V/Lu, are prone to vary according to  
1230 melting conditions (e.g., P and T), however, and the distinction between these  
1231 effects and the lithology of the source is thus difficult to make (cf. Paper III). On  
1232 the other hand, Le Roux *et al.* (2010) recently argued that elevated Zn/Fe ratio of  
1233 several OIBs is hard to explain by melting of peridotitic mantle at varying  
1234 temperature or pressure, but rather indicates pyroxene- and garnet-rich sources for  
1235 the parental magmas. The purported peridotite-origin of the Vestfjella depleted  
1236 ferropicrites is compatible with this claim: they show Zn/Fe ratios similar to  
1237 peridotites and MORBs (Fig. 12). East Greenland and Steep Rock ferropicrites  
1238 also show peridotitic Zn/Fe ratios, whereas the Vestfjella enriched type and the  
1239 Ahlmannryggen ferropicrites exhibit consistently high Zn/Fe ratios suggestive of  
1240 more pyroxene-rich sources for these magma types. Other ferropicrites show less  
1241 coherent and/or less definitive Zn/Fe ratios: this may reflect heterogeneous  
1242 sources and/or, especially in the case of Precambrian ferropicrites, secondary  
1243 alteration and metamorphism.

1244 Compositions of olivine phenocrysts have also been used to estimate the  
1245 nature of the mantle sources of intraplate basalts. Sobolev *et al.* (2007, 2008)  
1246 suggested that the proportion of pyroxenitic source component could be  
1247 quantitatively assessed on the basis of Ni, Mn, Fe, and Mg contents of primitive  
1248 olivine phenocrysts: relatively high Ni and low Mn/Fe were thought to be  
1249 unaffected by melting conditions and indicate predominantly pyroxenitic mantle  
1250 sources for several intraplate suites (e.g., Hawaii, Karoo, Siberian Traps; Sobolev  
1251 *et al.* 2007). The lack of olivine chemical data on Precambrian ferropicrites  
1252 restricts the assessment of these methods in their case and the olivine analyzes on  
1253 Phanerozoic ferropicrites (Karoo, Paraná-Etendeka, and Emeishan) do not meet  
1254 the high analytical standards [e.g., high probe currents (~300 nA) and long  
1255 counting times (> 100 s)] required by the formulas of Sobolev *et al.* (2007, 2008).  
1256 It should also be noted that recent studies indicate negative depth effect on  $K_d^{ol-}$   
1257  $^{liq}(Ni)$  thus undermining the basis of the equations of Sobolev *et al.* (2007) (Li &  
1258 Ripley 2010). Nevertheless, the evaluation of ferropicrite sources on the basis of  
1259 very high-precision olivine chemical data may be considered a potential subject  
1260 for future studies.

1261 Sobolev *et al.* (2008) also found out a quantitative link between purported  
1262 pyroxenite sources (on the basis of olivine chemistry) and Os isotopic  
1263 composition in Icelandic lavas: samples that indicated more pyroxene-rich sources  
1264 also showed more radiogenic <sup>187</sup>Os/<sup>188</sup>Os. Radiogenic Os in volcanic rocks has  
1265 been considered as evidence of pyroxene-rich sources also in several other studies  
1266 (e.g., Hauri & Hart 1993; Reisberg *et al.* 1993; Hauri *et al.* 1996; Carlson &  
1267 Nowell 2001; Carlson *et al.* 2006; Day *et al.* 2009), mainly because mantle  
1268 peridotites are characterized by relatively unradiogenic <sup>187</sup>Os/<sup>188</sup>Os in general

(initial  $\gamma_{\text{Os}}^* \leq 0$ ; Shirey & Walker 1998; Chesley *et al.* 2004). Os isotopic data are available for the ferropicrites of Vestfjella and Pechenga only. The Vestfjella depleted ferropicrites have inherited their relatively unradiogenic Os (initial  $\gamma_{\text{Os}}$  from -0.5 to -2.1 at 180 Ma) from their highly magnesian parental magmas derived from depleted peridotite sources (Paper III). The Vestfjella enriched ferropicrites (initial  $\gamma_{\text{Os}}$  from +9.2 to +11.1 at 180 Ma) and Pechenga ferropicrites (initial  $\gamma_{\text{Os}}$  from +4.1 to +5.5 at 1980 Ma), however, show relatively radiogenic Os composition that has been linked to entrainment of lithospheric materials (Paper III; Walker *et al.* 1997) and thus imply pyroxene-rich sources for them (cf. Sobolev *et al.* 2005, 2007, 2008).

In summary, the issue of pyroxenite vs. peridotite sources is hard to assess in the case of many ferropicrites due to difficulties in interpreting major element data and inadequate mineral chemical and Os isotopic data. In addition, most incompatible trace element ratios are dependent on melting conditions and are generally difficult to utilize in order to distinguish mantle source lithologies. Nevertheless, the importance of recycled-origin pyroxenites as potential mantle source components has probably increased through time and this progress may reflect also on ferropicrites (cf. Fig. 11 and 12). Moreover, the fact that at least the Phanerozoic ferropicrites represent melts generated at very high pressures beneath continental lithosphere indicate that they derive by melting of the most fusible (e.g., pyroxene-rich) mantle materials (cf. Gibson 2002; Sobolev *et al.* 2005; Tuff *et al.* 2005). On the other hand, the most important findings of my work is that ferropicritic magmas may also evolve by fractionation from even more magnesian (meimechitic/komatiitic) parental melts. In such case, peridotite is the primary source contributor (Paper II).

\* = Calculated using bulk-earth parameters of  $^{187}\text{Os}/^{188}\text{Os} = 0.1296$  and  $^{187}\text{Re}/^{188}\text{Os} = 0.4353$ .

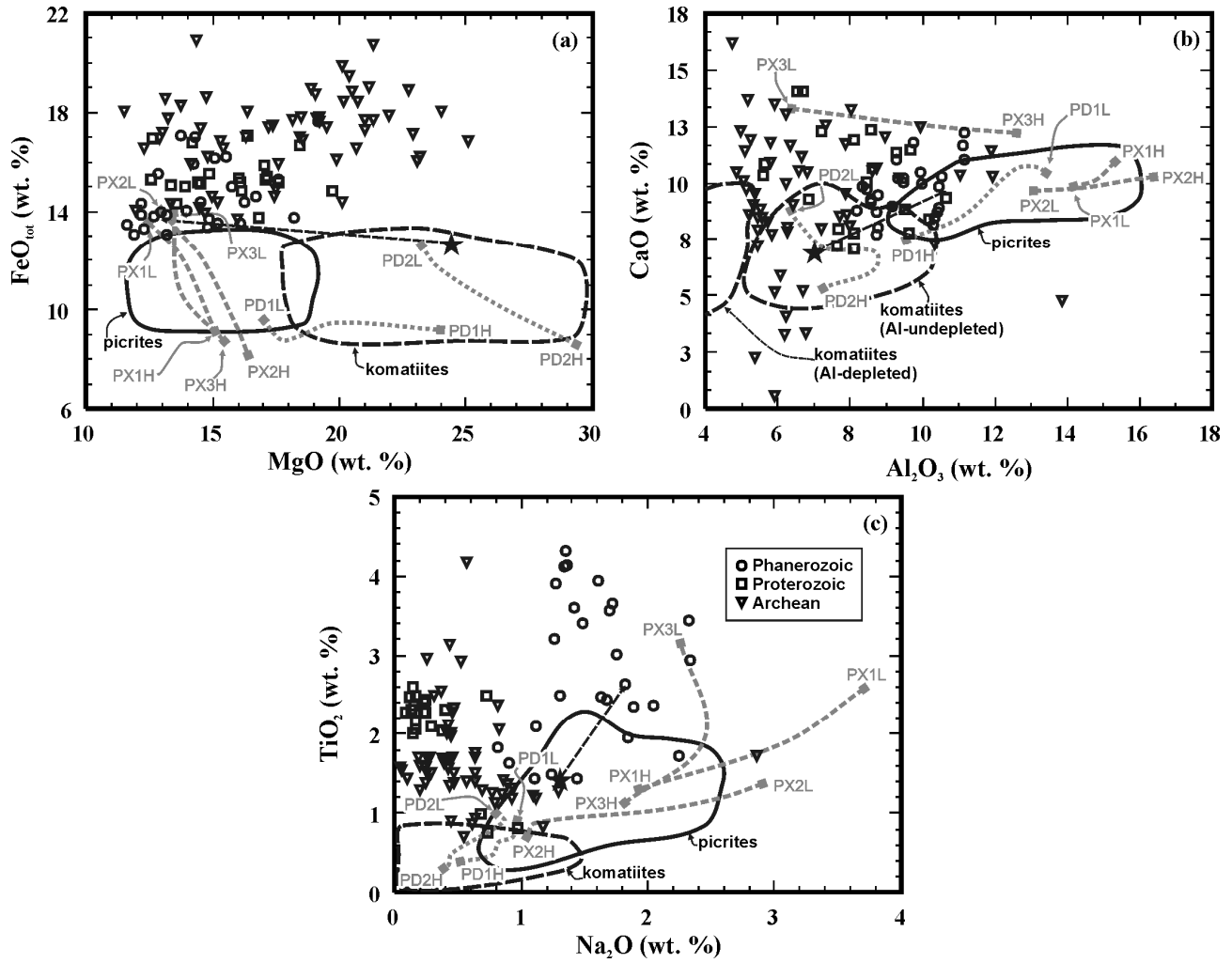


**Figure 11.** Geochemical characteristics of ferropicrites compared with peridotite and pyroxenite experimental partial melts and continental picrites and komatiites in FeO<sub>tot</sub> vs. MgO (a), CaO vs. Al<sub>2</sub>O<sub>3</sub> (b), and TiO<sub>2</sub> vs. Na<sub>2</sub>O (c) diagrams. Star indicates Vestfjella meimechite sample AL/B9-03 that closely corresponds to a parental melt composition of the Vestfjella depleted type (Paper II); stippled line corresponds to ~30% fractionation of olivine. Gray stippled lines approximate the compositional progression of partial melt composition between low- and high-degree melt end-members: PD1L–PD1H = peridotite at 3 GPa and 14–53% of melting (Walter 1998); PD2L–PD2H = peridotite at 6 GPa and 11–65% of melting (Walter 1998); PX1L–PX1H = pyroxenite at 2.5 GPa and 21–67% of melting (Hirschmann *et al.* 2003); PX2L–PX2H = pyroxenite at 2.5 GPa and 18–99% of melting (Keshav *et al.* 2004); PX3L–PX3H = pyroxenite at 5 GPa and 19–75% of melting (Kogiso *et al.* 2003). Legend is given in c.

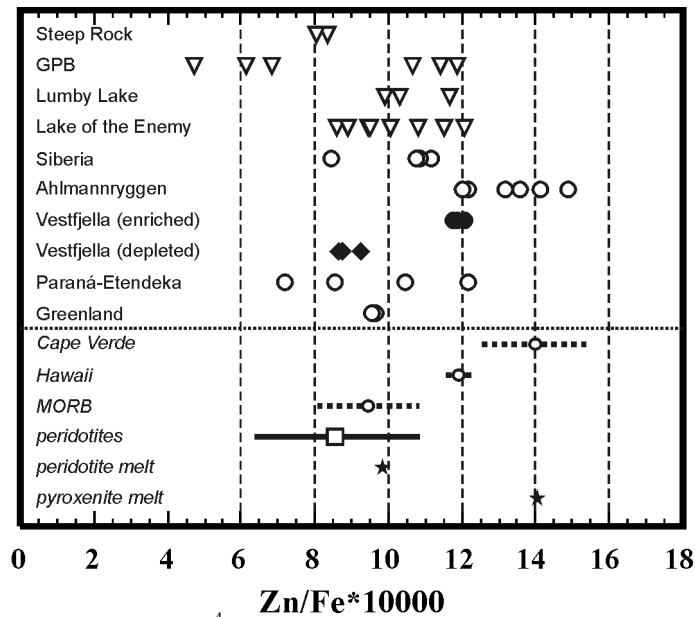


**Figure 12.** Ferropicrites shown in  $\text{Zn/Fe} (*10^4)$  diagram. Selected oceanic suites (Cape Verde, Hawaii, and MORB), peridotites, and representative experimental peridotite and pyroxenite partial melts shown for comparison. Cape Verde has the highest  $\text{Zn/Fe}$  ratios of oceanic rocks reported in Le Roux *et al.* (2010). In the case of oceanic suites, the circle represents the value calculated for the entire suite at  $\text{MgO} = 12$  wt. % with standard error bars (stippled lines) shown (cf. Le Roux *et al.* 2010). In the case of peridotites, the square represents the average value and the line represents the range of compositions. Data sources for ferropicrites are reported in Table 1, for other data sources see Le Roux *et al.* (2010).  $\text{Zn/Fe}$  ratios are not prone to vary by fractional crystallization in basaltic/picritic magmas that have  $\text{MgO} > 8.5$  wt. % (Le Roux *et al.* 2010). GPB = Grassy Portage Bay.

### 3.3.3. Hydrous or anhydrous magmas?

The significance of water in the petrogenesis of ferropicrites is poorly understood. Despite the presence of primary igneous amphibole in some Precambrian ferropicrites (e.g., Hanski 1992; Stone *et al.* 1997), Gibson (2002) concluded that ferropicrites derive from anhydrous mantle sources. The Vestfjella samples are the first Phanerozoic ferropicrites that have been found out to contain igneous amphibole (Paper I–III). The presence of these amphiboles (as well as the Precambrian ones) as inclusions in olivine that likely crystallized at significant depths (cf. Paper II) is difficult to explain by reaction with meteoric waters (cf. Stone *et al.*, 1995). The amphibole-bearing inclusions likely represent melt droplets that got trapped within olivine phenocrysts during the early stages of magma evolution. In addition, the overall uncontaminated nature of the ferropicrites does not suggest contamination with water-rich lithosphere either. These constraints strongly suggest primary mantle-derived high  $\text{H}_2\text{O}$  content for the parental melts (Paper II; Stone *et al.* 1997). In the Vestfjella depleted type, amphibole is confined to olivine-hosted inclusions and is not found in the groundmass at all. Moreover, the absence of any other  $\text{H}_2\text{O}$ -rich groundmass phases indicates that the original high water contents were lost (e.g., by degassing) prior to groundmass crystallization (Paper II). This possibility should also be considered in the case of other Phanerozoic ferropicrites and future studies should concentrate on evaluating the role of volatiles by, e.g., focusing on mapping and analyzing possible olivine-hosted melt inclusions. In standard petrographical inspection using optical microscopes, the presence of small amphibole crystals in olivine-hosted inclusions can easily go unnoticed.

Whether water was involved in the petrogenesis of ferropicrites, the characteristic high Fe contents of ferropicrites are not likely the result of wet

mantle melting (e.g., Hanski 1992; Paper II; cf. Gibson 2002), because experimental water-bearing and dry systems tend to produce melts with comparable Fe contents at similar degrees of melting (cf. Hirose & Kawamoto 1995). I consider that the most important consequences of elevated water contents in the source are to promote partial melting and decrease both the density and viscosity of ultramafic magmas thus allowing their rapid ascent through thick lithosphere without significant interaction with country rocks (Paper II, III; cf. Arndt *et al.* 1998).

### 3.3.4. Mantle thermometry and relation to mantle plumes

Despite the debate on the water contents of the ferropicrite primary melts and their mantle sources, ferropicrites have generally been associated with anomalously hot mantle (e.g., Hanski & Smolkin 1995; Stone *et al.* 1995; Gibson *et al.* 2000; Gibson 2002; Riley *et al.* 2005; Goldstein & Francis 2008). Findings on the Vestfjella ferropicrites provide support for this view (Paper I, II).

The purported high temperatures are not necessarily indicative of plumes reaching the upper mantle, however; ferropicrites are commonly related to supercontinent break-up processes and thus may record high temperatures induced by internal mantle heating (cf. Coltice *et al.* 2007, 2009). The Vestfjella depleted type, for example, exhibits Indian Ridge MORB-like isotopic (Sr, Nd, Pb, and Os) compositions and low Nb/Y at a given Zr/Y that provide strong evidence of an ambient upper mantle (i.e. non-plume) source (Paper III).

Isotopic and trace element data of ferropicrites and volcanic rocks derived from distinct mantle reservoirs are presented in Fig. 13 and 14. In order to minimize time-integrated correction (and uncertainties it induces) and maximize readability, only Phanerozoic ferropicrites are shown in the isotope diagrams (Fig. 13). It is evident from Fig. 13 that, except for the Vestfjella depleted type, none of the Phanerozoic ferropicrites exhibit depleted-mantle- or MORB-like isotopic signatures. In particular, Phanerozoic ferropicrites are rather characterized by relatively elevated initial  $^{87}\text{Sr}/^{86}\text{Sr}$  ratios. Although this is compatible with relatively enriched mantle sources, it could also indicate minor lithospheric contamination (Fig. 13). The fact that the great majority of ferropicrites plot within the fields of OIBs and “Iceland Plume Array” in Nb/Y vs. Zr/Y diagram, however, is difficult to explain solely by minor lithospheric contamination of depleted mantle-derived magmas, and strongly suggest a major role for relatively Nb-enriched and anomalous mantle sources in their petrogenesis (Fig. 14; cf. Fitton *et al.* 1997; Paper III). Relating these anomalous signatures strictly to mantle plumes is quite an extrapolation, however, because enriched components are believed to form an intrinsic part of the upper mantle as well (Cooper *et al.* 2009; cf. Paper III). In addition to the Vestfjella depleted type, ferropicrites that derive from Nb-poor sources are found in Ahlmannryggen, the Keweenawan Rift, and the Kolar Schist Belt. Similarly, as all OIB-like signatures do not necessarily derive from mantle plumes, all these low-Nb magmas do not necessarily derive from low-degree high-pressure partial melts of MORB-source upper mantle. For example, the very high HFSE contents (e.g.,  $\text{TiO}_2 \approx 4$  wt. %), high Zn/Fe (Fig. 12), and the combination of relatively radiogenic initial  $^{87}\text{Sr}/^{86}\text{Sr}$  and very high initial  $\epsilon_{\text{Nd}}$  of the Ahlmannryggen ferropicrites provide strong evidence for some anomalous depleted, possibly pyroxenitic, source component (cf. Section 3.3.2; Riley *et al.* 2005).

In summary, given the deficiencies of the plume theory to explain the origin of many CFB provinces (e.g., Foulger *et al.* 2005) and growing evidence on other processes capable of creating significant sublithospheric temperature anomalies (e.g. Coltice *et al.* 2007), association of ferropicrite sources and their high potential temperatures with deep-seated mantle plumes is not straightforward. The generally anomalous isotopic signatures and high Nb/Y indicate that the great majority of ferropicrites sampled anomalous and/or enriched mantle sources, however. The evaluation of whether all these sources are related to mantle plumes is beyond the scope of this thesis and must be considered separately in every case (cf. Paper III).

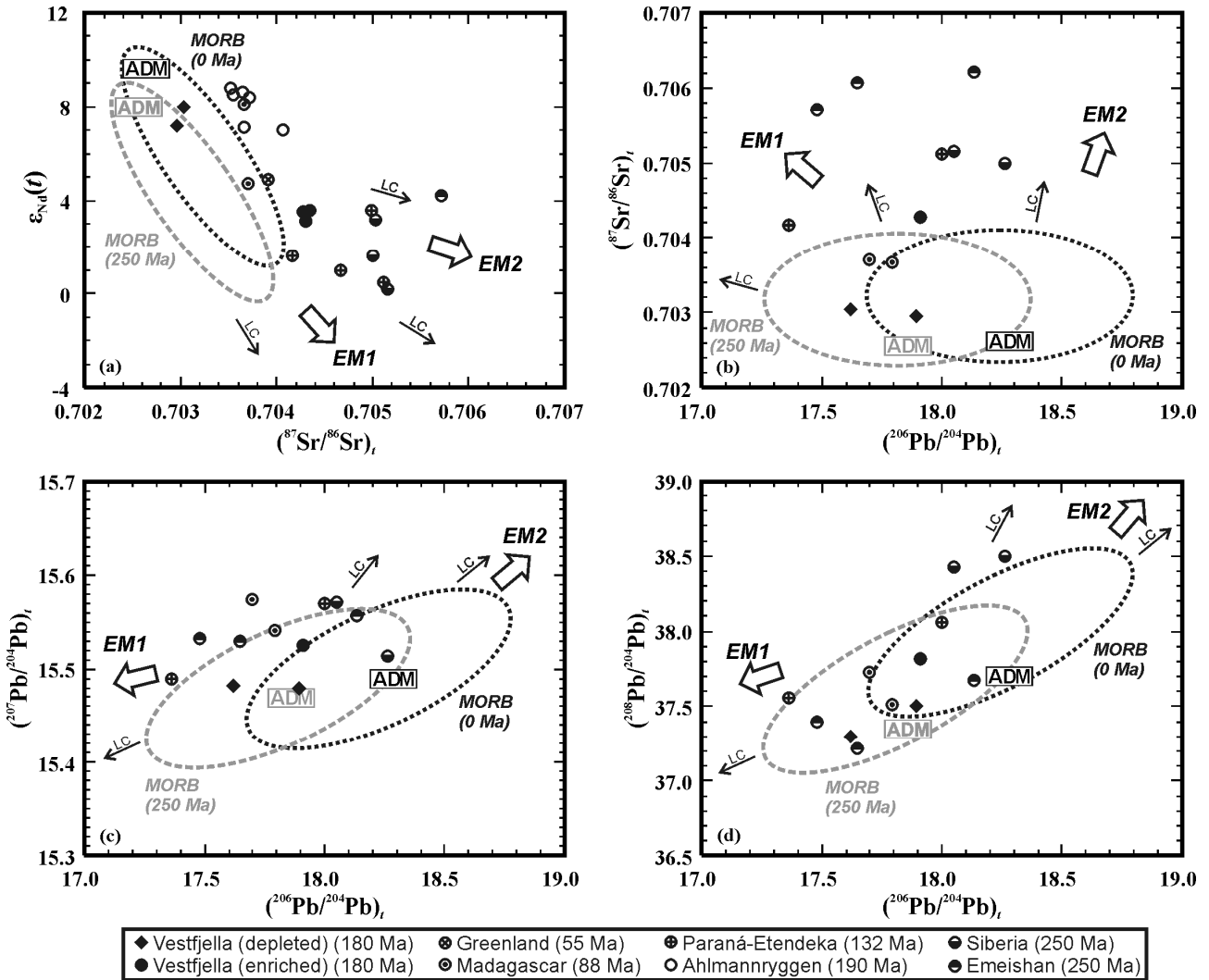


**Figure 13.** Phanerozoic ferropicrites shown in initial  $\epsilon_{Nd}$  vs.  $^{87}Sr/^{86}Sr$  (a),  $^{87}Sr/^{86}Sr$  vs.  $^{206}Pb/^{204}Pb$  (b),  $^{207}Pb/^{204}Pb$  vs.  $^{206}Pb/^{204}Pb$  (c), and  $^{208}Pb/^{204}Pb$  vs.  $^{206}Pb/^{204}Pb$  (d) diagrams. Average depleted MORB mantle (ADM; Workman & Hart, 2005) and field of worldwide MORBs (estimated after Klein 2003) shown at 0 and 250 Ma. The compositions at 250 Ma were back-calculated by using ADM mantle reservoir composition recommended by Workman & Hart (2005). Approximate compositions of EM1 and EM2 mantle reservoirs estimated after Eisele *et al.* (2002) and Workman *et al.* (2004), respectively (cf. Paper III). LC arrows denote the effect of lithospheric contamination with variable contaminant compositions (cf. Paper III).

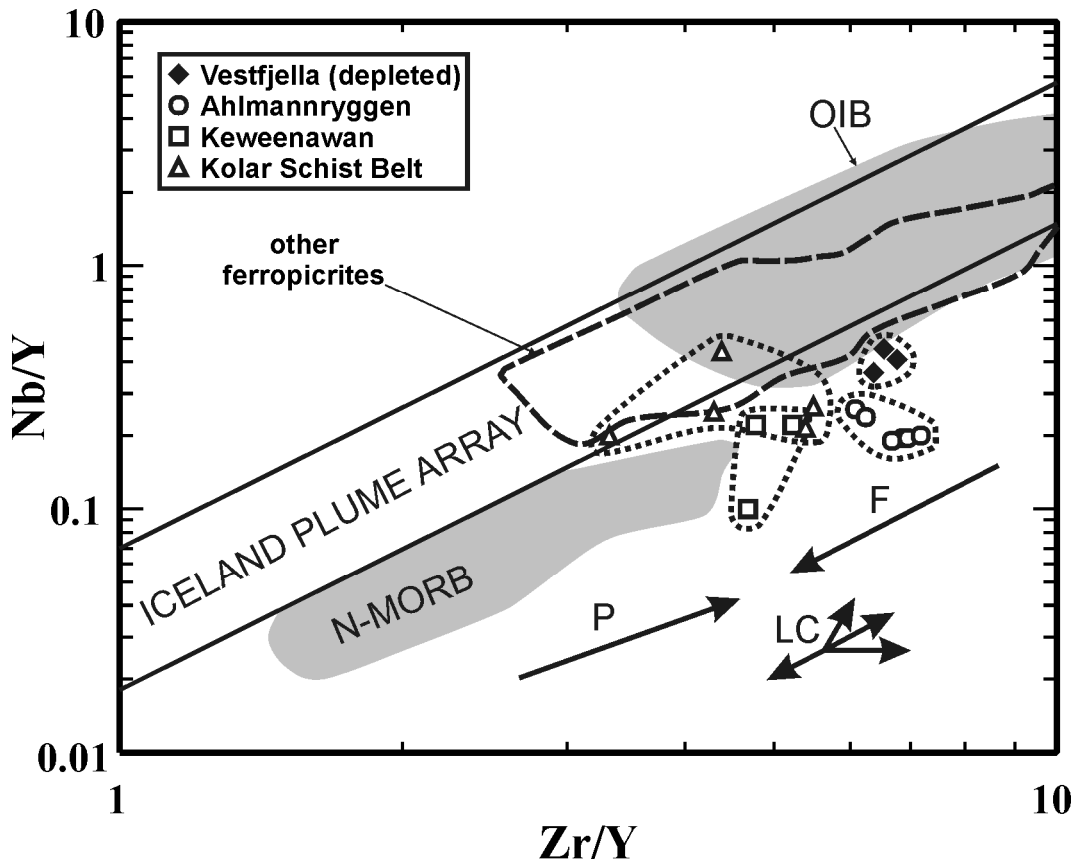


**Figure 14.** Ferropicrites shown in logarithmic Nb/Y vs. Zr/Y diagram (data sources listed in Table 1). The Iceland Plume Array and fields for N-MORB and OIB after Fitton *et al.* (2003). P and F arrows denote the effect of increasing pressure and degree of melting, respectively (cf. Fitton *et al.* 1997). LC arrows denote the effect of lithospheric contamination with variable contaminant compositions (cf. Paper III).

### 3.3.5. The origin of the relative Fe enrichment

On the basis of this thesis and earlier studies on ferropicrite petrogenesis (Hanski & Smolkin, 1995; Gibson *et al.*, 2000; Gibson, 2002; Goldstein & Francis, 2008), I present three fundamental ferropicrite factors that promote generation of these exceptional subalkaline melt compositions:

#### 1. Relatively low degree of melting

Low-degree melting of mantle lithologies results in relatively Fe-rich partial melts (cf. Fig. 11a). At very low-degrees of melting (e.g.,  $F \leq 0.01$ ) the partial melts tend to be alkaline in character, however.

#### 2. Melting at relatively high pressures

High-pressure melting of mantle lithologies results in relatively Fe-rich partial melts (cf. Fig. 11a).

#### 3. Enriched source components

Enriched source components may be needed in order to result in  $\text{FeO}_{\text{tot}}^{\text{liq}} > 14$  wt. % (cf. Fig. 11a; Section 3.3.2.). Fertile source composition also promotes melting at higher pressures.

As a result of these factors, ferropicritic magmas can be generated in several ways. The most well-established models include the following examples: (1) fractional crystallization of olivine from highly magnesian parental magmas

1471 derived from predominantly ambient peridotitic sources at high pressures (the  
1472 Vestfjella depleted type; Paper II), (2) high-pressure partial melting of relatively  
1473 Fe-rich (metasomatized?) peridotite (e.g., some Precambrian ferropicrites; Hanski  
1474 and Smolkin 1995; Stone *et al.* 1995), and (3) high-pressure partial melting of  
1475 pyroxenite that possibly contains recycled components (e.g., the Vestfjella  
1476 enriched type and Paraná-Etendeka; cf. Paper I, III; Tuff *et al.* 2005). Combining  
1477 geochemical, mineral chemical, and isotopic data and tracking down the primary  
1478 melt compositions is important in addressing the various possibilities. It should  
1479 also be noted that thick continental lithosphere appears to be prerequisite for the  
1480 preservation of ferropicrite parental melts until their eruption: thick lithospheric  
1481 lid effectively prevents subsequent mixing with mantle melts generated at higher  
1482 degree of melting, at lower pressures, and from less fertile mantle components (cf.  
1483 Fig. 2; Gibson 2002).

1484

#### 1485 **4. In conclusion**

1486 Ferropicrites (and related meimechites, picrites, picrobasalts, and basalts) of  
1487 Vestfjella, western Dronning Maud Land, are found as dikes that crosscut the  
1488 continental flood basalts of the Antarctic extension of the Jurassic Karoo LIP. The  
1489 dikes show division into two distinct geochemical types, one showing relatively  
1490 flat primitive-mantle-normalized incompatible element contents (depleted type)  
1491 and the other showing more enrichment in the highly incompatible elements  
1492 (enriched type). The depleted type is related to the main phase of Karoo  
1493 magmatism at ~180 Ma and originated as highly magnesian (MgO up to 25 wt. %)   
1494 partial melts from Indian Ocean MORB-source upper mantle at considerable  
1495 temperatures ( $T_p > 1600$  °C) and pressures (5–6 GPa) beneath the Gondwana  
1496 supercontinent. The enriched type was derived from pyroxenitic components that  
1497 were formed either by melt metasomatism or by recycling of oceanic crust in the  
1498 subcontinental mantle. The source of the depleted type represents an important  
1499 sublithospheric end-member for Karoo CFBs and its purported origin is  
1500 compatible with the theory that the Karoo LIP was formed in an extensive melting  
1501 episode caused mainly by internal heating of the upper mantle beneath the  
1502 Gondwana supercontinent. The relative Fe-enrichment of primary ferropicrites  
1503 seems to require one or more of the following: (1) relatively low degree of partial  
1504 melting, (2) high pressure of partial melting, and (3) melting of enriched source  
1505 components. Nevertheless, I address the importance in identifying the parental  
1506 magma composition, because ferropicritic whole-rock compositions could also  
1507 result from accumulation, secondary alteration, and fractional crystallization.

1508

1509



## 5. References

- Adam, J. & Green, T.H. (2006) Trace element partitioning between mica- and amphibole-bearing garnet lherzolite and hydrous basanitic melt: 1, Experimental results and the investigation of controls on partitioning behaviour. *Contributions to Mineralogy and Petrology*, **152**, 1–17.
- Anderson, D.L. (1994) The sublithospheric mantle as the source of continental flood basalts: the case against the continental lithosphere and plume head reservoirs. *Earth and Planetary Science Letters*, **123**, 269–280.
- Anderson, D.L. (2000) The thermal state of the upper mantle: no role for mantle plumes. *Geophysical Research Letters*, **27**, 3623–3626.
- Anderson, D.L. (2005) Large igneous provinces, delamination, and fertile mantle. *Elements*, **1**, 271–275.
- Anderson, D.L. (2007) The eclogite engine: chemical geodynamics as a Galileo thermometer. In *Plates, Plumes, and Planetary Processes* (eds G.R. Foulger & D.M. Jurdy), pp. 47–64. Geological Society of America, Special Paper, **430**.
- Arndt, N.T., Chauvel, C., Czamanske, G.K., & Fedorenko, V.A. (1998) Two mantle sources, two plumbing systems: tholeiitic and alkaline magmatism of the Maymecha River basin, Siberian flood volcanic province. *Contributions to Mineralogy and Petrology*, **133**, 297–313.
- Bercovici, D. & Mahoney, J.J. (1994) Double flood basalts and plume head separation at the 660-kilometer discontinuity. *Science*, **266**, 1367–1369.
- Bohrson, W.A. & Spera, F.J. (2001) Energy-constrained open-system magmatic processes II: Application of energy-constrained assimilation-fractional crystallization (EC-AFC) model to magmatic systems. *Journal of Petrology*, **42**, 1019–1041.
- Bryan, S.E. & Ernst, R.E. (2008) Revised definition of large igneous provinces (LIPs). *Earth-Science Reviews*, **86**, 175–202.
- Burke, K. & Dewey, J.F. (1973) Plume-generated triple junctions: key indicators in applying plate tectonics to old rocks. *Journal of Geology*, **81**, 406–433.
- Campbell, I.H. & Griffiths, R.W. (1990) Implications of mantle plume structure for the evolution of flood basalts. *Earth and Planetary Science Letters*, **99**, 79–93.
- Carlson, R.W. & Nowell, G.M. (2001) Olivine-poor sources for mantle-derived magmas: Os and Hf isotopic evidence from potassic magmas of the Colorado Plateau. *Geochemistry, Geophysics, Geosystems*, **2**, doi:10.1029/2000GC000128.
- Carlson, R.W., Czamanske, G.K., Fedorenko, V.A., & Ilupin, I. (2006) A comparison of Siberian meimechites and kimberlites: implications for the source of high-Mg alkalic magmas and flood basalts. *Geochemistry, Geophysics, Geosystems*, **7**, doi:10.1029/2006GC001342.
- Chesley, J.T., Righter, K., & Ruiz, J. (2004) Large-scale mantle metasomatism: a Re/Os perspective. *Earth and Planetary Science Letters*, **219**, 49–60.
- Clifford, P.M. (1968) Flood basalts, dike swarms and sub-crustal flow. *Canadian Journal of Earth Sciences*, **5**, 93–96.
- Coltice, N., Phillips, B.R., Bertrand, H., Ricard, Y., & Rey, P. (2007) Global warming of the mantle at the origin of flood basalts over supercontinents. *Geology (Boulder)*, **35**, 391–394.
- Coltice, N., Bertrand, H., Rey, P., Jourdan, F., Phillips, B.R., & Ricard, Y. (2009) Global warming of the mantle beneath continents back to the Archaean. *Gondwana Research*, **15**, 254–266.
- Cooper, K.M., Eiler, J.M., Sims, K.W.W., & Langmuir, C.H. (2009) Distribution of recycled crust within the upper mantle: Insights from the oxygen isotope composition of MORB from the Australian-Antarctic Discordance. *Geochemistry, Geophysics, Geosystems*, **10**, doi:10.1029/2009GC002728.
- Corner, B. (1994) Geological evolution of western Dronning Maud Land within a Gondwana framework: Geophysics subprogramme. Final project report to SACAR, Department of Geophysics, Witwaterstrand University, South Africa.
- Cox, K.G. (1970) Tectonics and volcanism of the Karoo period and their bearing on the postulated fragmentation of Gondwanaland. In *African Magmatism and Tectonics* (eds T.N. Clifford & I.G. Gass), pp. 211–235. Oliver & Boyd, Edinburgh.
- Cox, K.G. (1972) The Karoo volcanic cycle. *Journal of the Geological Society of London*, **128**, 311–336.
- Cox, K.G. (1978) Flood basalts, subduction and the break-up of Gondwanaland. *Nature*, **274**, 47–49.
- Cox, K.G. (1988) The Karoo province. In *Continental Flood Basalts* (ed J.D. MacDougall), pp. 239–271. Kluwer Academic Publishers, Dordrecht.
- Cox, K.G., Johnson, R.L., Monkman, L.J., Stillman, C.J., Vail, J.R., & Wood, D.S. (1965) The geology of the Nuanetsi igneous province. *Philosophical Transactions of the Royal Society of London, Series A: Mathematical and Physical Sciences*, **257**, 71–218.
- Cox, K.G., Macdonald, R., & Hornung, G. (1967) Geochemical and petrographic provinces in the Karoo basalts of southern Africa. *American Mineralogist*, **52**, 1451–1474.

- 1564 Curtis, M.L., Riley, T.R., Owens, W.H., Leat, P.T., & Duncan, R.A. (2008) The form, distribution and anisotropy of  
1565 magnetic susceptibility of Jurassic dykes in H.U. Sverdrupfjella, Dronning Maud Land, Antarctica. Implications for dyke  
1566 swarm emplacement. *Journal of Structural Geology*, **30**, 1429–1447.
- 1567 Dasgupta, R., Hirschmann, M.M., & Stalker, K. (2006) Immiscible transition from carbonate-rich to silicate-rich melts in the  
1568 3 GPa melting interval of eclogite + CO<sub>2</sub> and genesis of silica-undersaturated ocean island lavas. *Journal of Petrology*, **47**,  
1569 647–671.
- 1570 Dasgupta, R., Hirschmann, M.M., & Smith, N.D. (2007) Partial Melting Experiments of Peridotite + CO<sub>2</sub> at 3 GPa and  
1571 Genesis of Alkalic Ocean Island Basalts. *Journal of Petrology*, **48**, 2093–2124.
- 1572 Davis, F.A., Tangeman, J.A., Tenner, T.J., & Hirschmann, M.M. (2009) The composition of KLB-1 peridotite. *American*  
1573 *Mineralogist*, **94**, 176–180.
- 1574 Day, J.M.D., Pearson, D.G., Macpherson, C.G., Lowry, D., & Carracedo, J. (2009) Pyroxenite-rich mantle formed by  
1575 recycled oceanic lithosphere: oxygen-osmium isotope evidence from Canary Island lavas. *Geology (Boulder)*, **37**, 555–558.
- 1576 DePaolo, D.J. (1981a) Neodymium isotopes in the Colorado Front Range and crust-mantle evolution in the Proterozoic.  
1577 *Nature*, **291**, 193–196.
- 1578 DePaolo, D.J. (1981b) Trace element and isotopic effects of combined wallrock assimilation and fractional crystallization.  
1579 *Earth and Planetary Science Letters*, **53**, 189–202.
- 1580 Duncan, A.R., Erlank, A.J., & Marsh, J.S. (1984) Regional geochemistry of the Karoo igneous province. In *Petrogenesis of*  
1581 *the Volcanic Rocks of the Karoo Province* (ed A.J. Erlank), pp. 355–388. Geological Society of South Africa, Special  
1582 Publication, **13**.
- 1583 Duncan, A.R., Armstrong, R.A., Erlank, A.J., Marsh, J.S., & Watkins, R.T. (1990) MORB-related dolerites associated with  
1584 the final phases of Karoo flood basalt volcanism in Southern Africa. In *Mafic Dykes and Emplacement Mechanisms;*  
1585 *Proceedings of the Second International Dyke Conference* (eds A.J. Parker, P.C. Rickwood & D.H. Tucker), pp. 119–129.  
1586 Balkema, Rotterdam.
- 1587 Duncan, R.A., Hooper, P.R., Rehacek, J., Marsh, J.S., & Duncan, A.R. (1997) The timing and duration of the Karoo igneous  
1588 event, southern Gondwana. *Journal of Geophysical Research*, **102**, 18,127–18,138.
- 1589 Eisele, J., Sharma, M., Galer, S.J.G., Blichert-Toft, J., Devey, C.W., & Hofmann, A.W. (2002) The role of sediment  
1590 recycling in EM-1 inferred from Os, Pb, Hf, Nd, Sr isotope and trace element systematics of the Pitcairn Hotspot. *Earth and*  
1591 *Planetary Science Letters*, **196**, 197–212.
- 1592 Elburg, M. & Goldberg, A. (2000) Age and geochemistry of Karoo dolerite dykes from Northeast Botswana. *Journal of*  
1593 *African Earth Sciences*, **31**, 539–554.
- 1594 Elkins, L.J., Gaetani, G.A., & Sims, K. (2008) Partitioning of U and Th during garnet pyroxenite partial melting: Constraints  
1595 on the source of alkaline ocean island basalts. *Earth and Planetary Science Letters*, **265**, 270–286.
- 1596 Elkins-Tanton, L.T. (2005) Continental magmatism caused by lithospheric delamination. In *Plates, Plumes, and Paradigms*  
1597 (eds G.R. Foulger, J.H. Natland, D.C. Presnall & D.L. Anderson), pp. 449–461. Geological Society of America, Special  
1598 Publication, **388**.
- 1599 Elkins-Tanton, L.T. & Hager, B.H. (2000) Melt intrusion as a trigger for lithospheric foundering and the eruption of the  
1600 Siberian flood basalts. *Geophysical Research Letters*, **27**, 3937–3940.
- 1601 Elkins-Tanton, L.T., Draper, D.S., Agee, C.B., Jewell, J., Thorpe, A., & Hess, P.C. (2007) The last lavas erupted during the  
1602 main phase of the Siberian flood volcanic province: results from experimental petrology. *Contributions to Mineralogy and*  
1603 *Petrology*, **153**, 191–209.
- 1604 Ellam, R.M. (2006) New constraints on the petrogenesis of the Nuanetsi picrite basalts from Pb and Hf isotope data. *Earth*  
1605 *and Planetary Science Letters*, **245**, 153–161.
- 1606 Ellam, R.M. & Cox, K.G. (1989) A Proterozoic lithospheric source for Karoo magmatism: evidence from the Nuanetsi  
1607 picrites. *Earth and Planetary Science Letters*, **92**, 207–218.
- 1608 Ellam, R.M. & Cox, K.G. (1991) An interpretation of Karoo picrite basalts in terms of interaction between asthenospheric  
1609 magmas and the mantle lithosphere. *Earth and Planetary Science Letters*, **105**, 330–342.
- 1610 Ellam, R.M. & Stuart, F.M. (2000) The sub-lithospheric source of North Atlantic basalts: evidence for, and significance of, a  
1611 common end-member. *Journal of Petrology*, **41**, 919–932.
- 1612 Ellam, R.M., Carlson, R.W., & Shirey, S.B. (1992) Evidence from Re-Os isotopes for plume-lithosphere mixing in Karoo  
1613 flood basalt genesis. *Nature*, **359**, 718–721.
- 1614 Erlank, A.J. (ed) (1984) *Petrogenesis of the Volcanic Rocks of the Karoo Province*. Geological Society of South Africa,  
1615 Special Publication, **13**.
- 1616 Ewart, A., Milner, S.C., Armstrong, R.A., & Duncan, A.R. (1998) Etendeka volcanism of the Goboboseb Mountains and  
1617 Messum igneous complex, Namibia. Part I: Geochemical evidence of Early Cretaceous Tristan plume melts and the role of  
1618 crustal contamination in the Paraná-Etendeka CFB. *Journal of Petrology*, **39**, 191–225.
- 1619 Farnetani, C.G. & Richards, M.A. (1994) Numerical investigations of the mantle plume initiation model for flood basalt  
1620 events. *Journal of Geophysical Research*, **99**, 13,813–13,833.

- 1621 Fitton, J.G., Saunders, A.D., Norry, M.J., Hardarson, B.S., & Taylor, R.N. (1997) Thermal and chemical structure of the  
1622 Iceland Plume. *Earth and Planetary Science Letters*, **153**, 197–208.
- 1623 Fitton, J.G., Saunders, A.D., Kempton, P.D., & Hardarson, B.S. (2003) Does depleted mantle form an intrinsic part of the  
1624 Iceland Plume? *Geochemistry, Geophysics, Geosystems*, **4**, doi:10.1029/2002GC000424.
- 1625 Foulger, G.R. (2007) The "plate" model for the genesis of melting anomalies. In *Plates, Plumes, and Planetary Processes*  
1626 (eds G.R. Foulger & D.M. Jurdy), pp. 1–28. Geological Society of America, Special Paper, **430**.
- 1627 Foulger, G.R., Natland, J.H., Presnall, D.C., & Anderson, D.L. (eds) (2005) *Plates, Plumes, and Paradigms*. Geological  
1628 Society of America, Special Publication, **388**.
- 1629 Fram, M.S. & Leshner, C.E. (1997) Generation and polybaric differentiation of East Greenland early Tertiary flood basalts.  
1630 *Journal of Petrology*, **38**, 231–275.
- 1631 Francis, D., Ludden, J., Johnstone, R., & Davis, W. (1999) Picrite evidence for more Fe in Archean mantle reservoirs. *Earth*  
1632 *and Planetary Science Letters*, **167**, 197–213.
- 1633 Gaetani, G.A., Kent, A.J.R., Grove, T.L., Hutcheon, I.D., & Stolper, E.M. (2003) Mineral/melt partitioning of trace elements  
1634 during hydrous peridotite partial melting. *Contributions to Mineralogy and Petrology*, **145**, 391–405.
- 1635 Gibson, I.L. (1966) Crustal flexures and flood basalts. *Tectonophysics*, **3**, 447–456.
- 1636 Gibson, S.A. (2002) Major element heterogeneity in Archean to Recent mantle plume starting-heads. *Earth and Planetary*  
1637 *Science Letters*, **195**, 59–74.
- 1638 Gibson, S.A., Thompson, R.N., & Dickin, A.P. (2000) Ferropicrites: geochemical evidence for Fe-rich streaks in upwelling  
1639 mantle plumes. *Earth and Planetary Science Letters*, **174**, 355–374.
- 1640 Gibson, S.A., Thompson, R.N., & Day, J.A. (2006) Timescales and mechanisms of plume-lithosphere interactions:  $^{40}\text{Ar}/^{39}\text{Ar}$   
1641 geochronology and geochemistry of alkaline igneous rocks from the Parana-Etendeka large igneous province. *Earth and*  
1642 *Planetary Science Letters*, **251**, 1–17.
- 1643 Goldstein, S.B. & Francis, D. (2008) The petrogenesis and mantle source of Archean ferropicrites from the Western  
1644 Superior Province, Ontario, Canada. *Journal of Petrology*, **49**, 1729–1753.
- 1645 Gudfinnsson, G.H. & Presnall, D.C. (2005) Continuous gradations among primary carbonatitic, kimberlitic, melilititic,  
1646 basaltic, picritic, and komatiitic melts in equilibrium with garnet lherzolite at 3–8 GPa. *Journal of Petrology*, **46**, 1645–1659.
- 1647 Gurnis, M. (1988) Large-scale mantle convection and the aggregation and dispersal of supercontinents. *Nature*, **332**, 695–  
1648 699.
- 1649 Hanski, E.J. (1992) Petrology of the Pechenga ferropicrites and cogenetic Ni-bearing gabbro-wehrlite intrusions, Kola  
1650 Peninsula, Russia. *Geological Survey of Finland – Bulletin*, **367**.
- 1651 Hanski, E.J. & Smolkin, V.F. (1989) Pechenga ferropicrites and other early Proterozoic picrites in the eastern part of the  
1652 Baltic Shield; Papers from the meeting on Proterozoic geochemistry. *Precambrian Research*, **45**, 63–82.
- 1653 Hanski, E.J. & Smolkin, V.F. (1995) Iron- and LREE-enriched mantle source for early Proterozoic intraplate magmatism as  
1654 exemplified by the Pechenga ferropicrites, Kola Peninsula, Russia; Picrites, komatiites and their ore deposits. *Lithos*, **34**,  
1655 107–125.
- 1656 Hargraves, R.B., Rehacek, J., & Hooper, P.R. (1997) Palaeomagnetism of the Karoo igneous rocks in Southern Africa. *South*  
1657 *African Journal of Geology*, **100**, 195–212.
- 1658 Harmer, R.E., Lee, C.A., & Eglington, B.M. (1998) A deep mantle source for carbonatite magmatism: evidence from the  
1659 nephelinites and carbonatites of the Buhera District, SE Zimbabwe. *Earth and Planetary Science Letters*, **158**, 131–142.
- 1660 Hauri, E.H. & Hart, S.R. (1993) Re-Os isotope systematics of HIMU and EMII oceanic island basalts from the South Pacific  
1661 Ocean. *Earth and Planetary Science Letters*, **114**, 353–371.
- 1662 Hauri, E.H., Lassiter, J.C., & DePaolo, D.J. (1996) Osmium isotope systematics of drilled lavas from Mauna Loa, Hawaii.  
1663 *Journal of Geophysical Research*, **101**, 11,793–11,806.
- 1664 Hawkesworth, C.J., Marsh, J.S., Duncan, A.R., Erlank, A.J., & Norry, M.J. (1984) The role of continental lithosphere in the  
1665 generation of the Karoo volcanic rocks: evidence from combined Nd- and Sr-isotope studies. In *Petrogenesis of the Volcanic*  
1666 *Rocks of the Karoo Province* (ed A.J. Erlank), pp. 341–354. Geological Society of South Africa, Special Publication, **13**.
- 1667 Hawkesworth, C.J., Gallagher, K., Kelley, S., Mantovani, M., Peate, D.W., Regelous, M., & Rogers, N.W. (1992) Parana  
1668 magmatism and the opening of the South Atlantic. In *Magmatism and the Causes of Continental Break-Up* (eds B.C. Storey,  
1669 T. Alabaster & R.J. Pankhurst), pp. 221–240. Geological Society of London, Special Publication, **68**.
- 1670 Hergt, J.M., Peate, D.W., & Hawkesworth, C.J. (1991) The petrogenesis of Mesozoic Gondwana low-Ti flood basalts. *Earth*  
1671 *and Planetary Science Letters*, **105**, 134–148.
- 1672 Herzberg, C. (2006) Petrology and thermal structure of the Hawaiian plume from Mauna Kea volcano. *Nature*, **444**, 605–  
1673 609.
- 1674 Herzberg, C. & Zhang, J. (1996) Melting experiments on anhydrous peridotite KLB-1: composition of magmas in the upper  
1675 mantle and transition zone. *Journal of Geophysical Research*, **101**, 8271–8295.
- 1676 Hirose, K. & Kawamoto, T. (1995) Hydrous partial melting of lherzolite at 1 GPa: the effect of H<sub>2</sub>O on the genesis of  
1677 basaltic magmas. *Earth and Planetary Science Letters*, **133**, 463–473.

- 1678 Hirschmann, M.M., Ghiorso, M.S., & Stolper, E.M. (1999) Calculation of peridotite partial melting from thermodynamic  
1679 models of minerals and melts. II. Isobaric variations in melts near the solidus and owing to variable source composition.  
1680 *Journal of Petrology*, **40**, 297–313.
- 1681 Hirschmann, M.M., Kogiso, T., Baker, M.B., & Stolper, E.M. (2003) Alkalic magmas generated by partial melting of garnet  
1682 pyroxenite. *Geology (Boulder)*, **31**, 481–484.
- 1683 Hooper, P.R. & Hawkesworth, C.J. (1993) Isotopic and geochemical constraints on the origin and evolution of the Columbia  
1684 River Basalt. *Journal of Petrology*, **34**, 1203–1246.
- 1685 Horan, M.F., Walker, R.J., Fedorenko, V.A., & Czamanske, G.K. (1995) Osmium and neodymium isotopic constraints on  
1686 the temporal and spatial evolution of Siberian flood basalt sources. *Geochimica et Cosmochimica Acta*, **59**, 5159–5168.
- 1687 Ichiyama, Y., Ishiwatari, A., Hirahara, Y., & Shuto, K. (2006) Geochemical and isotopic constraints on the genesis of the  
1688 Permian ferropicritic rocks from the Mino-Tamba belt, SW Japan. *Lithos*, **89**, 47–65.
- 1689 Ichiyama, Y., Ishiwatari, A., Koizumi, K., Ishida, Y., & Machi, S. (2007) Olivine-spinifex basalt from the Tamba Belt,  
1690 Southwest Japan: evidence for Fe- and high field strength element-rich ultramafic volcanism in Permian Ocean. *Island Arc*,  
1691 **16**, 493–503.
- 1692 Jahn, B., Gruau, G., & Glikson, A.Y. (1982) Komatiites of the Onverwacht Group, S. Africa: REE geochemistry, Sm/Nd age  
1693 and mantle evolution. *Contributions to Mineralogy and Petrology*, **80**, 25–40.
- 1694 Jakobsen, J.K., Veksler, I.V., Tegner, C., & Brooks, C.K. (2005) Immiscible iron- and silica-rich melts in basalt petrogenesis  
1695 documented in the Skaergaard Intrusion. *Geology (Boulder)*, **33**, 885–888.
- 1696 Janney, P.E., le Roex, A.P., & Carlson, R.W. (2005) Hafnium isotope and trace element constraints on the nature of mantle  
1697 heterogeneity beneath the central Southwest Indian Ridge (13°E to 47°E). *Journal of Petrology*, **46**, 2427–2464.
- 1698 Johnson, D.M., Hooper, P.R., & Conrey, R.M. (1999) XRF Analysis of Rocks and Minerals for Major and Trace Elements  
1699 on a Single Low Dilution Li-tetraborate Fused Bead. *Advances in X-ray Analysis*, **41**, 843–867.
- 1700 Johnston, S.T. & Thorkelson, D.J. (2000) Continental flood basalts: episodic magmatism above long-lived hotspots. *Earth  
1701 and Planetary Science Letters*, **175**, 247–256.
- 1702 Jones, A.P., Price, G.D., Price, N.J., DeCarli, P.S., & Clegg, R.A. (2002) Impact induced melting and the development of  
1703 large igneous provinces. *Earth and Planetary Science Letters*, **202**, 551–561.
- 1704 Jourdan, F., Féraud, G., Bertrand, H., Kampunzu, A.B., Tshoso, G., Watkeys, M.K., & Le Gall, B. (2005) Karoo large  
1705 igneous province: Brevity, origin, and relation to mass extinction questioned by new <sup>40</sup>Ar/<sup>39</sup>Ar age data. *Geology (Boulder)*,  
1706 **33**, 745–748.
- 1707 Jourdan, F., Féraud, G., Bertrand, H., Watkeys, M.K., Kampunzu, A.B., & Le Gall, B. (2006) Basement control on dyke  
1708 distribution in large igneous provinces: case study of the Karoo triple junction. *Earth and Planetary Science Letters*, **241**,  
1709 307–322.
- 1710 Jourdan, F., Bertrand, H., Schaerer, U., Blichert-Toft, J., Féraud, G., & Kampunzu, A.B. (2007) Major and trace element and  
1711 Sr, Nd, Hf, and Pb isotope compositions of the Karoo large igneous province, Botswana-Zimbabwe: lithosphere vs mantle  
1712 plume contribution. *Journal of Petrology*, **48**, 1043–1077.
- 1713 Jourdan, F., Féraud, G., Bertrand, H., & Watkeys, M.K. (2007) From flood basalts to the inception of oceanization: example  
1714 from the <sup>40</sup>Ar/<sup>39</sup>Ar high-resolution picture of the Karoo large igneous province. *Geochemistry, Geophysics, Geosystems*, **8**,  
1715 doi:10.1029/2006GC001392.
- 1716 Kent, R.W., Storey, M., & Saunders, A.D. (1992) Large igneous provinces: sites of plume impact or plume incubation?  
1717 *Geology (Boulder)*, **20**, 891–894.
- 1718 Keshav, S., Gudfinnsson, G.H., Sen, G., & Fei, Y. (2004) High-pressure melting experiments on garnet clinopyroxenite and  
1719 the alkalic to tholeiitic transition in ocean-island basalts. *Earth and Planetary Science Letters*, **223**, 365–379.
- 1720 King, S.D. & Anderson, D.L. (1995) An alternative mechanism of flood basalt formation. *Earth and Planetary Science  
1721 Letters*, **136**, 269–279.
- 1722 King, S.D. & Anderson, D.L. (1998) Edge-driven convection. *Earth and Planetary Science Letters*, **160**, 289–296.
- 1723 Klein, E.M. (2003) Geochemistry of the Igneous Ocean Crust. In *The Crust* (ed R.L. Rudnick), *Treatise on Geochemistry*, **3**,  
1724 pp. 433–463. Elsevier-Pergamon, Oxford.
- 1725 Kleinhanns, I.C., Kramers, J.D., & Kamber, B.S. (2003) Importance of water for Archaean granitoid petrology: a  
1726 comparative study of TTG and potassic granitoids from Barberton Mountain Land, South Africa. *Contributions to  
1727 Mineralogy and Petrology*, **145**, 377–389.
- 1728 Knaack, C., Cornelius, S.B., & Hooper, P.R. (1994) Trace Element Analyses of Rocks and Minerals by ICP-MS.  
1729 GeoAnalytical Lab, Washington State University, <http://www.sees.wsu.edu/Geolab/equipment/icpms.html>.
- 1730 Kogiso, T., Hirschmann, M.M., & Frost, D.J. (2003) High-pressure partial melting of garnet pyroxenite: possible mafic  
1731 lithologies in the source of ocean island basalts. *Earth and Planetary Science Letters*, **216**, 603–617.
- 1732 Kreissig, K., Naegler, T.F., Kramers, J.D., van Reenen, D.D., & Smit, C.A. (2000) An isotopic and geochemical study of the  
1733 northern Kaapvaal Craton and the Southern Marginal Zone of the Limpopo Belt: are they juxtaposed terranes? *Lithos*, **50**, 1–  
1734 25.

- 1735 Kurhila, M.I., Luttinen, A.V., Foland, K.A., & Heinonen, J.S. (2008)  $^{40}\text{Ar}/^{39}\text{Ar}$  ages of Karoo-related basaltic dikes from  
1736 Vestfjella, Dronning Maud Land, Antarctica. The Gondwana 13 Conference, Program & Abstracts, Institute of Geology and  
1737 Geophysics, Chinese Academy of Sciences, Beijing, China, p. 100.
- 1738 Larsen, L.M. & Pedersen, A.K. (2000) Processes in high-Mg, high-T magmas: evidence from olivine, chromite and glass in  
1739 Palaeogene picrites from West Greenland. *Journal of Petrology*, **41**, 1071–1098.
- 1740 Le Bas, M.J. (2000) IUGS reclassification of the high-Mg and picritic volcanic rocks. *Journal of Petrology*, **41**, 1467–1470.
- 1741 Le Bas, M.J., Le Maitre, R.W., Streckeisen, A., & Zanettin, B.A. (1986) Chemical classification of volcanic rocks based on  
1742 the total alkali-silica diagram. *Journal of Petrology*, **27**, 745–750.
- 1743 Le Roux, V., Lee, C.A., & Turner, S.J. (2010) Zn/Fe systematics in mafic and ultramafic systems: implications for detecting  
1744 major element heterogeneities in the Earth's mantle. *Geochimica et Cosmochimica Acta*, **74**, 2779–2796.
- 1745 Leat, P.T., Luttinen, A.V., Storey, B.C., & Millar, I.L. (2006) Sills of the Theron Mountains, Antarctica: evidence for long  
1746 distance transport of mafic magmas during Gondwana break-up. In *Dyke Swarms: Time Markers of Crustal Evolution* (eds  
1747 E.J. Hanski, S. Mertanen, O.T. Rämö & J. Vuollo), pp. 183–199. Taylor & Francis, Abingdon.
- 1748 Lee, C.A., Luffi, P., Plank, T., Dalton, H., & Leeman, W.P. (2009) Constraints on the depths and temperatures of basaltic  
1749 magma generation on Earth and other terrestrial planets using new thermobarometers for mafic magmas. *Earth and  
1750 Planetary Science Letters*, **279**, 20–33.
- 1751 Li, C. & Ripley, E.M. (2010) The relative effects of composition and temperature on olivine-liquid Ni partitioning:  
1752 Statistical deconvolution and implications for petrologic modeling. *Chemical Geology*, **275**, 99–104.
- 1753 Lightfoot, P.C., Naldrett, A.J., Gorbachev, N.S., Doherty, W., & Fedorenko, V.A. (1990) Geochemistry of the Siberian Trap  
1754 of the Noril'sk area, USSR, with implications for the relative contributions of crust and mantle to flood basalt magmatism.  
1755 *Contributions to Mineralogy and Petrology*, **104**, 631–644.
- 1756 Lightfoot, P.C., Hawkesworth, C.J., Hergt, J.M., Naldrett, A.J., Gorbachev, N.S., Fedorenko, V.A., & Doherty, W. (1993)  
1757 Remobilisation of the continental lithosphere by a mantle plume: major-, trace-element, and Sr-, Nd-, and Pb-isotope  
1758 evidence from picritic and tholeiitic lavas of the Noril'sk District, Siberian Trap, Russia. *Contributions to Mineralogy and  
1759 Petrology*, **114**, 171–188.
- 1760 Luttinen, A.V. & Furnes, H. (2000) Flood basalts of Vestfjella: Jurassic magmatism across an Archaean-Proterozoic  
1761 lithospheric boundary in Dronning Maud Land, Antarctica. *Journal of Petrology*, **41**, 1271–1305.
- 1762 Luttinen, A.V. & Huhma, H. (2005) Source characteristics of Jurassic ferropicrites from Dronning Maud Land, Antarctica.  
1763 *Geochimica et Cosmochimica Acta Supplement*, **69**, Goldschmidt Conference Abstracts 2005, p. A106.
- 1764 Luttinen, A.V., Rämö, O.T., & Huhma, H. (1998) Neodymium and strontium isotopic and trace element composition of a  
1765 Mesozoic CFB suite from Dronning Maud Land, Antarctica: Implications for lithosphere and asthenosphere contributions to  
1766 Karoo magmatism. *Geochimica et Cosmochimica Acta*, **62**, 2701–2714.
- 1767 Luttinen, A.V., Zhang, X., & Foland, K.A. (2002) 159 Ma Kjakebeinet lamproites (Dronning Maud Land, Antarctica) and  
1768 their implications for Gondwana breakup processes. *Geological Magazine*, **139**, 525–539.
- 1769 MacDougall, J.D. (ed) (1988) *Continental Flood Basalts*. Kluwer Academic Publishers, Dordrecht, The Netherlands.
- 1770 McDonough, W.F. & Sun, S.S. (1995) The composition of the Earth. *Chemical Geology*, **120**, 223–253.
- 1771 McKenzie, D. (1985) The extraction of magma from the crust and mantle. *Earth and Planetary Science Letters*, **74**, 81–91.
- 1772 Menzies, M.A. (1992) The lower lithosphere as a major source for continental flood basalts: a re-appraisal. In *Magmatism  
1773 and the Causes of Continental Break-Up* (eds B.C. Storey, T. Alabaster & R.J. Pankhurst), pp. 31–39. Geological Society of  
1774 London, Special Publication, **68**.
- 1775 Morgan, W.J. (1971) Convection plumes in the lower mantle. *Nature*, **230**, 42–43.
- 1776 Nishio, Y., Nakai, S., Ishii, T., & Sano, Y. (2007) Isotope systematics of Li, Sr, Nd, and volatiles in Indian Ocean MORBs  
1777 of the Rodrigues triple junction: Constraints on the origin of the DUPAL anomaly. *Geochimica et Cosmochimica Acta*, **71**,  
1778 745–759.
- 1779 Niu, Y. (2009) Some basic concepts and problems on the petrogenesis of intra-plate ocean island basalts. *Chinese Science  
1780 Bulletin*, **54**, 4148–4160.
- 1781 Niu, Y. & O'Hara, M.J. (2003) Origin of ocean island basalts: A new perspective from petrology, geochemistry, and mineral  
1782 physics considerations. *Journal of Geophysical Research*, **108**, doi:10.1029/2002JB002048.
- 1783 Pearce, J.A. (1996) A user's guide to basalt discrimination diagrams. In *Trace Element Geochemistry of Volcanic Rocks:  
1784 Applications for Massive Sulphide Exploration* (ed D.A. Wyman), pp. 79–113. Geological Association of Canada, Short  
1785 Course Notes, **12**.
- 1786 Peate, D.W., Baker, J.A., Blichert-Toft, J., Hilton, D.R., Storey, M., Kent, A.J.R., Brooks, C.K., Hansen, H., Pedersen, A.K.,  
1787 & Duncan, R.A. (2003) The Prinsen af Wales Bjerre Formation lavas, East Greenland: the transition from tholeiitic to  
1788 alkalic magmatism during Palaeogene continental break-up. *Journal of Petrology*, **44**, 279–304.
- 1789 Peters, M. (1989) Die Vulkanite im westlichen und mittleren Neuschwabenland, Vestfjella und Ahlmannryggen, Antarktika;  
1790 Petrographie, Geochemie, Geochronologie, Palaeomagnetismus, geotektonische Implikationen. Berichte zur Polarforschung  
1791 61, Alfred Wegener-Institut für Polar- und Maareforschung, Bremerhaven. (In German)

- 1792 Pik, R., Deniel, C., Coulon, C., Yirgu, G., & Marty, B. (1999) Isotopic and trace element signatures of Ethiopian flood  
1793 basalts: evidence for plume-lithosphere interactions. *Geochimica et Cosmochimica Acta*, **63**, 2263–2279.
- 1794 Putirka, K.D. (1999) Melting depths and mantle heterogeneity beneath Hawaii and the East Pacific Rise: constraints from  
1795 Na/Ti and rare earth element ratios. *Journal of Geophysical Research*, **104**, 2817–2829.
- 1796 Putirka, K.D., Perfit, M., Ryerson, F.J., & Jackson, M.G. (2007) Ambient and excess mantle temperatures, olivine  
1797 thermometry, and active vs. passive upwelling. *Chemical Geology*, **241**, 177–206.
- 1798 Rajamani, V., Shivkumar, K., Hanson, G.N., & Shirey, S.B. (1985) Geochemistry and petrogenesis of amphibolites, Kolar  
1799 schist belt, South India: evidence for komatiitic magma derived by low percentages of melting of the mantle. *Journal of*  
1800 *Petrology*, **26**, 92–123.
- 1801 Reiners, P.W. & Nelson, B.K. (1998) Temporal-compositional-isotopic trends in rejuvenated-stage magmas of Kauai,  
1802 Hawaii, and implications for mantle melting processes. *Geochimica et Cosmochimica Acta*, **62**, 2347–2368.
- 1803 Reisberg, L., Zindler, A., Marcantonio, F., White, W.M., Wyman, D., & Weaver, B.L. (1993) Os isotope systematics in  
1804 ocean island basalts. *Earth and Planetary Science Letters*, **120**, 149–167.
- 1805 Richards, M.A., Duncan, R.A., & Courtillot, V.E. (1989) Flood basalts and hot-spot tracks: plume heads and tails. *Science*,  
1806 **246**, 103–107.
- 1807 Riley, T.R., Leat, P.T., Curtis, M.L., Millar, I.L., Duncan, R.A., & Fazel, A. (2005) Early-Middle Jurassic dolerite dykes  
1808 from Western Dronning Maud Land (Antarctica): Identifying mantle sources in the Karoo Large Igneous Province. *Journal*  
1809 *of Petrology*, **46**, 1489–1524.
- 1810 Riley, T.R., Curtis, M.L., Leat, P.T., Watkeys, M.K., Duncan, R.A., Millar, I.L., & Owens, W.H. (2006) Overlap of Karoo  
1811 and Ferrar magma types in KwaZulu-Natal, South Africa. *Journal of Petrology*, **47**, 541–566.
- 1812 Rudnick, R.L. & Gao, S. (2003) The Composition of the Continental Crust. In *The Crust* (ed R.L. Rudnick), *Treatise on*  
1813 *Geochemistry*, **3**, pp. 1–64. Elsevier-Pergamon, Oxford.
- 1814 Ryabov, V.V., Bakumenko, I.T., & Fominykh, I.M. (1977) Dendritic megacrystals of clinopyroxene in trap rocks of the  
1815 Norilsk region and some questions concerning their formation. *Akade. Nauk SSSR, Sibirskoe Otdelenie, Instituta Geologii i*  
1816 *Geofiziki Trudy*, **349**, 47–74. (in Russian)
- 1817 Sano, T., Fujii, T., Deshmukh, S.S., Fukuoka, T., & Aramaki, S. (2001) Differentiation processes of Deccan Trap basalts:  
1818 contribution from geochemistry and experimental petrology. *Journal of Petrology*, **42**, 2175–2195.
- 1819 Saunders, A.D. (2005) Large igneous provinces: origin and environmental consequences. *Elements*, **1**, 259–263.
- 1820 Saunders, A.D., Norry, M.J., & Tarney, J. (1988) Origin of MORB and chemically-depleted mantle reservoirs: trace element  
1821 constraints. *Journal of Petrology*, Special Volume, **1**, 415–445.
- 1822 Segev, A. (2002) Flood basalts, continental breakup and the dispersal of Gondwana: evidence for periodic migration of  
1823 upwelling mantle flows (plumes). *European Geosciences Union Stephan Mueller Special Publication Series*, **2**, 171–191.
- 1824 Shirey, S.B. & Walker, R.J. (1998) The Re-Os isotope system in cosmochemistry and high-temperature geochemistry.  
1825 *Annual Review of Earth and Planetary Sciences*, **26**, 423–500.
- 1826 Shirey, S.B., Klewin, K.W., Berg, J.H., & Carlson, R.W. (1994) Temporal changes in the sources of flood basalts: isotopic  
1827 and trace element evidence from the 1100 Ma old Keweenaw Mamainse Point Formation, Ontario, Canada. *Geochimica et*  
1828 *Cosmochimica Acta*, **58**, 4475–4490.
- 1829 Silver, P.G., Behn, M.D., Kelley, K.A., Schmitz, M., & Savage, B. (2006) Understanding cratonic flood basalts. *Earth and*  
1830 *Planetary Science Letters*, **245**, 190–201.
- 1831 Sobolev, A.V., Hofmann, A.W., Sobolev, S.V., & Nikogosian, I.K. (2005) An olivine-free mantle source of Hawaiian shield  
1832 basalts. *Nature*, **434**, 590–597.
- 1833 Sobolev, A.V., Hofmann, A.W., Kuzmin, D.V., Yaxley, G.M., Arndt, N.T., Chung, S., Danyushevsky, L.V., Elliott, T., Frey,  
1834 F.A., Garcia, M.O., Gurenko, A.A., Kamenetsky, V.S., Kerr, A.C., Krivolutsкая, N.A., Matvienkov, V.V., Nikogosian,  
1835 I.K., Rocholl, A., Sigurdsson, I.A., Sushchevskaya, N.M., & Teklay, M. (2007) The amount of recycled crust in sources of  
1836 mantle-derived melts. *Science*, **316**, 412–417.
- 1837 Sobolev, A.V., Hofmann, A.W., Brüggemann, G., Batanova, V.G., & Kuzmin, D.V. (2008) A quantitative link between  
1838 recycling and osmium isotopes. *Science*, **321**, 536.
- 1839 Song, X., Qi, H., Robinson, P.T., Zhou, M., Cao, Z., & Chen, L. (2008) Melting of the subcontinental lithospheric mantle by  
1840 the Emeishan mantle plume: evidence from the basal alkaline basalts in Dongchuan, Yunnan, southwestern China. *Lithos*,  
1841 **100**, 93–111.
- 1842 Spera, F.J. & Bohron, W.A. (2001) Energy-constrained open-system magmatic processes I: General model and energy-  
1843 constrained assimilation and fractional crystallization (EC-AFC) formulation. *Journal of Petrology*, **42**, 999–1018.
- 1844 Srivastava, R.K., Chalapathi Rao, N.V., & Sinha, A.K. (2009) Cretaceous potassic intrusives with affinities to aillikites from  
1845 Jharia area: magmatic expression of metasomatically veined and thinned lithospheric mantle beneath Singhbhum Craton,  
1846 eastern India. *Lithos*, **112**, 407–418.
- 1847 Stolper, E.M., Sherman, S., Garcia, M.O., Baker, M.B., & Seaman, C. (2004) Glass in the submarine section of the HSDP2  
1848 drill core, Hilo, Hawaii. *Geochemistry, Geophysics, Geosystems*, **5**, doi:10.1029/2003GC000553.

- 1849 Stone, W.E., Crocket, J.H., Dickin, A.P., & Fleet, M.E. (1995) Origin of Archean ferropicrites: geochemical constraints from  
1850 the Boston Creek Flow, Abitibi greenstone belt, Ontario, Canada. *Chemical Geology*, **121**, 51–71.
- 1851 Stone, W.E., Deloule, E., Larson, M.S., & Leshner, C.M. (1997) Evidence for hydrous high-MgO melts in the Precambrian.  
1852 *Geology (Boulder)*, **25**, 143–146.
- 1853 Storey, B.C., Alabaster, T., Hole, M.J., Pankhurst, R.J., & Wever, H.E. (1992) Role of subduction-plate boundary forces  
1854 during the initial stages of Gondwana break-up: evidence from the proto-Pacific margin of Antarctica. In *Magmatism and*  
1855 *the Causes of Continental Break-Up* (eds B.C. Storey, T. Alabaster & R.J. Pankhurst), pp. 149–163. Geological Society of  
1856 London, Special Publication, **68**.
- 1857 Storey, M., Mahoney, J.J., & Saunders, A.D. (1997) Cretaceous basalts in Madagascar and the transition between plume and  
1858 continental lithosphere mantle sources. In *Large Igneous Provinces: Continental, Oceanic, and Planetary Flood Volcanism*  
1859 (eds J.J. Mahoney & M.F. Coffin), pp. 95–122. American Geophysical Union, Geophysical Monograph, **100**.
- 1860 Stracke, A., Bizimis, M., & Salters, V.J.M. (2003) Recycling oceanic crust: quantitative constraints. *Geochemistry,*  
1861 *Geophysics, Geosystems*, **4**, doi:10.1029/2001GC000223.
- 1862 Sun, S.S. & McDonough, W.F. (1989) Chemical and isotopic systematics of oceanic basalts: Implications for mantle  
1863 composition and processes. In *Magmatism in the Ocean Basins* (eds A.D. Saunders & M.J. Norry), pp. 313–345. Geological  
1864 Society, Special Publications, **42**.
- 1865 Sweeney, R.J., Falloon, T.J., Green, D.H., & Tatsumi, Y. (1991) The mantle origins of Karoo picrites. *Earth and Planetary*  
1866 *Science Letters*, **107**, 256–271.
- 1867 Sweeney, R.J., Duncan, A.R., & Erlank, A.J. (1994) Geochemistry and petrogenesis of central Lebombo basalts of the Karoo  
1868 igneous province. *Journal of Petrology*, **35**, 95–125.
- 1869 Talarico, F., Borsi, L., & Lombardo, B. (1995) Relict granulites in the Ross Orogen of northern Victoria Land (Antarctica),  
1870 II. Geochemistry and palaeo-tectonic implications. *Precambrian Research*, **75**, 157–174.
- 1871 Thompson, R.N. & Gibson, S.A. (2000) Transient high temperatures in mantle plume heads inferred from magnesian  
1872 olivines in Phanerozoic picrites. *Nature*, **407**, 502–506.
- 1873 Tommasini, S., Manetti, P., Innocenti, F., Abebe, T., Sintoni, M.F., & Conicelli, S. (2005) The Ethiopian subcontinental  
1874 mantle domains: geochemical evidence from Cenozoic mafic lavas. *Mineralogy and Petrology*, **84**, 259–281.
- 1875 Tuff, J., Takahashi, E., & Gibson, S.A. (2005) Experimental constraints on the role of garnet pyroxenite in the genesis of  
1876 high-Fe mantle plume derived melts. *Journal of Petrology*, **46**, 2023–2058.
- 1877 Turner, S., Hawkesworth, C.J., Gallagher, K., Stewart, K., Peate, D., & Mantovani, M.S.M. (1996) Mantle plumes, flood  
1878 basalts, and thermal models for melt generation beneath continents: assessment of a conductive heating model and  
1879 application to the Parana. *Journal of Geophysical Research*, **101**, 11,503–11,518.
- 1880 Walker, R.J., Morgan, J.W., Hanski, E.J., & Smolkin, V.F. (1997) Re-Os systematics of early Proterozoic ferropicrites,  
1881 Pechenga Complex, northwestern Russia: evidence for ancient <sup>187</sup>Os-enriched plumes. *Geochimica et Cosmochimica Acta*,  
1882 **61**, 3145–3160.
- 1883 Walter, M.J. (1998) Melting of garnet peridotite and the origin of komatiite and depleted lithosphere. *Journal of Petrology*,  
1884 **39**, 29–60.
- 1885 Wasserburg, B.J., Jacobsen, S.B., DePaolo, D.J., McCulloch, M.T., & Wen, T. (1981) Precise determination of Sm/Nd  
1886 ratios, Sm and Nd isotopic abundances in standard solutions. *Geochimica et Cosmochimica Acta*, **45**, 2311–2323.
- 1887 Watkeys, M.K. (2002) Development of the Lebombo rifted volcanic margin of Southeast Africa. In *Volcanic rift margins*  
1888 (eds M.A. Menzies, S.L. Klemperer, C.J. Ebinger & J. Baker), pp. 27–46. Geological Society of America, Special Paper,  
1889 **362**.
- 1890 White, R. & McKenzie, D. (1989) Magmatism at rift zones: the generation of volcanic continental margins and flood basalts.  
1891 *Journal of Geophysical Research*, **94**, 7685–7729.
- 1892 Wooden, J.L., Czamanske, G.K., Fedorenko, V.A., Arndt, N.T., Chauvel, C., Bouse, R.M., King, B.W., Knight, R.J., &  
1893 Siems, D.F. (1993) Isotopic and trace-element constraints on mantle and crustal contributions to Siberian continental flood  
1894 basalts, Noril'sk area, Siberia. *Geochimica et Cosmochimica Acta*, **57**, 3677–3704.
- 1895 Workman, R.K. & Hart, S.R. (2005) Major and trace element composition of the depleted MORB mantle (DMM). *Earth and*  
1896 *Planetary Science Letters*, **231**, 53–72.
- 1897 Workman, R.K., Hart, S.R., Jackson, M.G., Regelous, M., Farley, K.A., Blusztajn, J.S., Kurz, M., & Staudigel, H. (2004)  
1898 Recycled metasomatized lithosphere as the origin of the enriched mantle II (EM2) end-member: Evidence from the Samoan  
1899 volcanic chain. *Geochemistry, Geophysics, Geosystems*, **5**, doi:10.1029/2003GC000623.
- 1900 Xue, X., Baadsgaard, H., Irving, A.J., Scarfe, C.M., & Brearley, M. (1990) Geochemical and isotopic characteristics of  
1901 lithospheric mantle beneath West Kettle River, British Columbia: evidence from ultramafic xenoliths. *Journal of*  
1902 *Geophysical Research*, **95**, 15,879–15,891.
- 1903 Zhang, Z., Mahoney, J.J., Mao, J., & Wang, F. (2006) Geochemistry of picritic and associated basalt flows of the Western  
1904 Emeishan flood basalt province, China. *Journal of Petrology*, **47**, 1997–2019.

- 1905 Zhang, X., Luttinen, A.V., Elliot, D.H., Larsson, K., & Foland, K.A. (2003) Early stages of Gondwana breakup: the  
 1906  $^{40}\text{Ar}/^{39}\text{Ar}$  geochronology of Jurassic basaltic rocks from western Dronning Maud Land, Antarctica, and implications for the  
 1907 timing of magmatic and hydrothermal events. *Journal of Geophysical Research*, **108**, doi:10.1029/2001JB001070.
- 1908 Zolotukhin, V.V. & Al'mukhamedov, A.I. (1991) Basalts of the Siberian Platform: occurrence conditions, chemical  
 1909 composition, formation mechanism. *Akade. Nauk SSSR, Sibirskoe Otdelenie, Instituta Geologii i Geofiziki Trudy*, **803**, 7–39.  
 1910 (in Russian)
- 1911 Zolotukhin, V.V., Al'mukhamedov, A.I., & Tkachenko, N.A. (1991) Composition of main rock-forming minerals in Deccan  
 1912 and Siberian trap rocks: a comparison. *Akade. Nauk SSSR, Sibirskoe Otdelenie, Instituta Geologii i Geofiziki Trudy*, **803**,  
 1913 140–177. (in Russian)



**Appendix I. Electron microprobe analyses of minerals of the Vestfjella ferropicrites and related rocks (data that was not published in Papers I–III).**

OLIVINE														
CR	Sample	Analysis	SiO <sub>2</sub>	TiO <sub>2</sub>	Al <sub>2</sub> O <sub>3</sub>	FeO	MnO	MgO	CaO	Cr <sub>2</sub> O <sub>3</sub>	NiO	Total	Notes	Fo
1	117-KHG-91	117KHG/r2/19	38.53	0.04	0.02	21.37	0.26	40.00	0.41	0.02	0.24	100.88	c	0.77
2	117-KHG-91	117KHG/r4/27	38.79	0.02	0.04	19.07	0.26	41.34	0.28	0.01	0.21	100.03	c	0.79
2	117-KHG-91	117KHG/r4/28	39.00	0.01	0.05	15.06	0.22	43.73	0.23	0.04	0.41	98.76	c	0.84
2	117-KHG-91	117KHG/r4/29	36.66	0.17	0.01	29.47	0.49	33.25	0.37	0.03	0.21	100.66	r	0.67
3	117-KHG-91	117KHG/r4/31	38.26	0.04	0.05	19.58	0.25	40.84	0.36	0.04	0.29	99.70	c	0.79
4	117-KHG-91	117KHG/r4/32	38.52	0.03	0.05	16.95	0.28	41.94	0.36	0.02	0.30	98.45	c	0.82
5	117-KHG-91	117KHG/r4/33	38.34	0.04	0.07	17.65	0.25	42.70	0.31	0.05	0.31	99.71	c	0.81
6	117-KHG-91	117KHG/36	38.40	0.03	0.04	17.34	0.26	41.83	0.26	0.04	0.30	98.50	c	0.81
7	117-KHG-91	117KHG/38	38.91	0.00	0.05	18.88	0.29	41.46	0.23	0.02	0.28	100.13	c	0.80
8	117-KHG-91	117KHG/37	38.03	0.02	0.06	16.33	0.27	42.43	0.27	0.03	0.35	97.79	c	0.82
9	117-KHG-91	117KHG/39	39.18	0.05	0.08	16.19	0.20	43.55	0.25	0.03	0.39	99.94	c	0.83
1	AL/WM1e-98	WM1e/r1/1	39.64	0.02	0.02	18.51	0.27	41.45	0.32	0.02	0.32	100.59	c	0.80
2	AL/WM1e-98	WM1e/r1/2	40.76	0.06	0.11	13.77	0.18	44.92	0.47	0.10	0.39	100.75	c	0.85
3	AL/WM1e-98	WM1e/r2/6	40.01	0.04	0.12	14.87	0.20	43.14	0.45	0.04	0.33	99.19	c	0.84
4	AL/WM1e-98	WM1e/r2/9	39.93	0.02	0.05	14.64	0.22	44.50	0.41	0.07	0.37	100.21	c	0.84
5	AL/WM1e-98	WM1e/r2/12	40.45	0.03	0.04	14.61	0.20	44.61	0.47	0.09	0.35	100.86	c	0.84
6	AL/WM1e-98	WM1e/r2/13	39.95	0.00	0.07	15.27	0.22	43.89	0.41	0.10	0.38	100.30	mi1	0.84
6	AL/WM1e-98	WM1e/r2/18	40.10	0.04	0.02	14.60	0.20	44.22	0.47	0.08	0.38	100.12	spl17	0.84
6	AL/WM1e-98	WM1e/r2/20	40.07	0.01	0.04	14.65	0.21	44.61	0.50	0.02	0.34	100.44	mi2	0.84
7	AL/WM1e-98	WM1e/r4/27	39.76	0.04	0.02	17.69	0.20	42.44	0.29	0.04	0.36	100.84	c	0.81
7	AL/WM1e-98	WM1e/r4/28	40.78	0.01	0.04	13.86	0.19	44.87	0.34	0.04	0.38	100.50	r	0.85
8	AL/WM1e-98	WM1e/r4/29	39.72	0.07	0.05	17.53	0.26	41.95	0.45	0.06	0.29	100.38	c	0.81
9	AL/WM1e-98	WM1e/r4/30	39.23	0.03	0.01	19.25	0.31	41.26	0.29	0.04	0.30	100.71	c	0.79
9	AL/WM1e-98	WM1e/r4/31	40.02	0.00	0.06	16.20	0.23	43.28	0.37	0.05	0.34	100.55	r	0.83
9	AL/WM1e-98	WM1e/ol	39.44	0.04	0.05	17.62	0.27	42.64	0.37	0.00	0.30	100.73	c	0.81
10	AL/WM1e-98	WM1e/ol2	39.34	0.04	0.03	17.85	0.16	42.31	0.40	0.02	0.32	100.46	c	0.81
11	AL/WM1e-98	WM1e/r2/Ol1/r	39.33	0.02	0.02	17.00	0.23	42.77	0.36	0.02	0.31	100.07	mi	0.82
12	AL/WM1e-98	WM1e/r2/Ol2/k	40.30	0.07	0.08	13.39	0.09	46.76	0.26	0.11	0.23	101.30	mi	0.86
13	AL/WM1e-98	WM1e/r2/Ol2/i	39.03	0.00	0.03	18.48	0.20	42.02	0.39	0.05	0.33	100.53	miD	0.80
14	AL/WM1e-98	WM1e/r2/Ol3/c	38.70	0.00	0.03	19.69	0.25	40.99	0.36	0.01	0.31	100.33	c	0.79
14	AL/WM1e-98	WM1e/r2/Ol3/r	39.92	0.10	0.01	14.15	0.16	46.15	0.42	0.06	0.33	101.30	r	0.85
1	AL/WM3a-03	WM3/r1/1	40.06	0.03	0.06	18.29	0.29	41.90	0.36	0.06	0.31	101.36	c	0.80
1	AL/WM3a-03	WM3/r1/2	39.63	0.00	0.04	18.82	0.28	42.09	0.34	0.04	0.32	101.57	mi	0.80
2	AL/WM3a-03	WM3/r3/27	39.42	0.05	0.03	19.58	0.27	41.48	0.45	0.08	0.36	101.72	spl26	0.79
2	AL/WM3a-03	WM3/r3/28	39.94	0.00	0.05	19.20	0.25	41.34	0.44	0.04	0.29	101.57	c	0.79
2	AL/WM3a-03	WM3/r3/29	40.29	0.04	0.06	17.36	0.26	42.46	0.46	0.14	0.30	101.37	spl30	0.81

Appendix I continued...

CLINOPYROXENE

CR	Sample	Analysis	SiO <sub>2</sub>	TiO <sub>2</sub>	Al <sub>2</sub> O <sub>3</sub>	FeO	MnO	MgO	CaO	Na <sub>2</sub> O	Cr <sub>2</sub> O <sub>3</sub>	V <sub>2</sub> O <sub>3</sub>	Total	Notes
1	14-KHG-90	14-KHG/1	52.06	1.09	2.14	6.93	0.13	15.60	21.86	0.35	0.39	0.04	100.59	pcc
1	14-KHG-90	14-KHG/2	51.63	1.17	2.36	5.90	0.10	15.66	22.08	0.34	0.73	0.06	100.02	pcr
1	14-KHG-90	14-KHG/3	50.67	1.46	3.51	7.41	0.13	14.57	21.71	0.38	0.54	0.06	100.44	pcc
2	14-KHG-90	14-KHG/4	48.95	2.17	4.23	7.71	0.12	13.71	21.75	0.46	0.31	0.05	99.48	pcc
3	14-KHG-90	14-KHG/5	51.56	1.24	2.37	7.87	0.17	15.13	21.32	0.32	0.18	0.07	100.24	pcc
4	14-KHG-90	14-KHG/6	51.12	1.25	2.41	7.19	0.14	15.15	21.69	0.37	0.17	0.06	99.54	pcc
4	14-KHG-90	14-KHG/7	48.47	2.39	4.51	8.23	0.13	13.83	21.28	0.45	0.37	0.09	99.75	pcz1
4	14-KHG-90	14-KHG/8	52.10	1.05	1.87	6.15	0.10	15.93	22.37	0.27	0.37	0.06	100.27	pcr
5	14-KHG-90	14-KHG/9	51.74	1.21	2.55	6.34	0.10	15.80	22.07	0.30	0.57	0.04	100.72	pcr
5	14-KHG-90	14-KHG/10	51.17	1.36	2.87	6.53	0.12	15.22	22.00	0.36	0.58	0.07	100.27	pcr
5	14-KHG-90	14-KHG/11	50.14	1.61	3.49	7.60	0.12	14.62	21.78	0.41	0.39	0.04	100.20	pcc
6	14-KHG-90	14-KHG/12	52.00	1.11	2.03	7.08	0.11	15.66	21.47	0.32	0.30	0.05	100.13	pcc
7	14-KHG-90	14-KHG/13	52.45	0.94	1.83	6.99	0.14	16.08	20.92	0.30	0.49	0.04	100.18	pcc
7	14-KHG-90	14-KHG/14	50.45	1.56	3.29	7.34	0.11	14.39	21.96	0.36	0.33	0.05	99.82	pcr
7	14-KHG-90	14-KHG/15	50.68	1.46	3.28	7.37	0.09	14.77	21.75	0.37	0.61	0.07	100.46	pcr
8	14-KHG-90	14-KHG/16	49.60	1.91	4.28	7.84	0.10	14.10	21.44	0.46	0.39	0.08	100.20	pcr
8	14-KHG-90	14-KHG/17	52.17	1.28	2.37	7.98	0.11	15.19	21.62	0.31	0.13	0.07	101.22	pcc
9	14-KHG-90	14-KHG/18	51.86	1.12	1.97	6.48	0.12	15.82	21.56	0.30	0.41	0.04	99.67	pcc
1	JSH/B006	B006a/1	52.06	1.09	2.11	7.47	0.15	15.49	21.77	0.30	0.29	0.04	100.76	gm
2	JSH/B006	B006a/2	48.94	2.05	4.25	8.73	0.14	13.67	21.70	0.46	0.07	0.09	100.09	gm/amph3
3	JSH/B006	B006a/r2/12	44.99	4.18	6.75	9.76	0.20	11.73	21.40	0.50	0.00	0.11	99.63	mi14r
3	JSH/B006	B006a/r2/13	47.33	2.72	4.71	8.27	0.16	13.23	21.80	0.45	0.12	0.11	98.89	mi14c
4	JSH/B006	B006a/r2/16	50.47	1.43	2.52	9.10	0.19	14.72	21.05	0.32	0.01	0.08	99.89	gmc/amph18
4	JSH/B006	B006a/r2/17	46.91	2.78	5.18	8.98	0.14	12.63	21.48	0.47	0.01	0.08	98.67	gmr/amph18
5	JSH/B006	B006a/r2/20	50.41	1.41	2.47	9.06	0.19	14.66	21.21	0.33	0.00	0.07	99.79	gm/amph19
6	JSH/B006	B006b/r4/10	47.09	3.18	7.07	12.33	0.24	10.12	21.42	0.56	0.01	0.10	102.10	mi~12
7	JSH/B006	B006b/r4/16	53.45	0.94	1.65	6.90	0.11	16.93	20.83	0.38	0.53	0.04	101.75	gm
8	JSH/B006	B006b/r4/17	50.26	1.43	3.24	7.58	0.12	14.77	22.15	0.43	0.42	0.04	100.44	gm
9	JSH/B006	B006b/r5/19	46.43	3.37	6.64	10.29	0.19	11.66	21.31	0.54	0.01	0.14	100.58	mi20-21
10	JSH/B006	B006b/r6/28	50.41	1.52	3.19	7.52	0.12	15.03	21.94	0.39	0.38	0.08	100.57	gmc
10	JSH/B006	B006b/r6/29	47.54	2.48	4.97	8.84	0.16	12.69	22.21	0.44	0.00	0.11	99.43	gmr
11	JSH/B006	B006b/r6/31	47.62	2.53	4.85	9.26	0.23	12.64	21.35	0.48	0.00	0.10	99.06	gm/amph32
12	JSH/B006	B006b/r7/36	51.12	1.43	2.86	6.84	0.08	15.39	21.78	0.43	0.76	0.05	100.74	gm/amph37
13	JSH/B006	B006b/r7/41	51.72	1.09	2.16	7.17	0.11	15.69	21.46	0.33	0.38	0.05	100.16	gm
1	AL/B7-98	B798/r1/4	51.24	1.00	1.93	11.47	0.28	15.60	18.83	0.22	0.00	0.04	100.61	
1	AL/B7-98	B798/r1/5	47.88	2.24	4.52	9.99	0.17	14.00	20.36	0.36	0.04	0.09	99.64	

Appendix I continued...

CLINOPYROXENE

CR	Sample	Analysis	SiO <sub>2</sub>	TiO <sub>2</sub>	Al <sub>2</sub> O <sub>3</sub>	FeO	MnO	MgO	CaO	Na <sub>2</sub> O	Cr <sub>2</sub> O <sub>3</sub>	V <sub>2</sub> O <sub>3</sub>	Total	Notes
2	AL/B7-98	B798/r1/7	48.08	1.35	2.95	8.32	0.14	15.80	19.91	0.30	0.46	0.04	97.36	
2	AL/B7-98	B798/r1/8	50.34	1.40	3.10	8.53	0.17	15.69	20.47	0.33	0.44	0.10	100.58	
3	AL/B7-98	B798/r1/9	49.85	1.69	3.59	9.39	0.18	14.86	20.00	0.33	0.10	0.08	100.07	
4	AL/B7-98	B798/r2/14	50.12	1.34	3.01	11.10	0.24	14.21	20.10	0.35	0.01	0.07	100.55	r
4	AL/B7-98	B798/r2/15	49.22	1.38	2.95	8.05	0.14	15.96	19.66	0.29	0.63	0.06	98.34	c
5	AL/B7-98	B798/r2/16	51.37	1.03	2.13	10.81	0.23	16.70	17.62	0.23	0.01	0.05	100.19	r
5	AL/B7-98	B798/r2/17	50.83	1.35	2.95	7.96	0.17	15.73	20.16	0.26	0.68	0.07	100.15	c
5	AL/B7-98	B798/r2/18	50.56	1.25	2.63	9.63	0.23	15.87	19.51	0.27	0.04	0.08	100.06	r
1	117-KHG-91	117KHG/r1/1	50.34	1.75	3.05	9.76	0.24	12.92	22.52	0.36	0.01	0.12	101.08	z1
1	117-KHG-91	117KHG/r1/2	44.62	3.93	8.00	9.03	0.13	11.28	22.32	0.44	0.02	0.18	99.95	z2
1	117-KHG-91	117KHG/r1/3	43.36	4.07	8.91	9.14	0.13	11.03	21.82	0.49	0.10	0.22	99.27	z2
1	117-KHG-91	117KHG/r1/4	48.93	2.07	4.41	8.21	0.14	13.42	22.31	0.30	0.03	0.15	99.98	z1
2	117-KHG-91	117KHG/r1/7	43.95	4.10	8.74	9.24	0.11	11.03	21.99	0.48	0.09	0.20	99.96	
2	117-KHG-91	117KHG/r1/8	43.62	4.20	9.01	8.91	0.13	11.24	22.36	0.36	0.17	0.20	100.21	
3	117-KHG-91	117KHG/r2/11	49.16	1.96	4.27	8.36	0.14	13.70	22.14	0.31	0.07	0.09	100.20	z1
3	117-KHG-91	117KHG/r2/12	44.73	3.85	8.30	9.00	0.16	11.43	22.10	0.43	0.07	0.22	100.29	z2
3	117-KHG-91	117KHG/r2/13	44.31	3.84	8.51	9.07	0.15	11.33	22.15	0.41	0.06	0.18	100.01	z2
3	117-KHG-91	117KHG/r2/14	48.94	1.87	3.96	7.63	0.12	13.34	22.42	0.38	0.08	0.11	98.84	z1
4	117-KHG-91	117KHG/r2/17	43.57	4.06	8.44	9.13	0.12	11.28	22.28	0.44	0.06	0.20	99.59	z2
4	117-KHG-91	117KHG/r2/18	48.00	2.02	4.07	7.91	0.16	13.43	22.59	0.34	0.03	0.16	98.72	z1
6	117-KHG-91	117KHG/r3/21	47.31	2.50	4.69	9.87	0.21	11.29	22.35	0.54	0.00	0.06	98.82	z2
6	117-KHG-91	117KHG/r3/22	48.29	2.01	3.68	7.99	0.17	13.30	22.20	0.34	0.01	0.14	98.15	z1
7	117-KHG-91	117KHG/r4/25	43.61	4.09	8.41	9.21	0.14	11.17	21.97	0.47	0.05	0.21	99.31	ac
8	117-KHG-91	117KHG/r4/34	43.23	3.75	7.48	8.07	0.13	11.74	22.40	0.44	0.08	0.17	97.50	z2
8	117-KHG-91	117KHG/r4/35	47.54	2.02	4.27	8.08	0.14	13.70	21.97	0.34	0.03	0.13	98.22	z1
1	AL/WM1e-98	WM1e/r1/4	44.75	2.90	8.01	11.69	0.14	11.11	19.37	0.59	0.05	0.15	98.76	gm
2	AL/WM1e-98	WM1e/r2/10	45.74	2.73	7.69	8.08	0.10	12.47	21.30	0.33	0.36	0.11	98.91	gm
3	AL/WM1e-98	WM1e/r2/11	46.85	2.59	6.48	8.22	0.15	12.58	20.48	0.31	0.49	0.11	98.26	gm
4	AL/WM1e-98	WM1e/r3/23	48.29	1.73	5.25	10.14	0.20	13.51	19.72	0.23	0.04	0.11	99.20	gm
5	AL/WM1e-98	WM1e/r3/24	45.27	2.95	8.33	9.20	0.13	11.61	21.25	0.35	0.20	0.14	99.44	gm
6	AL/WM1e-98	WM1e/r4/32	49.72	1.41	3.97	8.07	0.08	15.19	19.92	0.19	0.38	0.06	98.98	gm
7	AL/WM1e-98	WM1e/r4/36	47.22	2.23	6.64	8.45	0.13	12.81	20.81	0.35	0.35	0.12	99.11	gm
8	AL/WM1e-98	WM1e/r4/37	45.59	3.02	8.24	9.56	0.14	11.53	21.03	0.35	0.10	0.12	99.68	gm
9	AL/WM1e-98	WM1e-98/r4/s1	44.03	3.35	8.85	11.69	0.14	9.00	20.90	0.42	0.01	0.00	98.39	mi
10	AL/WM1e-98	WM1e-98/r4/1	43.76	3.85	8.88	12.01	0.22	8.69	20.95	0.41	0.00	0.00	98.78	mi
11	AL/WM1e-98	WM1e-98-2	41.87	4.65	10.03	11.35	0.20	8.15	21.36	0.40	0.00	0.00	98.01	mi

Appendix I continued...

CLINOPYROXENE

CR	Sample	Analysis	SiO <sub>2</sub>	TiO <sub>2</sub>	Al <sub>2</sub> O <sub>3</sub>	FeO	MnO	MgO	CaO	Na <sub>2</sub> O	Cr <sub>2</sub> O <sub>3</sub>	V <sub>2</sub> O <sub>3</sub>	Total	Notes
11	AL/WM1e-98	WM1e-98-2r	41.58	5.83	10.40	11.06	0.16	8.13	21.22	0.44	0.07	0.00	98.90	mi
12	AL/WM1e-98	WM1e-98-1b	40.69	4.81	11.28	12.75	0.18	6.33	21.78	0.45	0.07	0.00	98.34	mi
13	AL/WM1e-98	WM1e/r2/19	41.76	5.33	11.66	9.89	0.17	8.12	20.90	0.61	0.01	0.17	98.62	mi20
1	AL/WM1b-98	WM1b/amfs1	41.57	4.44	10.27	11.60	0.22	9.16	20.90	0.47	0.06	0.00	98.68	mi
2	AL/WM1b-98	WM1b/amfs2	44.56	3.10	8.58	14.11	0.31	8.31	20.21	0.48	0.00	0.00	99.66	mi
1	AL/WM3a-03	WM3/r1/5	42.78	3.67	10.66	11.95	0.16	8.90	21.03	0.41	0.10	0.22	99.90	mi2
2	AL/WM3a-03	WM3/r1/6	46.08	3.06	8.65	9.17	0.11	11.63	21.34	0.36	0.13	0.11	100.64	gm
3	AL/WM3a-03	WM3/r1/7	45.09	3.24	8.31	9.70	0.14	11.82	21.34	0.37	0.20	0.16	100.37	gm
4	AL/WM3a-03	WM3/r2/12	45.91	3.09	7.97	9.16	0.12	11.78	21.29	0.35	0.33	0.18	100.17	gm
5	AL/WM3a-03	WM3/r2/13	46.10	2.86	7.92	8.90	0.10	11.92	21.84	0.34	0.25	0.13	100.36	gm
6	AL/WM3a-03	WM3/r2/16	44.76	2.87	7.58	9.60	0.55	12.67	19.69	0.36	0.05	0.08	98.21	gm
7	AL/WM3a-03	WM3/r3/21	44.29	3.60	9.18	10.49	0.16	10.61	21.33	0.41	0.07	0.18	100.33	gm
8	AL/WM3a-03	WM3/r3/22	48.96	2.17	4.72	11.52	0.29	12.00	20.42	0.49	0.02	0.12	100.72	gm
9	AL/WM3a-03	WM3/r3/23	44.83	3.15	8.95	10.10	0.16	10.88	21.49	0.41	0.06	0.17	100.20	gm
10	AL/WM3a-03	WM3/r3/24	46.99	1.98	7.62	8.66	0.17	12.57	20.94	0.38	0.12	0.08	99.50	gm
1	AL/WM3a-03	WM3/r1/3	41.59	3.20	11.25	12.64	0.24	8.01	19.51	0.76	0.02	0.15	97.38	mi2
5	AL/B5-03	B5/r3/20	51.68	0.82	3.09	5.81	0.09	16.43	21.17	0.24	0.92	0.10	100.35	pcc
5	AL/B5-03	B5/r3/21	52.30	0.73	3.01	5.92	0.12	16.45	21.54	0.21	0.45	0.06	100.79	pcz1
5	AL/B5-03	B5/r3/26	52.37	0.58	2.60	5.25	0.06	16.94	21.04	0.22	1.22	0.02	100.29	pcz2
5	AL/B5-03	B5/r3/23	51.50	1.03	2.95	8.40	0.20	16.22	19.57	0.23	0.06	0.09	100.24	pcr
1	128-KHG-91	128KHG/r1/8	47.56	1.86	5.33	10.72	0.19	13.08	21.24	0.41	0.06	0.10	100.57	c
2	128-KHG-91	128KHG/r1/9	49.05	1.86	3.96	11.34	0.30	13.15	20.61	0.47	0.00	0.09	100.83	plag6
3	128-KHG-91	128KHG/r1/10	49.15	1.47	4.01	10.56	0.20	13.77	20.74	0.37	0.00	0.10	100.38	c
4	128-KHG-91	128KHG/r2/15	47.75	1.90	5.56	10.60	0.18	13.03	21.53	0.38	0.06	0.09	101.08	c
5	128-KHG-91	128KHG/r2/16	47.27	2.14	5.85	10.36	0.16	13.05	21.12	0.39	0.20	0.08	100.62	c
6	128-KHG-91	128KHG/r2/17	50.36	1.03	3.01	10.23	0.22	14.61	20.80	0.28	0.00	0.08	100.62	c
7	128-KHG-91	128KHG/r3/22b	31.49	32.57	3.37	4.65	0.04	1.79	25.63	0.00	0.02	0.61	100.16	ox22
7	128-KHG-91	128KHG/r3/23	47.36	1.91	5.03	11.01	0.22	13.21	21.10	0.40	0.02	0.10	100.34	c
8	128-KHG-91	128KHG/r3/24	46.58	1.96	5.52	11.02	0.17	12.37	21.58	0.38	0.06	0.12	99.75	r
8	128-KHG-91	128KHG/r3/25	49.99	1.06	2.92	10.03	0.21	14.86	20.42	0.30	0.08	0.07	99.94	c
9	128-KHG-91	128KHG/r3/26	47.02	1.79	5.64	9.93	0.19	13.28	21.40	0.36	0.18	0.10	99.88	c
1	X2-KHG-90	X2/r1/1	51.61	1.37	1.81	12.04	0.33	13.70	20.38	0.26	0.05	0.12	101.67	
1	X2-KHG-90	X2/r1/2	51.26	1.28	1.93	11.71	0.27	14.03	19.83	0.29	0.00	0.14	100.76	
2	X2-KHG-90	X2/r1/3	49.38	1.98	3.03	12.54	0.25	12.36	20.88	0.38	0.00	0.11	100.91	
3	X2-KHG-90	X2/r1/4	48.10	2.50	4.57	11.48	0.22	12.89	20.12	0.36	0.07	0.22	100.52	
4	X2-KHG-90	X2/r1/5	51.36	1.26	1.86	11.99	0.31	13.87	19.59	0.28	0.06	0.11	100.70	

Appendix I continued...

CLINOPYROXENE

CR	Sample	Analysis	SiO <sub>2</sub>	TiO <sub>2</sub>	Al <sub>2</sub> O <sub>3</sub>	FeO	MnO	MgO	CaO	Na <sub>2</sub> O	Cr <sub>2</sub> O <sub>3</sub>	V <sub>2</sub> O <sub>3</sub>	Total	Notes
5	X2-KHG-90	X2/r2/12	48.81	1.96	3.41	12.29	0.32	12.93	20.52	0.37	0.00	0.11	100.72	c
5	X2-KHG-90	X2/r2/13	50.83	1.24	1.50	13.81	0.36	12.68	20.29	0.32	0.01	0.00	101.05	r
6	X2-KHG-90	X2/r2/14	50.76	1.17	1.41	14.36	0.43	12.68	20.11	0.27	0.00	0.06	101.25	c
6	X2-KHG-90	X2/r2/15	50.49	0.81	0.85	18.52	0.51	10.07	19.97	0.27	0.02	0.04	101.54	r
7	X2-KHG-90	X2/r2/16	48.65	2.05	3.58	11.40	0.26	13.23	20.94	0.38	0.03	0.12	100.64	
8	X2-KHG-90	X2/r2/20	47.86	1.93	3.79	12.82	0.23	12.95	19.25	0.37	0.00	0.14	99.33	

AMPHIBOLE

CR	Sample	Analysis	SiO <sub>2</sub>	TiO <sub>2</sub>	Al <sub>2</sub> O <sub>3</sub>	FeO	MnO	MgO	CaO	Na <sub>2</sub> O	K <sub>2</sub> O	P <sub>2</sub> O <sub>5</sub>	Cr <sub>2</sub> O <sub>3</sub>	V <sub>2</sub> O <sub>3</sub>	Cl	F	Total	Notes
1	JSH/B006	B006a/3	39.28	5.46	13.16	16.74	0.23	9.60	10.94	2.47	0.76	0.15	0.00	0.04	0.03	0.48	99.34	cpx2
2	JSH/B006	B006a/r2/15	39.71	3.98	12.20	16.43	0.27	9.45	10.89	2.49	0.88	0.11	0.00	0.03	0.03	0.62	97.08	gm
3	JSH/B006	B006a/r2/18	39.42	3.60	13.08	16.80	0.25	9.66	11.01	2.48	0.88	0.40	0.01	0.04	0.02	0.61	98.26	cpx16-17
4	JSH/B006	B006a/r2/19	40.15	4.01	11.83	15.31	0.26	10.10	10.67	2.61	0.70	0.43	0.00	0.04	0.02	0.58	96.72	cpx20
5	JSH/B006	B006b/r4/8	41.32	5.32	10.22	13.06	0.16	10.52	14.74	1.94	0.69	0.01	0.02	0.17	0.02	0.36	98.54	mi14
6	JSH/B006	B006b/r6/30	39.20	5.47	13.03	15.84	0.24	9.80	10.99	2.47	0.69	0.23	0.00	0.05	0.01	0.46	98.48	gm
7	JSH/B006	B006b/r6/32	39.51	3.75	12.97	17.86	0.32	9.24	10.71	2.54	0.94	0.15	0.00	0.04	0.02	0.49	98.53	cpx31
8	JSH/B006	B006b/r6/33	39.56	5.23	12.49	15.26	0.26	9.94	10.82	2.60	0.70	0.19	0.00	0.05	0.01	0.50	97.62	gm
9	JSH/B006	B006b/r7/38	38.86	5.44	13	16.05	0.25	9.73	10.74	2.59	0.65	0.31	0.00	0.03	0.02	0.51	98.25	gm
1	AL/WM1b-98	WM1b/amf3	39.36	5.05	12.23	18.27	0.23	7.75	11.27	2.67	1.17	0.00	0.08	0.00	0.03	0.17	98.32	mi
1	AL/WM1b-98	WM1b/amf3-2	38.60	4.75	12.10	18.20	0.25	7.80	11.34	2.75	1.16	0.00	0.06	0.00	0.00	0.25	97.46	mi
1	AL/WM1b-98	WM1b/amf3-3	38.68	4.87	12.21	17.87	0.22	7.91	11.36	2.82	1.15	0.00	0.08	0.00	0.02	0.18	97.47	mi
1	AL/WM1e-98	WM1e/amf1	37.97	5.41	14.70	14.52	0.12	8.96	12.79	2.46	0.15	0.00	0.06	0.00	0.00	0.35	97.83	mi
1	AL/WM1e-98	WM1e/amf1-2	37.24	5.90	15.32	15.05	0.22	8.70	11.12	2.61	0.20	0.00	0.05	0.00	0.00	0.36	97.16	mi
2	AL/WM1e-98	WM1e/amf1r	38.64	5.62	14.90	13.60	0.20	10.00	10.98	2.70	0.20	0.00	0.03	0.00	0.01	0.40	97.58	mi
2	AL/WM1e-98	WM1e/amf1k	37.24	4.12	17.59	13.41	0.18	9.24	11.04	2.84	0.23	0.00	0.01	0.00	0.03	0.46	96.65	mi
3	AL/WM1e-98	WM1e/1a	37.66	5.79	14.52	14.59	0.15	8.78	12.67	2.41	0.18	0.00	0.05	0.00	0.01	0.42	97.57	mi-B
4	AL/WM1e-98	WM1e/1kev	37.36	4.63	17.40	13.87	0.29	9.03	11.03	2.80	0.23	0.00	0.05	0.00	0.00	0.44	97.38	mi
5	AL/WM1e-98	WM1e/r3/3-2	36.96	5.98	15.49	14.22	0.12	9.05	11.28	2.88	0.33	0.00	0.24	0.00	0.00	0.42	97.25	mi
6	AL/WM1e-98	WM1e/r4/2	38.53	5.62	14.54	13.73	0.19	10.03	11.22	2.76	0.21	0.00	0.00	0.00	0.00	0.40	97.55	mi

CR SPINEL

CR	Sample	Analysis	SiO <sub>2</sub>	TiO <sub>2</sub>	Al <sub>2</sub> O <sub>3</sub>	FeO	MgO	Cr <sub>2</sub> O <sub>3</sub>	NiO	V <sub>2</sub> O <sub>3</sub>	Total	Notes
1	JSH/B006	B006a/r2/10	0.02	7.80	6.60	45.25	8.14	26.97	0.28	0.38	95.45	ol9
2	JSH/B006	B006b/r6/27	0.00	6.61	6.86	46.73	7.53	29.08	0.23	0.39	97.43	ol-26
1	AL/WM1e-98	WM1e/r1/5	0.08	3.74	18.22	34.28	13.84	27.50	0.33	0.49	98.47	pc
2	AL/WM1e-98	WM1e/r2/15	0.53	2.97	18.66	32.22	11.52	30.48	0.31	0.37	97.05	mi13
3	AL/WM1e-98	WM1e/r2/16	2.35	3.14	19.47	30.58	12.07	27.87	0.31	0.37	96.15	ol18
4	AL/WM1e-98	WM1e/r2/17	0.17	3.21	20.02	31.62	12.52	28.74	0.28	0.42	96.98	ol18

Appendix I continued...

CR SPINEL

CR	Sample	Analysis	SiO <sub>2</sub>	TiO <sub>2</sub>	Al <sub>2</sub> O <sub>3</sub>	FeO	MgO	Cr <sub>2</sub> O <sub>3</sub>	NiO	V <sub>2</sub> O <sub>3</sub>	Total	Notes
5	AL/WM1e-98	WM1e/r3/22	0.21	2.44	15.30	34.54	11.10	32.83	0.23	0.27	96.92	pc
6	AL/WM1e-98	WM1e/r4/38	0.15	4.51	19.12	34.91	12.10	26.04	0.33	0.60	97.77	pc
7	AL/WM1e-98	WM1e/r4/39	0.11	3.02	18.93	31.04	13.08	30.51	0.33	0.42	97.44	pc
8	AL/WM1e-98	WM1e/OI/k	0.06	3.59	15.09	40.22	8.63	27.21	0.28	0.45	95.53	olD
9	AL/WM1e-98	WM1e-23	0.17	3.42	14.41	39.29	9.03	30.65	0.36	0.30	97.63	mi
1	AL/WM3a-03	WM3/r1/9	0.08	4.13	14.43	43.62	9.40	25.43	0.28	0.56	97.93	ol~1
2	AL/WM3a-03	WM3/r2/17	0.13	3.45	17.28	35.71	11.58	29.07	0.35	0.40	97.96	ol~15
3	AL/WM3a-03	WM3/r2/18	0.13	4.02	18.03	36.47	12.95	26.79	0.34	0.48	99.20	ol~15
4	AL/WM3a-03	WM3/r2/19	0.19	4.52	17.13	36.97	12.81	25.96	0.37	0.49	98.44	ol~15
5	AL/WM3a-03	WM3/r3/25	0.07	4.71	16.91	37.83	12.07	25.54	0.35	0.49	97.97	gm
6	AL/WM3a-03	WM3/r3/26	0.11	3.33	15.57	40.16	9.82	29.23	0.27	0.53	99.03	ol27
7	AL/WM3a-03	WM3/r3/30	0.92	3.23	15.48	36.39	10.92	29.73	0.33	0.51	97.51	ol29

FE-TI OXIDES

CR	Sample	Analysis	SiO <sub>2</sub>	TiO <sub>2</sub>	Al <sub>2</sub> O <sub>3</sub>	FeO	MgO	Cr <sub>2</sub> O <sub>3</sub>	NiO	V <sub>2</sub> O <sub>3</sub>	Total	Notes
1	JSH/B006	B006a/5	0.21	23.07	3.62	66.60	1.08	0.46	0.03	0.51	95.57	gm
2	JSH/B006	B006b/r4/11	0.03	24.31	3.14	62.42	1.44	0.22	1.28	0.94	93.78	mi~12
3	JSH/B006	B006b/r7/39	0.04	23.48	3.83	65.14	1.65	0.02	0.01	0.63	94.81	gm
4	JSH/B006	B006b/r7/40	0.13	24.31	4.36	64.40	0.40	0.02	0.02	0.73	94.37	gm
1	AL/B7-98	B798/r1/1	0.02	46.65	0.07	47.99	2.01	0.16	0.00	0.57	97.47	c
2	AL/B7-98	B798/r1/2	0.00	46.99	0.01	47.06	3.02	0.00	0.01	0.43	97.52	c
3	AL/B7-98	B798/r2/19	0.00	46.59	0.12	48.08	1.48	0.60	0.08	0.58	97.52	c
4	AL/B7-98	B798/r2/20	0.00	45.84	0.16	48.32	2.52	0.00	0.07	0.62	97.53	c
1	117-KHG-91	117KHG/r1/5	0.09	26.23	1.03	66.86	1.02	0.11	0.05	0.59	95.99	c
2	117-KHG-91	117KHG/r1/10	0.41	20.54	1.25	68.69	0.71	0.48	0.09	0.60	92.77	c
3	117-KHG-91	117KHG/r3/23	0.05	25.73	2.50	61.28	1.41	0.07	0.95	0.64	92.64	c
4	117-KHG-91	117KHG/r4/26	0.03	26.49	2.32	61.62	1.28	0.23	0.20	0.65	92.82	c
1	128-KHG-91	128KHG/r1/1	0.16	16.56	4.18	72.28	1.62	0.00	0.00	0.81	95.60	c
2	128-KHG-91	128KHG/r1/2	0.13	16.29	3.36	72.40	1.52	0.00	0.02	0.72	94.45	c
3	128-KHG-91	128KHG/r2/13	0.09	14.39	3.72	71.96	1.45	0.05	0.68	0.76	93.10	r
3	128-KHG-91	128KHG/r2/14	0.10	15.65	2.85	72.62	1.55	0.02	0.07	0.74	93.59	c
4	128-KHG-91	128KHG/r3/21	0.05	17.88	0.75	73.53	1.71	0.04	0.03	0.67	94.66	c
1	X2-KHG-90	X2/r1/10	0.82	23.99	0.52	69.66	1.00	0.40	0.02	0.47	96.89	c
2	X2-KHG-90	X2/r1/11	0.08	24.88	0.06	69.48	1.01	0.00	0.46	0.90	96.87	c
3	X2-KHG-90	X2/r2/21	0.08	25.40	1.88	67.39	0.98	0.00	0.06	0.98	96.76	c
3	X2-KHG-90	X2/r2/21	0.12	26.43	1.94	66.56	1.04	0.05	0.09	0.96	97.20	c

Appendix I continued...

PLAGIOCLASE

CR	Sample	Analysis	SiO <sub>2</sub>	Al <sub>2</sub> O <sub>3</sub>	FeO	MgO	CaO	Na <sub>2</sub> O	K <sub>2</sub> O	Total	Notes	An
1	JSH/B006	B006a/r2/21	59.22	24.18	0.45	0.00	6.47	6.57	0.82	97.73	gm	0.35
2	JSH/B006	B006b/r6/34	62.22	23.21	0.38	0.02	4.70	7.38	1.04	98.94	gm	0.26
3	JSH/B006	b006b/r7/c10	62.27	23.93	0.32	0.01	5.25	7.39	0.93	100.09	gm	0.28
1	AL/B7-98	B798/r1/3	55.22	26.39	0.62	0.05	10.07	5.34	0.31	98.00	c	0.51
2	AL/B7-98	B798/r1/6	57.41	25.22	0.57	0.09	8.30	6.34	0.42	98.34	c	0.42
3	AL/B7-98	B798/r2/10	54.36	27.16	0.71	0.07	10.91	4.97	0.31	98.49	c	0.55
4	AL/B7-98	B798/r2/11	53.82	26.85	0.65	0.07	11.16	4.85	0.30	97.70	c	0.56
5	AL/B7-98	B798/r2/12	54.32	27.15	0.79	0.10	10.94	4.98	0.30	98.58	c	0.55
6	AL/B7-98	B798/r2/13	58.29	24.02	0.49	0.01	7.23	6.65	0.52	97.21	c	0.38
1	117-KHG-91	117KHG/r1/6	54.10	28.13	0.42	0.05	11.45	4.46	0.40	99.01	c	0.59
2	117-KHG-91	117KHG/r1/9	50.51	30.65	0.67	0.08	14.44	3.06	0.25	99.67	c	0.72
3	117-KHG-91	117KHG/r2/15	51.54	30.07	0.61	0.07	13.45	3.38	0.21	99.33	c	0.69
4	117-KHG-91	117KHG/r2/16	51.01	29.66	0.60	0.09	13.95	3.27	0.22	98.80	c	0.70
5	117-KHG-91	117KHG/r4/30	50.42	29.20	0.57	0.08	13.41	3.56	0.26	97.50	c	0.68
1	AL/WM1e-98	WM1e/r1/3	58.06	25.84	0.81	0.09	8.24	5.82	0.36	99.22	gm	0.44
2	AL/WM1e-98	WM1e/r2/7	56.03	26.67	0.94	0.12	9.90	5.01	0.22	98.89	gm	0.52
3	AL/WM1e-98	WM1e/r3/25	55.04	26.94	1.14	0.10	10.36	4.68	0.18	98.44	gm	0.55
4	AL/WM1e-98	WM1e/r3/26	62.64	23.23	0.50	0.00	4.80	7.55	0.53	99.24	gm	0.26
5	AL/WM1e-98	WM1e/r4/33	53.42	27.15	2.73	0.32	10.44	4.27	0.18	98.50	gm	0.57
6	AL/WM1e-98	WM1e/r4/34	56.83	25.57	2.37	0.30	8.13	5.50	0.56	99.25	gm	0.45
7	AL/WM1e-98	WM1e/r4/35	55.86	26.45	1.30	0.14	9.73	5.00	0.23	98.70	gm	0.52
1	AL/WM3a-03	WM3/r1/8	56.78	26.56	0.97	0.42	9.61	5.13	0.20	99.68	gm	0.51
2	AL/WM3a-03	WM3/r2/10	52.56	26.40	2.09	0.33	10.44	4.01	0.22	96.05	gm	0.59
3	AL/WM3a-03	WM3/r2/14	55.43	27.23	0.96	0.11	10.69	4.57	0.20	99.18	gm	0.56
1	128-KHG-91	128KHG/r1/3	51.45	29.75	0.84	0.18	13.85	3.43	0.13	99.62	c	0.69
2	128-KHG-91	128KHG/r1/4	54.39	27.20	0.78	0.12	11.43	4.65	0.27	98.84	pcr	0.58
2	128-KHG-91	128KHG/r1/5	54.68	27.27	0.77	0.11	11.25	4.91	0.27	99.25	pcc	0.56
2	128-KHG-91	128KHG/r1/6	54.21	27.31	0.75	0.09	11.29	4.64	0.29	98.58	pcc	0.57
3	128-KHG-91	128KHG/r1/7	53.09	28.62	0.97	0.14	12.94	4.07	0.16	99.99	c	0.64
4	128-KHG-91	128KHG/r1/11	52.04	29.01	1.25	0.26	13.50	3.74	0.16	99.97	c	0.67
5	128-KHG-91	128KHG/r1/12	51.00	29.37	0.90	0.16	13.86	3.44	0.11	98.85	c	0.69
6	128-KHG-91	128KHG/r2/18	51.68	28.76	0.86	0.14	13.58	3.68	0.14	98.84	c	0.67
7	128-KHG-91	128KHG/r2/19	56.96	26.52	0.76	0.08	9.73	5.67	0.28	100.00	c	0.49
8	128-KHG-91	128KHG/r2/20	56.68	26.01	0.73	0.09	9.51	5.58	0.29	98.88	c	0.49
9	128-KHG-91	128KHG/r3/27	50.73	28.34	1.02	0.12	13.69	3.64	0.13	97.66	c	0.68
10	128-KHG-91	128KHG/r3/28	50.74	28.93	0.84	0.14	13.73	3.64	0.14	98.17	c	0.68

Appendix I continued...

PLAGIOCLASE

CR	Sample	Analysis	SiO <sub>2</sub>	Al <sub>2</sub> O <sub>3</sub>	FeO	MgO	CaO	Na <sub>2</sub> O	K <sub>2</sub> O	Total	Notes	An
11	128-KHG-91	128KHG/r3/29	50.66	28.65	0.91	0.15	13.85	3.45	0.11	97.77	c	0.69
12	128-KHG-91	128KHG/r3/30	51.89	28.50	0.99	0.12	13.16	3.96	0.14	98.74	c	0.65
1	X2-KHG-90	X2/r1/6	56.86	25.40	1.57	0.27	8.91	5.33	0.54	98.89	c	0.48
2	X2-KHG-90	X2/r1/7	54.11	27.25	0.81	0.15	11.23	4.27	0.33	98.16	c	0.59
3	X2-KHG-90	X2/r1/8	56.20	26.11	0.59	0.07	10.11	4.91	0.41	98.40	c	0.53
4	X2-KHG-90	X2/r1/9	59.72	24.39	0.42	0.08	7.42	6.20	0.73	98.97	c	0.40
5	X2-KHG-90	X2/r2/17	55.79	26.33	0.63	0.06	10.20	4.94	0.34	98.27	c	0.53
6	X2-KHG-90	X2/r2/18	56.60	25.69	0.61	0.10	9.71	5.22	0.42	98.34	c	0.51
7	X2-KHG-90	X2/r2/19	53.50	27.56	0.99	0.12	12.10	4.18	0.25	98.72	c	0.62

Mineral compositions determined at the Geological Survey of Finland with Cameca SX-100 electron microprobe. Analytical procedures given in Paper II. Abbreviations used in the dataset: CR = crystal, c = core, r = rim, mi = melt inclusion, gm = groundmass, z = zone, pc = phenocryst, spl = close to spinel inclusion, amph = clinopyroxene with amphibole rim, ox = close to oxide grain, cpx = amphibole rim in clinopyroxene, ol = inclusion in olivine, Fo = forsterite content ( $\text{Mg}/(\text{Mg}+\text{Fe}^{2+})$ ), An = anorthite content ( $\text{Ca}/(\text{Ca}+\text{Na})$ ).